A KINETIC THEORY APPROACH TO PEDESTRIAN MOTION AND ONSET OF DISEASE SPREADING

A Dissertation Presented to
the Faculty of the Department of Mathematics
University of Houston

In Partial Fulfillment
of the Requirements for the Degree
Doctor of Philosophy

By
Daewa Kim
May 2019

A KINETIC THEORY APPROACH TO PEDESTRIAN MOTION AND ONSET OF DISEASE SPREADING

Daewa Kim

APPROVED:

Prof. Annalisa Quaini, Committee Chair
Department of Mathematics

Prof. William Ott
Department of Mathematics, University of Houston

Prof. Ilya Timofeyev
Department of Mathematics, University of Houston

Prof. Natasha Sharma
Department of Mathematical Science,
Unversity of Texas at El Paso

Dean, College of Natural Sciences and Mathematics

Acknowledgements

I would like to express my deepest appreciation to my committee chair, Dr. Annalisa Quaini. I cannot begin to express how much I appreciate the time and effort that she put into helping and guiding me. Without her willingness and persistent help, this dissertation would not have been possible.

I am tremendously fortunate to have the committee members: Dr. William Ott, Dr. Ilya Timofeyev, and Dr. Natasha Sharma. I thank them for supporting me and giving such thoughtful feedback, which was always aimed at moving me forward.

The research was partially supported by the National Science Foundation through the NSF grant DMS-1620384. I am grateful for the Presidential Fellowship from the College of Natural Sciences and Mathematics, and also the University of Houston Alumni Association Scholarships from the University of Houston Alumni Association.

I would like to acknowledge the gratitude and love of my family who supported me throughout my entire study and encouraged my activities. They all kept me going and I give this honor to my mother in heaven.

Finally, I am thankful to all my friends: Mo Haque, Zach Hernandez, Nickos Karantzas, Kazem Safari, Duong Nguyen, Sarah Chehade, Prajakta Bedekar, and Krithika Rathinakumar. I would like to give special thanks to my academic sister and officemate, Kayla Bicol who have been always helping and encouraging me throughout the years.

Daewa Kim

A KINETIC THEORY APPROACH TO PEDESTRIAN MOTION AND ONSET OF DISEASE SPREADING

An Abstract of a Dissertation

Presented to

the Faculty of the Department of Mathematics

University of Houston

In Partial Fulfillment

of the Requirements for the Degree

Doctor of Philosophy

By

Daewa Kim

May 2019

Abstract

This dissertation shows a kinetic approach for pedestrian dynamics. First, we model the evacuation of a crowd from bounded domains. The interactions of a person with other pedestrians and the environment, which includes walls, exits, and obstacles, are modeled by using tools of game theory and are transferred to the crowd dynamics. The model allows to weight between two competing behaviors: the search for less congested areas and the tendency to follow the stream unconsciously in a panic situation. For the numerical approximation of the solution to our model, we apply an operator splitting scheme which breaks the problem into two pure advection problems and a problem involving the interactions. We compare our numerical results against the data reported in a recent empirical study on evacuation from a room with two exits. For medium and medium-to-large groups of people, we achieve good agreement between the computed average people density, flow rate, and the respective measured quantities. Through a series of numerical tests, we also show that our approach is capable of handling evacuation from a room with one or more exits with variable size, with and without obstacles, and can reproduce lane formation in bidirectional flow in a corridor.

Next, we consider a crowd model known as ASCRIBE that can also track the level of emotional contagion in evacuation scenarios. We propose a modification of this model to track disease contagion. Finally, we couple the disease contagion model with the one dimension kinetic approach for pedestrian dynamics to simulate the initial spreading of an infectious disease.

Contents

List of Figures

Chapter 1

Introduction

In recent years, the study of pedestrian dynamics has received much attention from the scientific community due to the large number of applications in engineering and social sciences. The interest in modeling pedestrian flow has strongly increased since reliable simulations of pedestrian flow may greatly aid mass transportation management, urban planning, and architecture. The challenging analytical and computational problems that arise from pedestrian flow models have also attracted the attention of many applied mathematicians.

Over the years, a very large variety of models have been developed, which can be divided into three different approaches related to three different scales [8]. One approach corresponds to the macroscopic description: evolution equations are derived for mass density and linear momentum, which are regarded as macroscopic observables of pedestrian flow, see, e.g., [31, 44]. Such an approach is suitable for high density, large-scale systems, which are not the focus of our work.

The second approach is related to the microscopic scale. There exists two categories of microscopic models: grid-based models and grid-free models. A grid-based model that has gained a lot of popularity is Cellular Automata [15, 16, 18, 23, 35]. These models describe pedestrian flow in space-time by assigning discrete states to a grid of space-cells. Cells can be occupied by a pedestrian or be empty. Thus, the movement of pedestrians in space is done by passing them from cell to cell (discrete space) in discrete time. Grid-free methods use Newtonian mechanics to interpret pedestrian movement as the physical interaction between the people and the environment, i.e. the action of other people and the environment on a given pedestrian is modeled with forces. These microscopic models, also called force-based models, are one of the most popular modeling paradigms of continuous models because they describe the movement of pedestrians qualitatively well, see, e.g., [21, 26, 29, 30, 36, 39, 49, 56] and references therein. Collective phenomena, like unidirectional or bidirectional flow in a corridor [38, 46, 53], lane formation [27, 29, 54], oscillations at bottlenecks [27, 29], the faster-is-slower effect [33, 40], emergency evacuation from buildings [27, 37, 54], are well reproduced. Other advantages of these methods are the ease of implementation, and in particular parallel implementation, and the fact that they permit higher resolution of geometry and time. Another type of frequently mentioned model is the agent-based model, see, e.g., [2, 3, 4, 20, 22] and references therein. Agent-based models allow for flexibility, extensibility, and capability to realize heterogeneity in crowd dynamics. Both force-based and agent-based models may introduce artifacts due to the force representation of human behavior, leading to unrealistic backward movement or oscillating trajectories. These artifacts can be reduced by incorporating extra rules and/or elaborate calibrations, at the price of increasing the computational cost.

The scale of observation for the third approach is between the previous two. Introduced in [5] and further developed in [1, 6, 7, 9, 10, 11, 12], this approach derives a Boltzmann-type evolution equation for the statistical distribution function of the position and velocity of the pedestrians, in a framework close to that of the kinetic theory of gases. See also [13] for a literature review on this approach. The model proposed in [5, 7, 12] is valid in unbounded domains and with a homogeneous distribution of walking ability for the pedestrians, while the extension to bounded domains is presented in [1] and further explored in [9, 10, 11]. In [9], more general features of behavioral-social dynamics are taken into account. In [10], Monte Carlo simulations are introduced to study pedestrians behavior in complex scenarios. The methodology in [10] is validated by comparing the computed fundamental density-velocity diagrams with empirically observed ones and by checking that well known emerging properties are reproduced. A kinetic theory approach for modeling pedestrian dynamics in presence of social phenomena, such as the propagation of stress conditions, is presented in [11]. Finally, we refer to [6] for a thorough description of how kinetic theory and evolutionary game theory can be used to understand the dynamics of living systems.

Most of the references cited so far have been shown to replicate various cases of pedestrian movement qualitatively through analysis and/or numerical simulations. Obviously, if a model cannot represent a certain phenomenon qualitatively, there is no hope for any quantitative agreement between model prediction and practical experiments. However before using a model for quantitative predictions, the model itself must be validated and the numerical method used to implement the model must be verified [24]. A verified method is capable of correctly solving the problem equations, while a valid model is able to correctly describe the features of the problem (i.e. it uses the right equations). Validation of pedestrian flow models is complicated by the lack of reliable experimental data. In addition, the few available datasets show large differences [43, 41, 55]. In order to make the models more reliable, evolutionary adjustment of the parameters and data assimilations have also been proposed in [32, 52], respectively.

This thesis deals with a kinetic theory approach to model pedestrian dynamics. We reproduce the models and simulations from [1] and compare the results given by our model with the empirical data in [50]. In our model, pedestrians are considered as active particles and their movement is influenced by the environment, i.e. walls and exits, and by other pedestrians.

Moreover, we introduce another model of pedestrian dynamics with emotional contagion [51]. This model can track the level of emotional contagion. Also, this model has been used to model evacuation scenarios [48] and compared to other models [47]. For more details, see [14]. In this dissertation, we propose the modification of this model in order to track disease contagion level and test some particular simulations.

The dissertation is organized as follows. Chapter 2 introduces the representation of the system and the modeling of pedestrian interactions. In Chapter 3, we propose the Lie splitting algorithm for the model described in Chapter 2. Chapter 4 presents the numerical results. We first focus on validating our implementation of the numerical approach described in Chapter 3 with an academic benchmark tests and empirical data. We analyze the role of the exit size, the influence of the level of panic, study the influence of the quality of the environment, and devise a strategy to handle obstacles within the domain evacuating the room with two exits in order to compare with experimental data in [50]. Finally, we see the bidirectional motion in a straight periodic corridor to compare the numerical results with the experimental data in [28]. In Chapter 5, we propose a model to track the contagion level of a disease called ASCRIBE which allows tracking the emotional contagion level in evacuation scenarios. We present a one dimensional kinetic approach to model pedestrian dynamics in Chapter 6. Last, in Chapter 7, we couple the model for the spreading of an infectious disease presented in Chapter 5 with the one dimensional model for pedestrian dynamics presented in Chapter 6.

Chapter 2

Mathematical Model

In this chapter, we describe a kinetic theory approach for pedestrian dynamics. Pedestrians are viewed as active particles, whose micro-states are defined by position and velocity direction, and the state of the overall system is given by a probability distribution function over the micro-state. The equations which model the time and space dynamics of this distribution function are obtained by a balance of "particles" in an elementary volume. The net flow into this volume is due to transport and interactions.

The numerical results obtained with this approach will be shown and compared against experimental data in Chapter 4. The approach we choose is suitable to model pedestrian dynamics in a domain with boundaries, which consists of walls and exits. Modeling the interactions of pedestrians with walls can be viewed as a statement of boundary conditions for kinetic equations. This is conceptually more complicated than imposing boundary conditions in the classical theory of particles, where it is possible to implement suitable reflection rules [19]. Individuals feel the presence of walls at a distance and modify their dynamics in order to avoid them. Another advantage of the model described in this chapter is that it takes into account the granular feature of pedestrian dynamics, which does not justify the assumption of continuity of the distribution function over the micro-variable. Thus, we expect this model to give more realistic pedestrian dynamics than classical kinetic theory approaches.

2.1 Representation of the system

Let $\Omega \subset \mathbb{R}^2$ be the bounded domain where pedestrians move. We assume that the boundary $\partial\Omega$ includes the exit zone E, while the remaining part of the boundary constitutes the wall W. It is worth mentioning that E could be the finite union of disjoint sets, i.e. the domain may have more than one exit. The quality of the domain where pedestrians move is given by parameter $\alpha \in [0, 1]$, where $\alpha = 0$ corresponds to the worst quality which forces pedestrians to slow down or stop, while the value $\alpha = 1$ corresponds to the best quality, which contributes to walk at the desired speed.

Let $\boldsymbol{x} = (x, y)$ denote position, which is supposed to be a continuous variable defined over Ω. Let $\boldsymbol{v} = (v_1, v_2) = v(\cos\theta, \sin\theta)$ denote a velocity field defined over $D_{\boldsymbol{v}}$, where $D_{\boldsymbol{v}} \subset \mathbb{R}^2$ is the velocity domain. We assume that angle θ, that identifies the velocity direction, can only take a finite number of values in the interval $[0, 2\pi)$, i.e. we consider only uniformly spaced angles θ_i in the set:

$$I_\theta = \left\{ \theta_i = \frac{i-1}{N_d} 2\pi : i = 1, \ldots, N_d \right\}.$$

The velocity magnitude v is modeled as a continuous deterministic variable which evolves in time and space according to macroscopic effects determined by the overall dynamics. The use of discrete variables for the individual velocity states v and θ is due to granular nature of pedestrian dynamics, as explained in the previous section. In fact, we do not want to assume to have such a large crowd to justify a continuous distribution function over direction angle θ. Instead, we want to be able to deal with a wide spectrum of crowd sizes.

For a system composed by a number of pedestrians distributed inside a bounded domain $\Omega \subset \mathbb{R}^2$, the distribution function is given by

$$f = f(t, \boldsymbol{x}, \boldsymbol{v}) \quad \text{for all } \ t \geq 0, \ \boldsymbol{x} \in \Omega, \ \boldsymbol{v} \in D_{\boldsymbol{v}}.$$

Under suitable integrability conditions, $f(t, \boldsymbol{x}, \boldsymbol{v}) d\boldsymbol{x} d\boldsymbol{v}$ represents the number of individuals who, at time t , are located in the infinitesimal rectangle $[x, x+dx] \times [y, y+dy]$ and have a velocity belonging to $[v_1, v_1 + dv_1] \times [v_2, v_2 + dv_2]$. Notice that when we use polar coordinates for the velocity, we can write the distribution function as $f = f(t, \boldsymbol{x}, v, \theta)$.

Concerning the velocity modulus v, we assume that pedestrians adjust their speed according to the level of congestion around them. So higher densities induce people to reduce their velocity modulus, while in less congested areas people can increase their speed. Due to the deterministic nature of the variable v, the kinetic type representation is given by the *reduced* distribution function

$$f(t, \boldsymbol{x}, \theta) = \sum_{i=1}^{N_d} f^i(t, \boldsymbol{x}) \delta(\theta - \theta_i), \tag{2.1}$$

where $f^i(t, \boldsymbol{x}) = f(t, \boldsymbol{x}, \theta_i)$ represents the active particles that, at time t and position $\boldsymbol{x}$, move with direction θ_i. In (2.1), δ denotes the Dirac delta function.

We will make use of dimensionless quantities. For this purpose, we introduce the following reference quantities:

- D: the diameter of the domain Ω.
- v_M: the highest velocity modulus that a pedestrian can reach in low density and optimal environmental conditions.
- T: reference time given by D/v_M.
- ρ_M: the maximal admissible number of pedestrians per unit area.

We can now define the following dimensionless variables: position $\hat{\boldsymbol{x}} = \boldsymbol{x}/D$, time $\hat{t} = t/T$, velocity modulus $\hat{v} = v/v_M$ and distribution function $\hat{f} = f/\rho_M$. From now on, all the variables will be dimensionless and hats will be omitted to simplify notation.

Due to the normalization of f and each f^i, the dimensionless local density is obtained by summing the distribution functions over the set of directions:

$$\rho(t, \boldsymbol{x}) = \sum_{i=1}^{N_d} f^i(t, \boldsymbol{x}). \tag{2.2}$$

As mentioned earlier, we assume that pedestrians adjust their speed depending on the the level of congestion around them. This means that their speed depends formally on the local density, i.e. $v = v[\rho](t, \boldsymbol{x})$. The square brackets are used to denote that v depends on ρ in a functional way. For instance, v can depend on ρ and on its gradient.

We assume that the maximum dimensionless speed v_M a pedestrian can reach depends linearly on the quality of the environment. In particular, we take $v_M = \alpha$. Velocity magnitude v is set equal to the maximal speed v_m under low density conditions (free flow regime), i.e. for $\rho \in [0, \rho_c)$ where $\rho_c = \rho_c(\alpha)$ is a critical density that can be experimentally measured, see [42]. We take $\rho_c = \alpha/5$. For values of ρ greater than ρ_c, the velocity modulus decreases to zero (slowdown zone). In the slowdown zone, pedestrians have a velocity modulus which is here heuristically modeled by third-order polynomial. We have

$$v = v(\rho) = \begin{cases} \alpha & \text{for} \quad \rho \leq \rho_c(\alpha) = \alpha/5 \\ a_3\rho^3 + a_2\rho^2 + a_1\rho + a_0 & \text{for} \quad \rho > \rho_c(\alpha) = \alpha/5, \end{cases} \tag{2.3}$$

where a_i, with $i = 0, 1, 2, 3$, is constant. To find these constants, we impose the following conditions: $v(\rho_c) = v_m$, $\partial_\rho v(\rho_c) = 0$, $v(1) = 0$ and $\partial_\rho v(1) = 0$. This leads to:

$$\begin{cases} a_0 & = (1/(\alpha^3 - 15\alpha^2 + 75\alpha - 125))(75\alpha^2 - 125\alpha) \\ a_1 & = (1/(\alpha^3 - 15\alpha^2 + 75\alpha - 125))(-150\alpha^2) \\ a_2 & = (1/(\alpha^3 - 15\alpha^2 + 75\alpha - 125))(75\alpha^2 + 375\alpha) \\ a_3 & = (1/(\alpha^3 - 15\alpha^2 + 75\alpha - 125))(-250\alpha). \end{cases} \tag{2.4}$$

See Figure 2.1. This shows the dependence of the dimensionless velocity modulus v on the dimensionless density ρ for three different values of the parameter α, i.e. the quality of the environment. In the free flow zone, pedestrians move with the maximal velocity modulus $v_m = \alpha$. In the slowdown zone, pedestrians have a velocity modulus by the third-order polynomial from the point $(\rho_c(\alpha), v_m(\alpha))$ to the point $(1, 0)$.

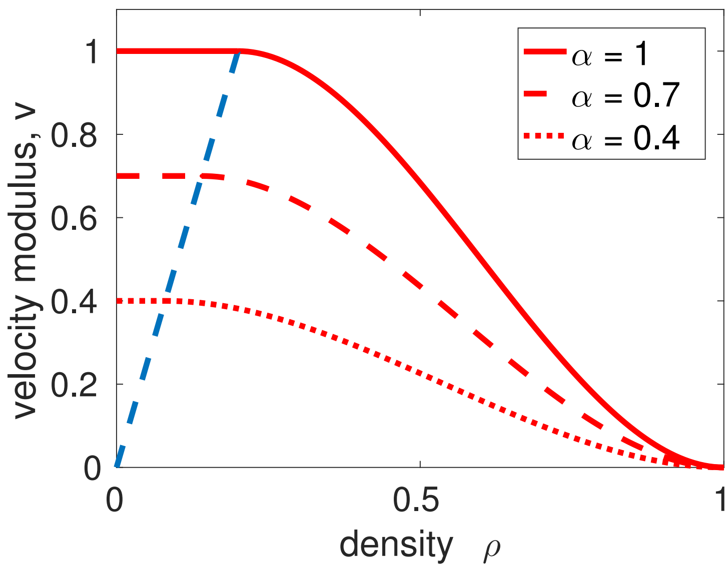

Figure 2.1: Dependence of the dimensionless velocity modulus v on the dimensionless density ρ for different values of the parameter α representing the quality of the environment.

2.2 Modeling interactions

This section is devoted to the modeling of pedestrian-pedestrian and pedestrian-environment interactions. To model interaction dynamics, we assume that pedestrians modify their walking direction by taking into account various inputs: the desire to reach the exit (or another target destination) and avoid the wall, the search for less congested directions, and the unconscious attraction to the stream of people. It is worth noting that this last input models an irrational behavior which is always present but might be stronger in panic situations. The remaining inputs describe the behavior of a rational crowd. Interactions are nonlinearly additive, meaning that they produce a global effect which is not given by the sum of all the individual interactions.

We refer to an i-particle to mean a pedestrian moving with direction θ_i. Interactions involve three types of particles:

- *test particles* with state $(\boldsymbol{x}, \theta_i)$: they are representative of the whole system;
- *candidate particles* with state $(\boldsymbol{x}, \theta_h)$: they can reach in probability the state of the test particles after individual-based interactions with the environment or with field particles;
- *field particles* with state $(\boldsymbol{x}, \theta_k)$: their presence triggers the interactions of the candidate particles.

As mentioned above, the process through which a pedestrian decides the direction to take is the results of several factors. Our model that takes into account four factors:

(F1) *The goal to reach the exit.*

Given a candidate particle at the point $\boldsymbol{x}$, we define its distance to the exit as

$$d_E(\boldsymbol{x}) = \min_{\boldsymbol{x}_E \in E} ||\boldsymbol{x} - \boldsymbol{x}_E||,$$

and we consider the unit vector $\boldsymbol{u}_E(\boldsymbol{x})$, pointing from $\boldsymbol{x}$ to the exit. See Figure 2.2.

(F2) *The desire to avoid the collision with walls.*

Given a candidate particle at the point $\boldsymbol{x}$, we define the distance $d_W(\boldsymbol{x}, \theta_h)$ from the particle to a wall at a point $\boldsymbol{x}_W(\boldsymbol{x}, \theta_h)$. We select the unit tangent vector $\boldsymbol{u}_W(\boldsymbol{x}, \theta_h)$ to the boundary $\partial\Omega$ at $\boldsymbol{x}_W$ that points to the direction a pedestrian would take to get closer to the exit. See Figure 2.2.

(F3) *The tendency to look for less congested area.*

A candidate particle $(\boldsymbol{x}, \theta_h)$ may decide to change direction in order to avoid congested areas. This is achieved by considering the direction that gives the minimal directional derivative of the density at the point $\boldsymbol{x}$. This direction is denoted by the unit vector $\boldsymbol{u}_C(\theta_h, \rho)$.

(F4) *The tendency to follow the stream.*

A candidate particle modifies its state, in probability, into that of the test particle due to interactions with field particles, while the test particle loses its state as a result of these interactions. A candidate pedestrian h interacting with a field pedestrian k may decide to follow him/her and thus adopt his/her direction. We define the unit vector $\boldsymbol{u}_F = (\cos\theta_k, \sin\theta_k)$.

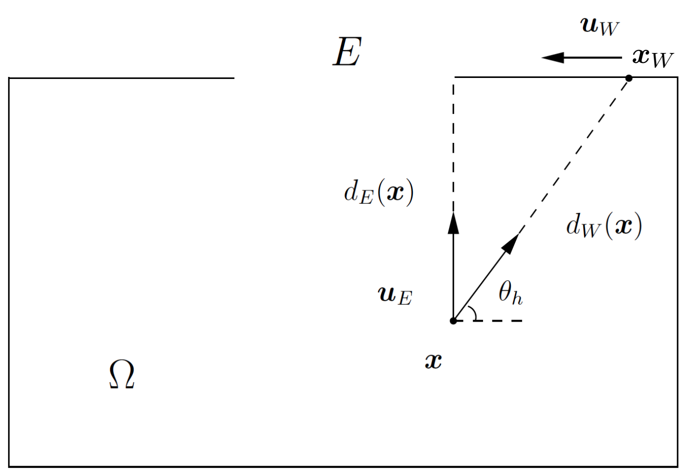

Figure 2.2: A particle located at point $\boldsymbol{x}$.

See Figure 2.2. A particle located at point $\boldsymbol{x}$ tries to reach the exit E walking through the shortest path, which is the distance $d_E(\boldsymbol{x})$ from a particle to the exit by the unit vector $\boldsymbol{u}_E(\boldsymbol{x})$ pointing from $\boldsymbol{x}$ to the exit. Also, a particle moving with direction θ_h is expected to collide the wall, then it computes not only the distance from $\boldsymbol{x}$ to the wall but also the unit tangent vector $\boldsymbol{u}_w(\boldsymbol{x})$ toward the exit.

Factors (F1) and (F2) are related to geometric aspects of the domain, while factors

(F3) and (F4) consider that people's behavior is strongly affected by surrounding crowd.

The effects related to assumptions (F3)-(F4) compete with each other. We introduce a parameter $\varepsilon \in [0,1]$, that varies according to the particular situation to be modeled: the value $\varepsilon = 0$ corresponds to the situation in which only the research of less congested areas is considered, while $\varepsilon = 1$ corresponds to the situation in which only the tendency to follow the stream is taken into account. The case $\varepsilon = 1$ represents a panic situation.

2.2.1 Interaction with the bounding walls

The interaction with the environment is modeled with two terms:

- $\mu[\rho]$: the *interaction rate* models the frequency of interactions between candidate particles and the boundary of the domain. If the local density is getting lower, it is easier for pedestrians to see the walls and doors. Following this idea, we set $\mu[\rho] = 1 - \rho$.
- $\mathcal{A}_h(i)$: the *transition probability* gives the probability that a candidate particle h, i.e. with direction θ_h adjusts its direction into that of the test particle θ_i due to the presence of the walls and/or and exit. The following constraint for $\mathcal{A}_h(i)$ has to be satisfied:

$$\sum_{i=1}^{N_d} \mathcal{A}_h(i) = 1 \quad \text{for all } h \in \{1, \dots, N_d\}.$$

We assume that particles change direction, in probability, only to an adjacent clockwise or counterclockwise direction in the discrete set I_θ. This means a candidate particle h may end up into the states $h-1, h+1$ or remain in the state h. In the case $h = 1$, we set $\theta_{h-1} = \theta_{N_d}$ and, in the case $h = N_d$, we set $\theta_{h+1} = \theta_1$. The set of all transition probabilities $\mathcal{A} = \{\mathcal{A}_h(i)\}_{h,i=1,\ldots,N_d}$ forms the so-called *table of games* that models the game played by active particles interaction with the geometry of the environment.

To take into account factors (F1) and (F2), we define the vector

$$\boldsymbol{u}_G(\boldsymbol{x}, \theta_h) = \frac{(1 - d_E(\boldsymbol{x}))\boldsymbol{u}_E(\boldsymbol{x}) + (1 - d_W(\boldsymbol{x}, \theta_h))\boldsymbol{u}_W(\boldsymbol{x}, \theta_h)}{||(1 - d_E(\boldsymbol{x}))\boldsymbol{u}_E(\boldsymbol{x}) + (1 - d_W(\boldsymbol{x}, \theta_h))\boldsymbol{u}_W(\boldsymbol{x}, \theta_h)||} = (\cos\theta_G, \sin\theta_G). \quad (2.5)$$

Here θ_G is the *geometrical preferred direction*, which is the ideal direction that a pedestrian should take in order to reach the exit and avoid the walls in an optimal way.

A candidate particle h will update its direction by choosing the angle closest to θ_G among the three allowed angles θ_{h-1}, θ_h and θ_{h+1}. The transition probability is given by:

$$\mathcal{A}_h(i) = \beta_h(\alpha)\delta_{s,i} + (1 - \beta_h(\alpha))\delta_{h,i}, \quad i = h-1, h, h+1, \quad (2.6)$$

where

$$s = \underset{j\in\{h-1,h+1\}}{\arg\min} \{d(\theta_G, \theta_j)\},$$

with

$$d(\theta_p, \theta_q) = \begin{cases} |\theta_p - \theta_q| & \text{if } |\theta_p - \theta_q| \leq \pi, \\ 2\pi - |\theta_p - \theta_q| & \text{if } |\theta_p - \theta_q| > \pi. \end{cases} \quad (2.7)$$

In (2.6), δ denotes the Kronecker delta function. Coefficient β_h, proportional to parameter α, is defined by:

$$\beta_h(\alpha) = \begin{cases} \alpha & \text{if } d(\theta_h, \theta_G) \geq \Delta\theta, \\ \alpha\dfrac{d(\theta_h, \theta_G)}{\Delta\theta} & \text{if } d(\theta_h, \theta_G) < \Delta\theta, \end{cases}$$

where $\Delta\theta = 2\pi/N_d$. The role of β_h is to allow for a transition to θ_{h-1} or θ_{h+1} even in the case that the geometrical preferred direction θ_G is closer to θ_h. Such a transition is more likely to occur the more distant θ_h and θ_G are. Notice that if $\theta_G = \theta_h$, then $\beta_h = 0$ and $\mathcal{A}_h(h) = 1$, meaning that a pedestrian keeps the same direction (in the absence of interactions other than with the environment) with probability 1.

2.2.2 Interaction with obstacles

The strategy reported in the previous section to avoid collisions with the walls works well when the pedestrian is sufficiently far from the walls. If pedestrians get too close to the bounding walls, and in particular if they are close to an exit, the definition of $\boldsymbol{u}_G$ in (2.5) does not prevent collisions with the walls. Thus, obstacles within the domain Ω cannot be avoided just by adjusting $\boldsymbol{u}_W$. In this section, we report an effective strategy to handle obstacles.

Three ingredients are needed to exclude the real obstacle area from the walkable domain:

1. An effective area: an enlarged area that encloses the real obstacle.
2. A definition of $\boldsymbol{u}_W$ to account for the effective area.
3. A setting of the parameter α in the effective area depending on the shape of the obstacle.

The effective area is necessary especially if the obstacle is close to an exit: it allows to define $\boldsymbol{u}_W$ with respect to a larger area than the one occupied by the obstacle to achieve the goal of having no pedestrian walking on the real obstacle area. In the numerical results reported in Section 4.4, we used an effective area that is four times bigger than the real obstacle area.

Since some pedestrians will walk on part of the effective area, one needs to set parameter α. By setting $\alpha = 1$ (i.e. best quality of the environment) in the effective area, pedestrians can move with the maximal velocity modulus as they approach the obstacle and thus they quickly adapt to the effective area through $\boldsymbol{u}_W$. However, some pedestrians will walk close to the top, bottom, and rear (with respect to the pedestrian motion) boundary of the effective area. Thus, the real obstacle is located at the front of the effective area. From the numerical results reported in Section 4.4, we also see that the shape of the obstacle is square. By setting $\alpha = 0$ (i.e. worst quality of the environment) in the effective area, pedestrians are forced to slow down at the front part of the effective area. The slow down leads to higher densities in the front part of the effective area, therefore direction $\boldsymbol{u}_W$ competes with direction $\boldsymbol{u}_C$. As a result some pedestrians walk on the front part of the effective area. However, as the congestion decreases pedestrians avoid the rear part of the effective area. From the numerical results shown in Section 4.4, we see that the shape of the obstacle for $\alpha = 0$ in the effective area is slender.

2.2.3 Interactions between pedestrians

The interaction with other pedestrians is also modeled with two terms:

- $\eta[\rho]$: the *interaction rate* defines the number of binary encounters per unit time. If a local density increases, then the interaction rate also increases. We take $\eta[\rho] = \rho$. Unlike the case of classical particles, this rate is not related to the relative velocity, but to the sensitivity of particles to surrounding pedestrians.

- $\mathcal{B}_{hk}(i)[\rho]$: the *transition probability* gives the probability that a candidate particle h modifies its direction θ_h into that of the test particle i, i.e. θ_i, due to the research of less congested areas and the interaction with a field particle k that moves with direction θ_k. The following constrain for $\mathcal{B}_{hk}(i)$ has to be satisfied:

$$\sum_{i=1}^{N_d} \mathcal{B}_{hk}(i)[\rho] = 1 \quad \text{for all } h, k \in \{1, \dots, N_d\},$$

where again the square brackets denote the dependence on the density ρ.

Concerning the search for less congested areas, the game consists in choosing the less congested direction among the three admissible ones. This direction can be computed for a candidate pedestrian h situated at $\boldsymbol{x}$, by taking

$$C = \underset{j \in \{h-1, h, h+1\}}{\arg\min} \{\partial_j \rho(t, \boldsymbol{x})\},$$

where $\partial_j \rho$ denotes the directional derivative of ρ in the direction given by angle θ_j. We have $\boldsymbol{u}_C(\theta_h, \rho) = (\cos\theta_C, \sin\theta_C)$. Also, we recall the unit vector $\boldsymbol{u}_F = (\cos\theta_k, \sin\theta_k)$ following the direction of a field particle.

To take into account (F3) and (F4), we define the vector

$$\boldsymbol{u}_P(\theta_h, \theta_k, \rho) = \frac{\varepsilon \boldsymbol{u}_F + (1-\varepsilon)\boldsymbol{u}_C(\theta_h, \rho)}{||\varepsilon \boldsymbol{u}_F + (1-\varepsilon)\boldsymbol{u}_C(\theta_h, \rho)||} = (\cos\theta_P, \sin\theta_P),$$

where the subscript P stands for *pedestrians*. Direction θ_P is the *interaction-based perferred direction*, obtained as a weighted combination between the trendency to follow the stream and the tendency to avoid crowded zones.

The transition probability is given by:

$$\mathcal{B}_{hk}(i)[\rho] = \beta_{hk}(\alpha)\rho\delta_{r,i} + (1 - \beta_{hk}(\alpha)\rho)\delta_{h,i}, \quad i = h-1, h, h+1,$$

where r and β_{hk} are defined by:

$$r = \underset{j \in \{h-1, h+1\}}{\arg\min} \{d(\theta_P, \theta_j)\},$$

$$\beta_{hk}(\alpha) = \begin{cases} \alpha & \text{if } d(\theta_h, \theta_P) \geq \Delta\theta \\ \alpha \dfrac{d(\theta_h, \theta_P)}{\Delta\theta} & \text{if } d(\theta_h, \theta_P) < \Delta\theta. \end{cases}$$

We recall that $d(\cdot, \cdot)$ is defined in (2.7).

2.3 Equation of balance

The derivation of the mathematical model can be obtained by a suitable balance of particles in an elementary volume of the space of microscopic states, considering the net flow into such volume due to transport and interactions [1].

Taking into account factors (F1)-(F4), we obtain:

$$\begin{aligned} &\frac{\partial f^i}{\partial t} + \nabla \cdot \Big(\boldsymbol{v}^i[\rho](t, \boldsymbol{x}) f^i(t, \boldsymbol{x}) \Big) \\ &\quad = \mathcal{J}^i[f](t, \boldsymbol{x}) \\ &\quad = \mathcal{J}^i_G[f](t, \boldsymbol{x}) + \mathcal{J}^i_P[f](t, \boldsymbol{x}) \\ &\quad = \mu[\rho] \left(\sum_{h=1}^{n} \mathcal{A}_h(i) f^h(t, \boldsymbol{x}) - f^i(t, \boldsymbol{x}) \right) \\ &\qquad + \eta[\rho] \left(\sum_{h,k=1}^{n} \mathcal{B}_{hk}(i)[\rho] f^h(t, \boldsymbol{x}) f^k(t, \boldsymbol{x}) - f^i(t, \boldsymbol{x}) \rho(t, \boldsymbol{x}) \right) \end{aligned} \tag{2.8}$$

for $i = 1, 2, \ldots, N_d$. Functional $\mathcal{J}^i[f]$ represents the net balance of particles that move with direction θ_i due to interactions. As seen in the previous subsection, we consider both the interaction with the environment and with the surrounding people.

Thus, we can write $\mathcal{J}^i$ as $\mathcal{J}^i = \mathcal{J}^i_G + \mathcal{J}^i_P$, where $\mathcal{J}^i_G$ is an interaction between candidate particles and the environment and $\mathcal{J}^i_P$ is an interaction between candidate and field particles.

Equation (2.8) is completed with Equation (2.2) for the density and Equation (2.3), (2.4) for the velocity. In the next chapter, we will discuss a numerical method for the solution of problem (2.2), (2.3), (2.4), and (2.8).

Chapter 3

Numerical Method

In this chapter, we propose a numerical method for the initial value problem in a bounded domain discussed in Chapter 2. The approach we consider is based on a splitting method, where the equation is split into the transport part and the interaction term. The idea is to split the problem into a set of subproblems that are easier to solve and for which practical algorithms are available. The numerical method is then completed by picking an appropriate numerical scheme for each subproblem. Among the available operator-splitting methods, we chose the Lie's splitting scheme because it provides a good compromise between accuracy and robustness as shown in [25].

3.1 The Lie operator-splitting scheme

Although the Lie splitting scheme is well-known, it may be useful to briefly present this scheme before applying it to the solution of problem (2.2), (2.3), (2.4), and (2.8).

Let us consider a first-order system in time:

$$\begin{aligned} \frac{\partial \phi}{\partial t} + A(\phi) &= 0, \quad \text{in } (0,T), \\ \phi(0) &= \phi_0, \end{aligned}$$

where A is an operator from a Hilbert space into itself. Operator A is then split, in a non-trivial decomposition, as

$$A = \sum_{i=1}^{I} A_i.$$

The Lie scheme consists of the following. Let $\Delta t > 0$ be a time discretization step for the time interval $[0,T]$. Denote $t^k = k\Delta t$, with $k = 0, \ldots, N_t$ and let ϕ^k be an approximation of $\phi(t^k)$. Set $\phi^0 = \phi_0$. Then, for $n \geq 0$ compute ϕ^{k+1} by solving

$$\frac{\partial \phi_i}{\partial t} + A_i(\phi_i) = 0 \quad \text{in } (t^k, t^{k+1}), \tag{3.1}$$

$$\phi_i(t^k) = \phi^{k+(i-1)/I}, \tag{3.2}$$

and then set $\phi^{k+i/I} = \phi_i(t^{k+1})$, for $i = 1, \ldots . I$.

This method is first-order accurate in time. More precisely, if (3.1) is defined on a finite-dimensional space, and if the operators A_i are smooth enough, then $\|\phi(t^k) - \phi^k\| = O(\Delta t)$ [25]. In our case, operator A that is associated with problem (2.8) will be split into a sum of three operators:

1. A pure advection problem in the x direction.
2. A pure advection problem in the y direction.
3. A problem involving the interaction with the environment and other pedestrians.

3.2 Lie scheme applied to problem (2.8)

Let us apply the Lie operator-splitting scheme described in the previous section to problem (2.8). Given an initial condition $f^{i,0} = f^i(0, \boldsymbol{x})$, for $i = 1, \ldots, N_d$, the algorithm reads: For $k = 0, 1, 2, \ldots, N_t - 2$, perform the following steps:

1. Find f^i, for $i = 1, \ldots, N_d$, such that

$$\begin{cases} \dfrac{\partial f^i}{\partial t} + \dfrac{\partial}{\partial x}\big((v[\rho]\cos\theta_i) f^i(t, \boldsymbol{x})\big) = 0, \ \text{ on } (t^k, t^{k+1}) \\ f^i(t^k, \boldsymbol{x}) = f^{i,k} \end{cases} \tag{3.3}$$

   Set $f^{i,k+\frac{1}{3}} = f^i(t^{k+1}, \boldsymbol{x})$.

2. Find f^i, for $i = 1, \ldots, N_d$, such that

$$\begin{cases} \dfrac{\partial f^i}{\partial t} + \dfrac{\partial}{\partial y}\big((v[\rho]\sin\theta_i) f^i(t, \boldsymbol{x})\big) = 0, \ \text{ on } (t^k, t^{k+1}) \\ f^i(t^k, \boldsymbol{x}) = f^{i,k+\frac{1}{3}} \end{cases} \tag{3.4}$$

   Set $f^{i,k+\frac{2}{3}} = f^i(t^{k+1}, \boldsymbol{x})$.

3. Find f_i, for $i = 1, \ldots, N_d$, such that

$$\begin{cases} \dfrac{\partial f^i}{\partial t} = \mathcal{J}^i[f](t, \boldsymbol{x}) \ \text{ on } (t^k, t^{k+1}) \\ , f^i(t^k, \boldsymbol{x}) = f^{i,k+\frac{2}{3}} \end{cases} \tag{3.5}$$

   Set $f^{i,k+1} = f^i(t^{k+1}, \boldsymbol{x})$.

Notice that with $f^{i,k+1}$, for $i = 1, \ldots, N_d$, we use an equation (2.2) to get the density ρ^{k+1} and equations (2.3),(2.4) to get the velocity magnitude at time t^{k+1}.

3.3 Space and time discretization

Let us assume for simplicity that the computational domain under consideration is a rectangle $[0, L] \times [0, H]$, for given L and H. We discretize the computational domain by choosing Δx and Δy to partition interval $[0, L]$ and $[0, H]$, respectively. Let $N_x = L/\Delta x$ and $N_y = H/\Delta y$. Then, we define the discrete mesh points $\boldsymbol{x}_{pq} = (x_p,\, y_q)$ by

$$
\begin{aligned}
x_p &= p\Delta x, \quad p = 0, 1, \ldots, N_x,\\
y_q &= q\Delta y, \quad q = 0, 1, \ldots, N_y.
\end{aligned}
$$

It will also be useful to define

$$
\begin{aligned}
x_{p+1/2} &= x_p + \Delta x/2 = \Big(p + \frac{1}{2}\Big)\Delta x,\\
y_{q+1/2} &= y_q + \Delta y/2 = \Big(q + \frac{1}{2}\Big)\Delta y.
\end{aligned}
$$

In order to simplify notation, let us set $\phi = f^i$, $\theta = \theta_i$, $t_0 = t^k$, $t_f = t^{k+1}$. Let M be a positive integer (≥ 3, in practice). We associate with M a time discretization step $\tau = (t_f - t_0)/M$ and set $t^m = t_0 + m\tau$.

Step 1

Let $\phi_0 = f^{i,k}$. Problem (3.3) can be rewritten as

$$
\begin{cases}
\dfrac{\partial \phi}{\partial t} + \dfrac{\partial}{\partial x}\big((v[\rho]\cos\theta)\phi(t, \boldsymbol{x})\big) = 0 \ \text{ on } (t_0, t_f),\\
\phi(t_0, \boldsymbol{x}) = \phi_0.
\end{cases}
\tag{3.6}
$$

The finite difference method we use produces an approximation $\Phi_{p,q}^m \in \mathbb{R}$ of the cell average

$$
\Phi_{p,q}^m \approx \frac{1}{\Delta x\, \Delta y} \int_{y_{q-1/2}}^{y_{q+1/2}} \int_{x_{p-1/2}}^{x_{p+1/2}} \phi(t^m, x, y) dx\, dy,
$$

where $m = 1, \ldots, M$, $1 \leq p \leq N_x - 1$ and $1 \leq q \leq N_y - 1$. Given an initial condition ϕ_0, function ϕ^m will be approximated by Φ^m with

$$\Phi^m \Big|_{[x_{p-1/2},\, x_{p+1/2}] \times [y_{q-1/2},\, y_{q+1/2}]} = \Phi^m_{p,q}$$

The Lax-Friedrichs method for problem (6.6) can be written in conservative form as follows:

$$\Phi^{m+1}_{p,q} = \Phi^m_{p,q} - \frac{\tau}{\Delta x}\Big(\mathcal{F}(\Phi^m_{p,q}, \Phi^m_{p+1,q}) - \mathcal{F}(\Phi^m_{p-1,q}, \Phi^m_{p,q})\Big)$$

where

$$\mathcal{F}(\Phi^m_{p,q}, \Phi^m_{p+1,q}) = \frac{\Delta x}{2\tau}(\Phi^m_{p,q} - \Phi^m_{p+1,q}) + \frac{1}{2}\Big((v[\rho^m_{p,q}]\cos\theta)\Phi^m_{p,q} + (v[\rho^m_{p+1,q}]\cos\theta)\Phi^m_{p+1,q}\Big).$$

Step 2

Let $\phi_0 = f^{i,k+\frac{1}{3}}$. Problem (3.4) can be rewritten as

$$\begin{cases} \dfrac{\partial \phi}{\partial t} + \dfrac{\partial}{\partial y}\big((v[\rho]\sin\theta)\phi(t, \boldsymbol{x})\big) = 0 \ \text{ on } (t_0, t_f), \\ \phi(t_0, \boldsymbol{x}) = \phi_0 \end{cases}$$

Similarly to step 1, we use the conservative Lax-Friedrichs scheme:

$$\Phi^{m+1}_{p,q} = \Phi^m_{p,q} - \frac{\tau}{\Delta y}\Big(\mathcal{F}(\Phi^m_{p,q}, \Phi^m_{p,q+1}) - \mathcal{F}(\Phi^m_{p,q-1}\Phi^m_{p,q})\Big)$$

where

$$\mathcal{F}(\Phi^m_{p,q}, \Phi^m_{p,q+1}) = \frac{\Delta y}{2\tau}(\Phi^m_{p,q} - \Phi^m_{p,q+1}) + \frac{1}{2}\Big((v[\rho^m_{p,q}]\sin\theta)\Phi^m_{p,q} + (v[\rho^m_{p,q+1}]\sin\theta)\Phi^m_{p,q+1}\Big).$$

Step 3

Let $\mathcal{J} = \mathcal{J}^i$ and $\phi_0 = f^{i,k+\frac{2}{3}}$. Problem (3.5) can be rewritten as

$$\begin{cases} \dfrac{\partial \phi}{\partial t} = \mathcal{J}[f](t, \boldsymbol{x}) \ \text{ on } (t_0, t_f), \\ \phi(t_0, \boldsymbol{x}) = \phi_0. \end{cases}$$

For the approximation of the above problem, we use the Forward Euler scheme:

$$\Phi_{p,q}^{m+1} = \Phi_{p,q}^{m} + \tau\Big(\mathcal{J}^m[F^m]\Big),$$

where F^m is the approximation of function (2.1) at time t^m.

Chapter 4

Numerical Results

In this chapter, we focus on the simulation of the evacuation from a room. The room has one or more exits and might have obstacles in it.

First, we consider a square domain with one exit door located on the right side. The goals of this first test are: to analyze the role of space discretizations and time discretizations, the role of the exit size, and the influence of the parameter ε. Next, we study the influence of α, which measures the quality of the environment, and devise a strategy to handle obstacles within the domain. Such obstacles will have different shapes and positions. As part of our validation effort, we consider a room with two exits and a different number of pedestrians evacuating the room in order to compare with experimental data. Finally, we show that our model successfully reproduces lane formation in a periodic corridor.

All the simulations in this chapter are performed with interaction rate $\mu = 1 - \rho$

and $\eta = \rho$. We consider eight different velocity directions $N_d = 8$ in the discrete set:

$$I_\theta = \left\{ \theta_i = \frac{i-1}{8} 2\pi : i = 1, \ldots, 8 \right\}.$$

The velocity modulus is assumed to depend on the density, as described (2.3) in Section 2.1.

4.1 Space and time discretizations

The first test we consider is taken from [1]. The computational domain encloses a square room with each as side 10 m, which features an exit door located on the middle of the right side. The exit size is 2.6 m. The computational domain is slightly larger than the room itself in order to simulate evacuation, i.e. pedestrians do not disappear from the computational domain when they leave the room. A group of 46 pedestrians is initially distributed into two equal-area circular clusters . The two groups are moving against the each other with opposite initial directions θ_3 and θ_7. Following [1], simulations are performed with $\varepsilon = 0.4$.

We are going to consider dimensionless quantities as described in Section 2.1. The dimensionless quantities are obtained by using the following reference quantities:

- $D = 10\sqrt{2}$ m;
- $v_M = 2$ m/s;
- $T = D/v_M = 5\sqrt{2}$ s;
- $\rho_M = 7$ people/m^2.

For the space discretization, we use three different meshes: a coarse mesh with $\Delta x = \Delta y = 0.5$ m, a medium mesh with $\Delta x = \Delta y = 0.25$ m, and a fine mesh with

$\Delta x = \Delta y = 0.125$ m. Similarly, for the time discretization we consider three different time steps: a large time step $\Delta t_{large} = 1.5$ s, a medium time step $\Delta t_{medium} = 0.75$ s, and a small time step $\Delta t_{small} = 0.375$ s. The value of M for the Lie splitting scheme is set to 3. In order to avoid stability issues, we consider six combinations of the above meshes and time steps:

1. coarse mesh and Δt_{large}; see Figure 4.1 for the density at times $t = 0$, 1.50, 3.00, 6.00, 10.50, and 13.50 s.
2. coarse mesh and Δt_{medium}; see Figure 4.2 for the density at times $t = 0$, 1.50, 3.00, 6.00, 10.50, and 13.50 s.
3. coarse mesh and Δt_{small}; see Figure 4.3 for the density at times $t = 0$, 1.50, 3.00, 6.00, 10.50, and 13.50 s.
4. medium mesh and Δt_{medium}; see Figure 4.4 for the density at times $t = 0$, 1.50, 3.00, 6.00, 10.50, 13.50 s.
5. medium mesh and Δt_{small}; see Figure 4.5 for the density at times $t = 0$, 1.50, 3.00, 6.00, 10.50, and 13.50 s.
6. fine mesh and Δt_{small}; see Figure 4.6 for the density at times $t = 0$, 1.50, 3.00, 6.00, 10.50, and 13.50 s.

For a more immediate comparison of the results on different meshes and with different time steps, Figure 4.7(a) shows how many pedestrians are left in the square room for the six combinations mentioned above. In all the cases the total evacuation time is around 18 s, which is in great agreement with the results reported in [1]. From Figure 4.7(a), one can observe that as the time step gets smaller with a given mesh, people evacuate the room faster. Vice versa, as the mesh gets finer with a

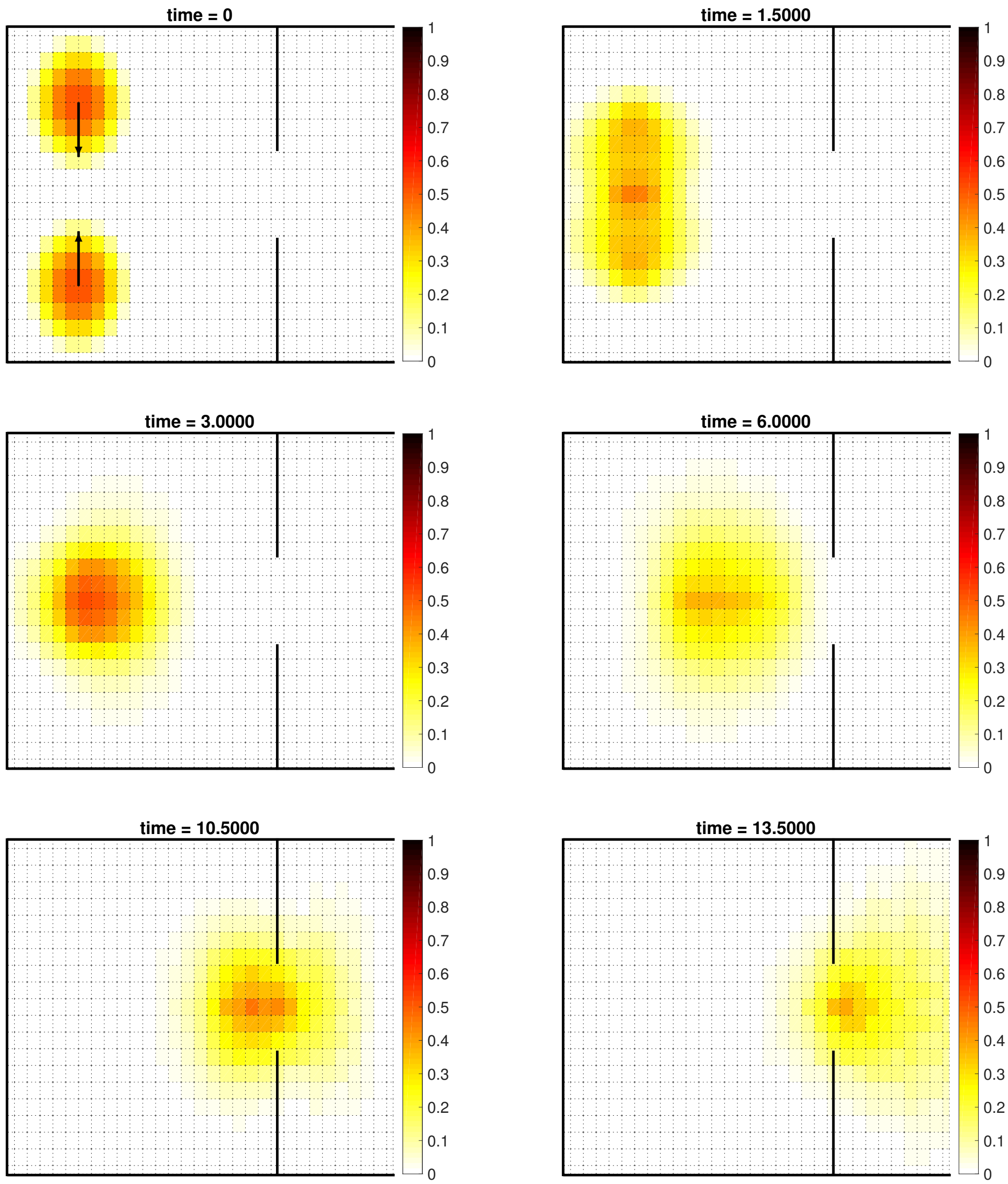

Figure 4.1: Evacuation process from a 10 m × 10 m room with a 2.6 m wide exit for $t = 0, 1.50, 3.00, 6.00, 10.50,$ and 13.50 s: 46 pedestrians initially grouped into two clusters, coarse mesh, and time step Δt_{large}. The color refers to density.

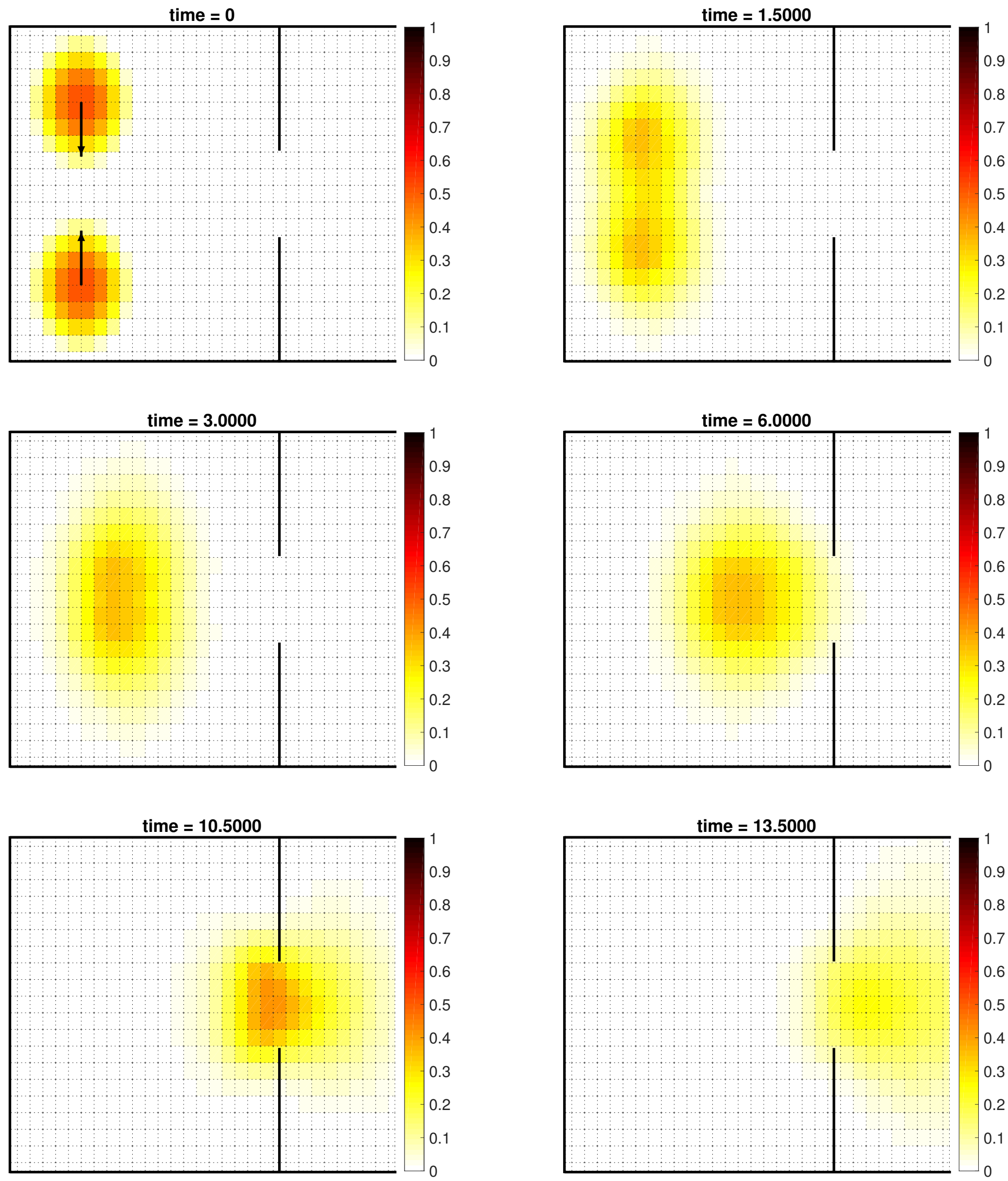

Figure 4.2: Evacuation process from a 10 m $\times$ 10 m room with a 2.6 m wide exit for $t = 0, 1.50, 3.00, 6.00, 10.50$, and 13.50 s: 46 pedestrians initially grouped into two clusters, coarse mesh, and time step Δt_{medium}. The color refers to density.

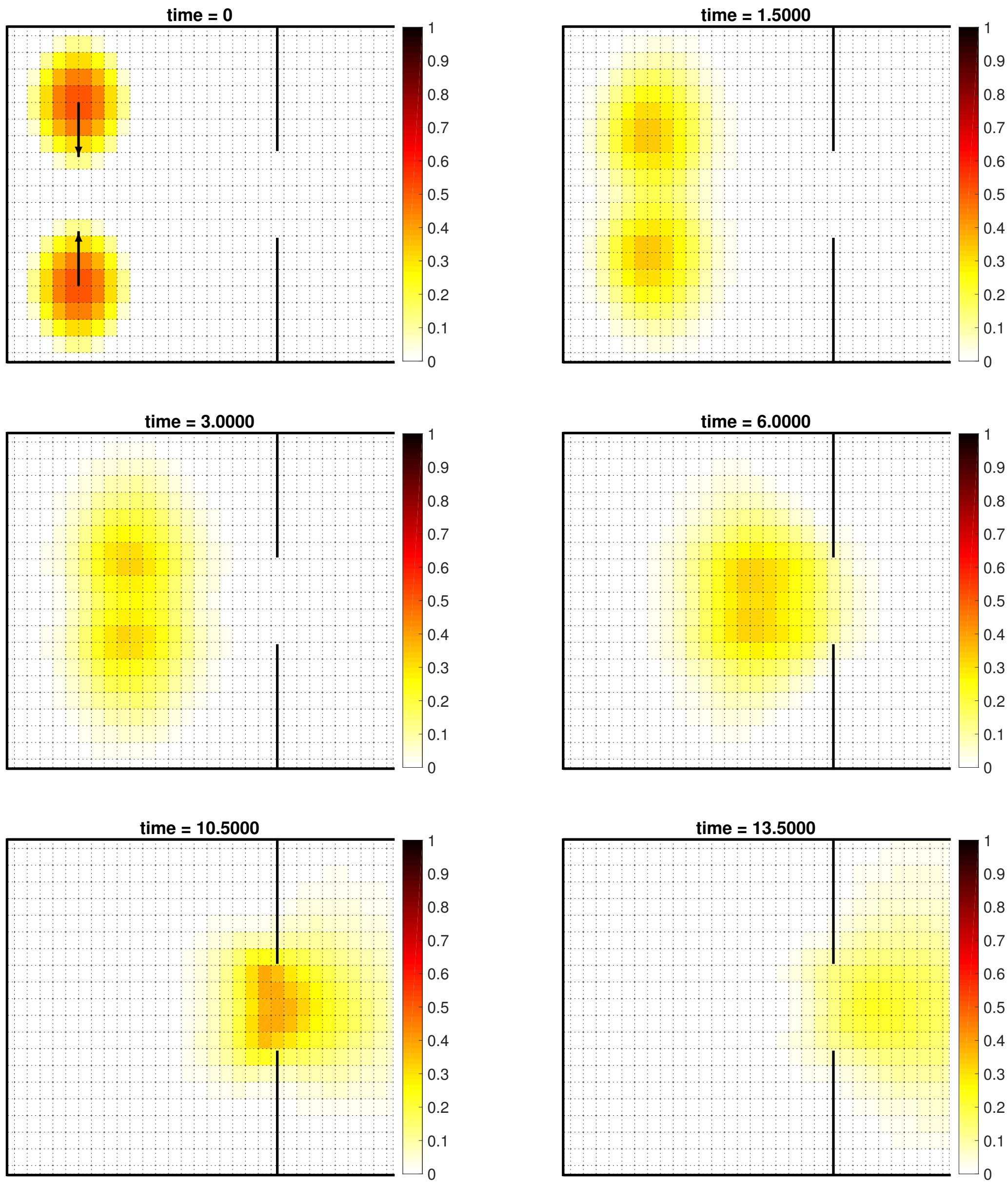

Figure 4.3: Evacuation process from a 10 m $\times$ 10 m room with a 2.6 m wide exit for $t = 0, 1.50, 3.00, 6.00, 10.50,$ and 13.50 s: 46 pedestrians initially grouped into two clusters, coarse mesh, and time step Δt_{small}. The color refers to density.

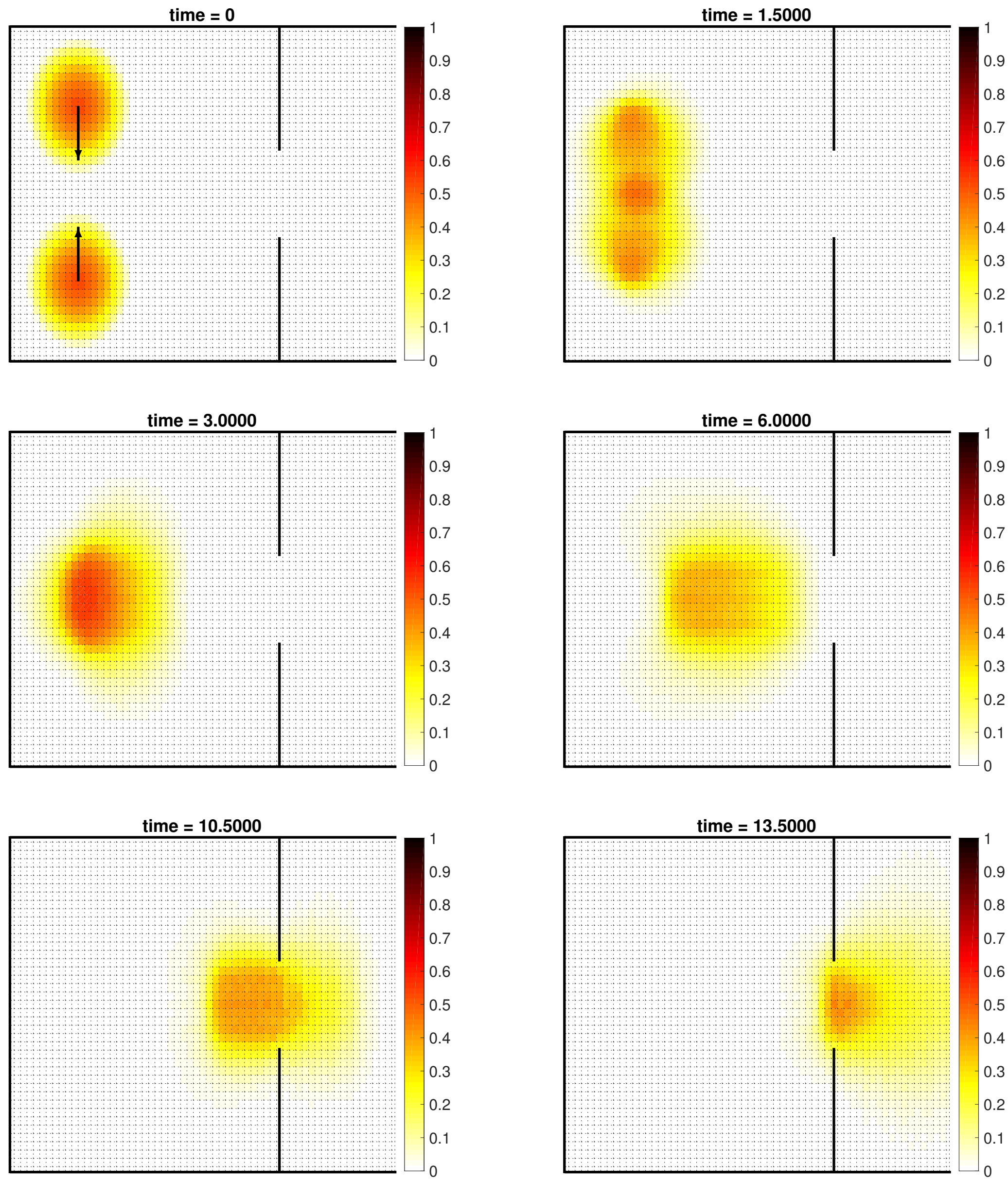

Figure 4.4: Evacuation process from a 10 m $\times$ 10 m room with a 2.6 m wide exit for $t = 0, 1.50, 3.00, 6.00, 10.50$, and 13.50 s: 46 pedestrians initially grouped into two clusters, medium mesh, and time step Δt_{medium}. The color refers to density.

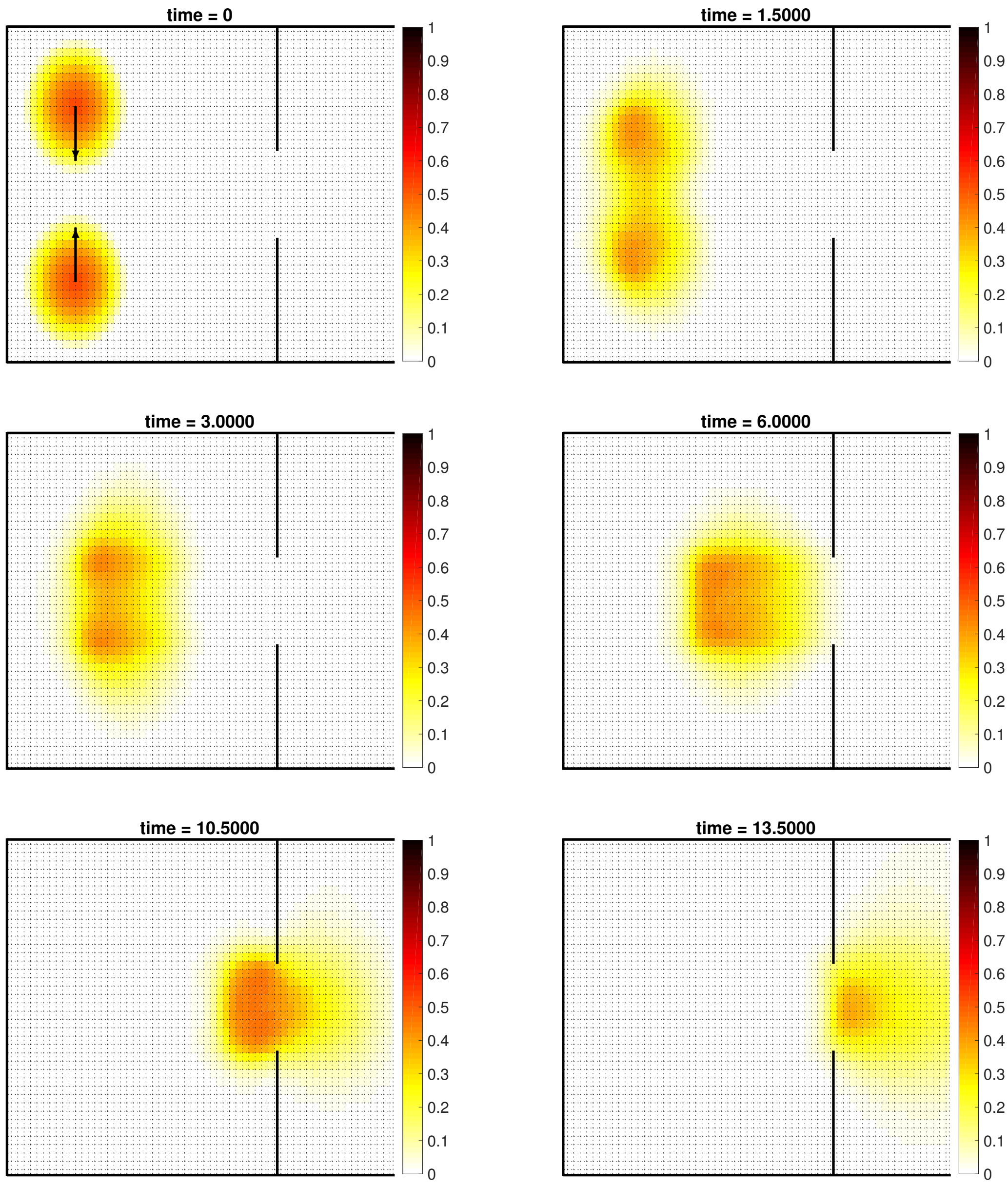

Figure 4.5: Evacuation process from a 10 m × 10 m room with a 2.6 m wide exit for $t = 0, 1.50, 3.00, 6.00, 10.50,$ and 13.50 s: 46 pedestrians initially grouped into two clusters, medium mesh, and time step Δt_{small}. The color refers to density.

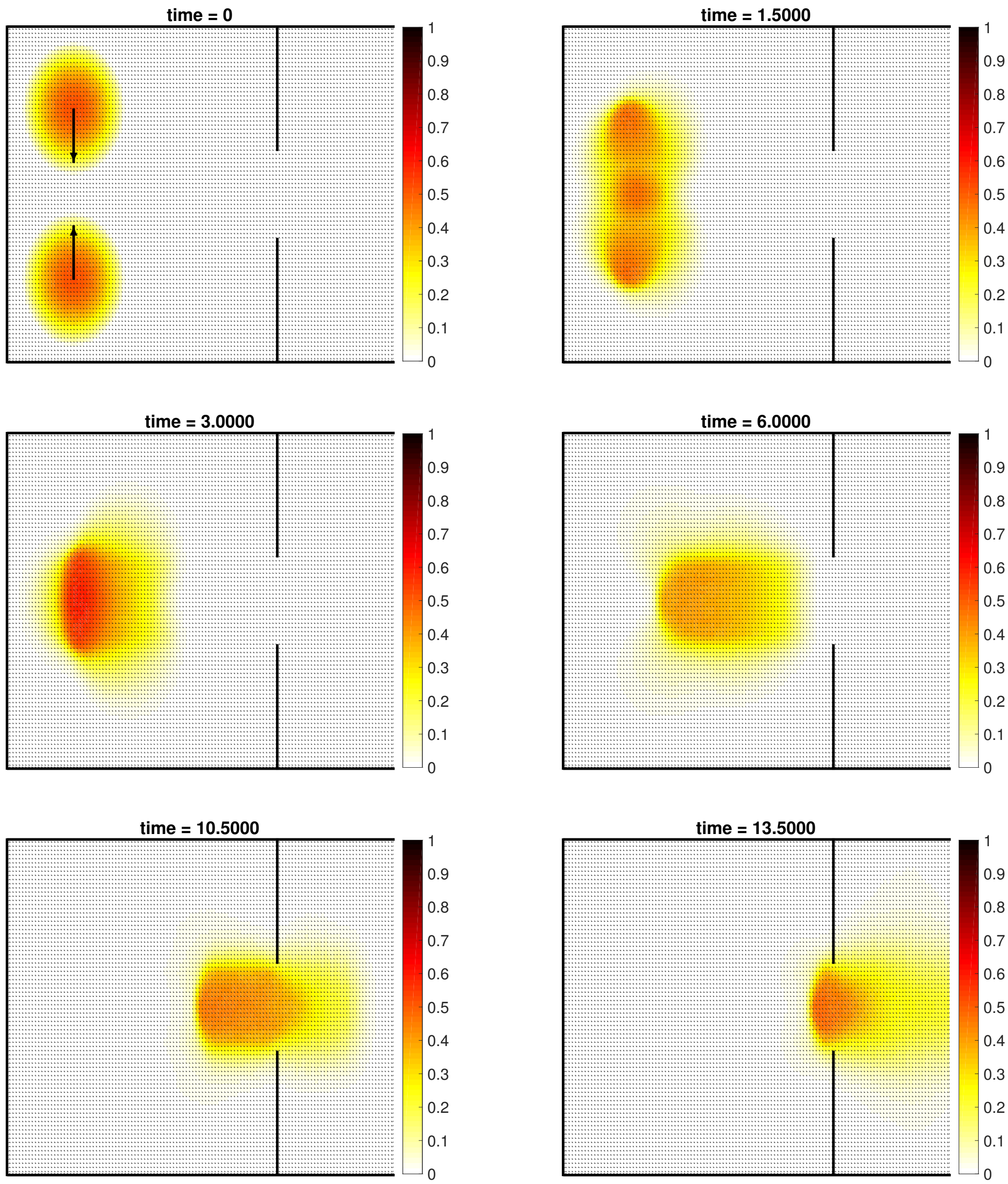

Figure 4.6: Evacuation process from a 10 m $\times$ 10 m room with a 2.6 m wide exit for $t = 0, 1.50, 3.00, 6.00, 10.50$, and 13.50 s: 46 pedestrians initially grouped into two clusters, small mesh, and time step Δt_{small}. The color refers to density.

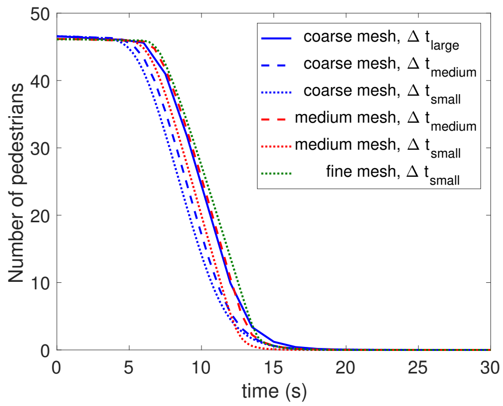

(a)

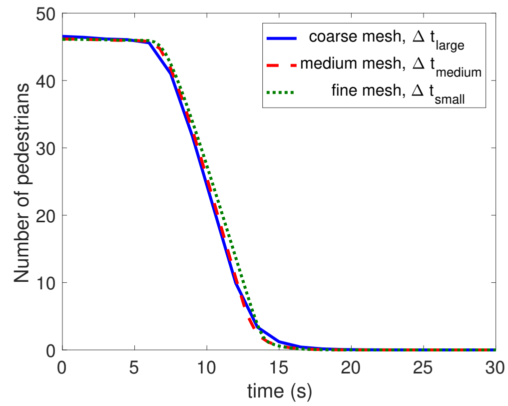

(b)

Figure 4.7: (a) Number of pedestrians for 6 different simulations combining different meshes and different time steps and (b) Change of the number of pedestrians under 3 different conditions.

given time step, pedestrians take longer to leave the room the room. Figure 4.7(b) compare the results from the cases 1, 4, and 6. We can see a very good agreement.

4.2 Different exit sizes

This second test is also taken from [1] for validation purposes. The aim of this test is to study how the evacuation time is affected by the exit size. We let the exit size vary from 1.5 m to 4 m. We consider the medium meshes and Δt_{medium} from Section 4.1, since it is an appropriate choice as we have seen in the previous section. All the other parameters are set like in Section 4.1.

Figure 4.8 shows the total evacuation time as a function of the exit size: Figure 4.8(a) from [1] and Figure 4.8(b) from our simulations. First, we notice that our results are in very good agreement with the results from [1]. As expected, the total evacuation time decreases with the exit size. However, we remark that once the exit is large enough for the crowd, the evacuation time does not change significantly of the exit is further enlarged.

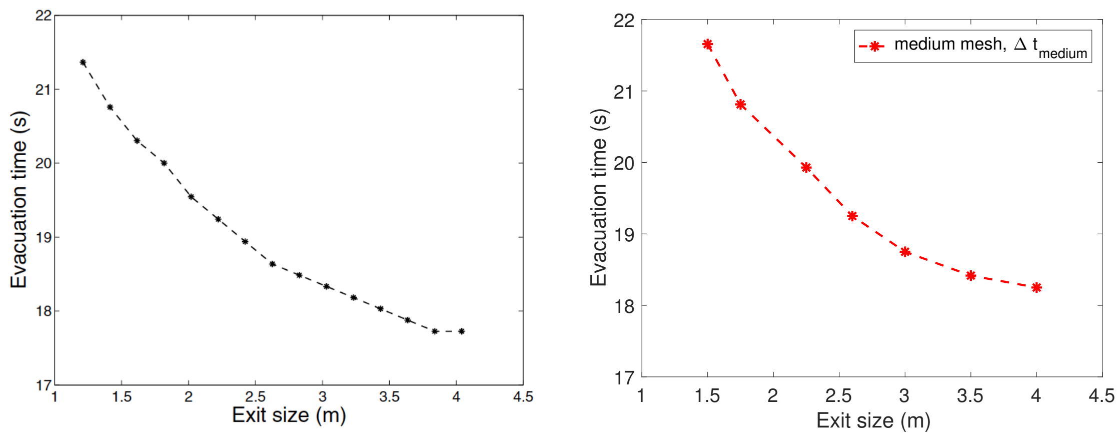

(a) (b)

Figure 4.8: The evacuation time on different exit sizes: (a) from [1] and (b) our simulation.

4.3 Influence of parameter ε

In the model introduced in Section 2.2, parameter ε can be interpreted as a measure of the level of panic: $\varepsilon = 0$ corresponds to the situation that pedestrians look for less congested, while $\varepsilon = 1$ represents a panic situation with pedestrians following the stream. In this section, we are interested in looking at how the evacuation from a room with one exit is affected by the level of panic.

We consider a square room of side 10 m. An exit door of size 2 m is centered in the middle of the right side of the room. Pedestrians are initially distributed in a

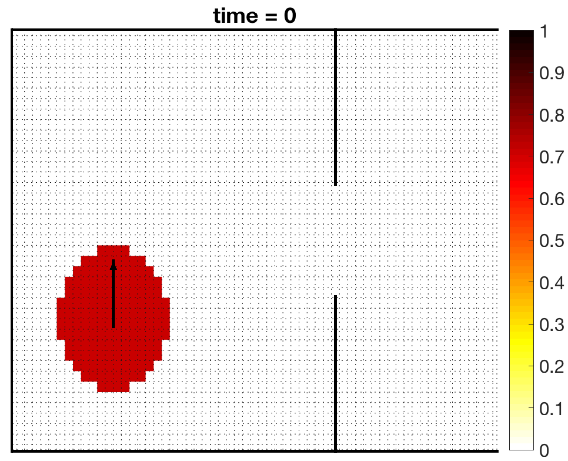

Figure 4.9: Initial distribution of about 46 pedestrians with direction θ_3 in a 10 m $\times$ 10 m room with a 2.6 m wide exit. The color refers to density.

circular region, with constant density $\rho = 0.70$. That corresponds approximately to 46 pedestrians. The pedestrians initially move with direction θ_3. See Figure 4.9.

Figure 4.10 show the computed density at times $t = 3$, 6, 13.5 s for $\varepsilon = 0$ (left) and $\varepsilon = 1$ (right). In the case when the pedestrians look for less congested areas, i.e. $\varepsilon = 0$, they take a longer path to approach the exit but they walk faster since the density is not high. On the other hand, when pedestrians follow the stream, i.e. $\varepsilon = 1$, the level of congestion is high and that leads to a decreased velocity modulus. In this particular case, the level of panic does not affect the overall evacuation time.

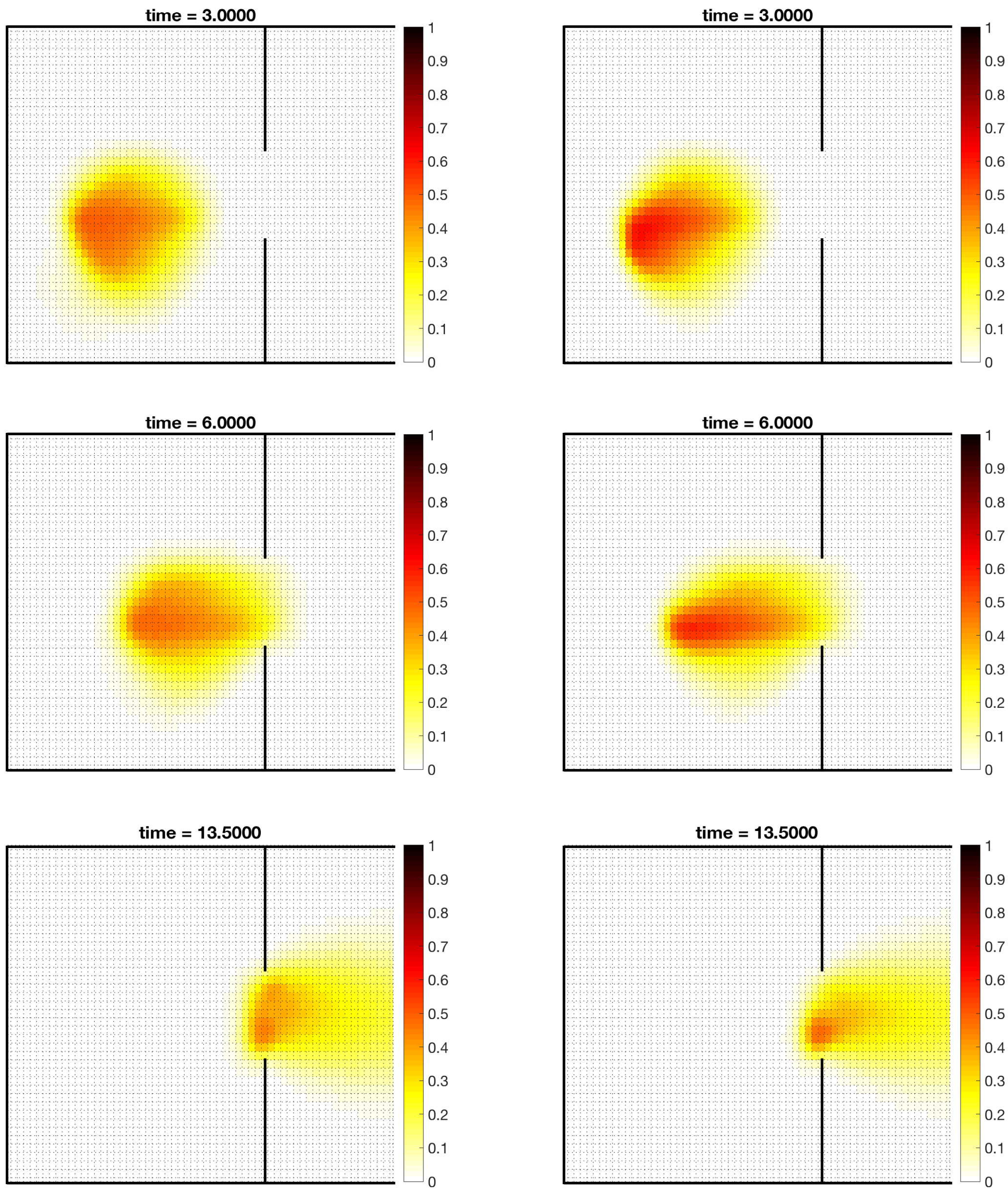

Figure 4.10: Computed density in a 10 m $\times$ 10 m room at $t = 3.00, 6.00$, and 13.50 s for $\varepsilon = 0$ (left) and $\varepsilon = 1$ (right). The color refers to density.

4.4 Influence of the parameter α and presence of obstacles

In the model introduced in Section 2.2, parameter α represents the quality of the environment, which influences also the maximal reachable dimensionless velocity modulus, Figure 2.1. In theory, parameter $\alpha = 0$ forces pedestrians to stop, while the value $\alpha = 1$ contributes to keep the maximal velocity modulus. However, in our experience this parameter alone is not very useful in modeling obstacles within the domain. Thus, after understanding the role and the limitations of parameter α, we present a new strategy to deal with obstacles.

We consider a square room of side 10 m with a 2.6 m wide exit located on the right wall and featuring either one obstacle (in two different positions) or two obstacles. Since as mentioned above $\alpha = 0$ does not prevent pedestrians from walking into the obstacle, we adopt the following strategy: define an *effective area* for the obstacle, i.e. an enlarged area with respect the real obstacle which corresponds to the area the pedestrian avoids to bypass the obstacle, and update the definition of $\boldsymbol{u}_W$ to account for the effective area. As we well see, the change of $\boldsymbol{u}_W$ does not prevent the pedestrians to walk through the effective area. Therefore, we explore the role of α in defining the shape of the real obstacle, i.e. the area all the pedestrians avoid.

Three configurations are considered:

a) One obstacle close to the exit, i.e. in the middle of the right wall; see Figure 4.19(a) for the effective area.

b) One obstacle close to the top of the right wall; see Figure 4.19(b) for the

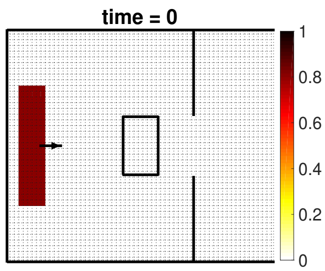

(a)

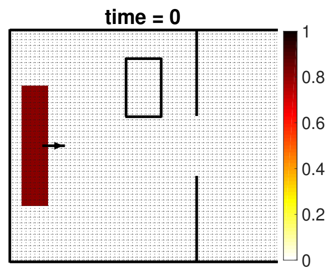

(b)

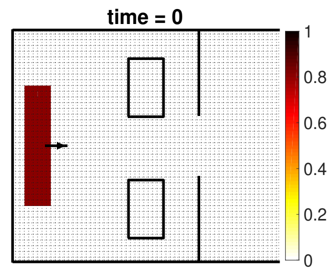

(c)

Figure 4.11: Set-up of the effective area; (a) placed in the middle, (b) placed on the right top and (c) placed symmetrically. The color refers to density.

effective area.

c) Two obstacles close to the right wall, place symmetrically with respect to the exit; see Figure 4.19(c) for the effective area.

Pedestrians are initially distributed in a rectangular region, with constant density $\rho = 0.80$, for a total of 44 pedestrians. Initially, pedestrians movies with direction θ_1. Other parameters are set the same way as in the previous subsection.

Before we present the results for the room with the obstacles, we show the evacuation progress in the absence of obstacles. Figure 4.12 displays the density at different times computed with $\alpha = 1$ everywhere in the domain. The total evacuation time for this case is 15.525 s.

Next, we present the results for the cases with obstacles. We first compare the evacuation process when in the effective area we prescribe $\alpha = 1$ and $\alpha = 0$, in order to identify the shape of the real obstacles. See Figure 4.13 and 4.14 for the density computed in case a) with $\alpha = 1$ and $\alpha = 0$ in the effective area, respectively. Likewise, see Figure 4.15 and 4.16 for the density computed in case b) with $\alpha = 1$ and $\alpha = 0$ in the effective area, respectively. Finally, see Figure 4.17 and 4.18 for the

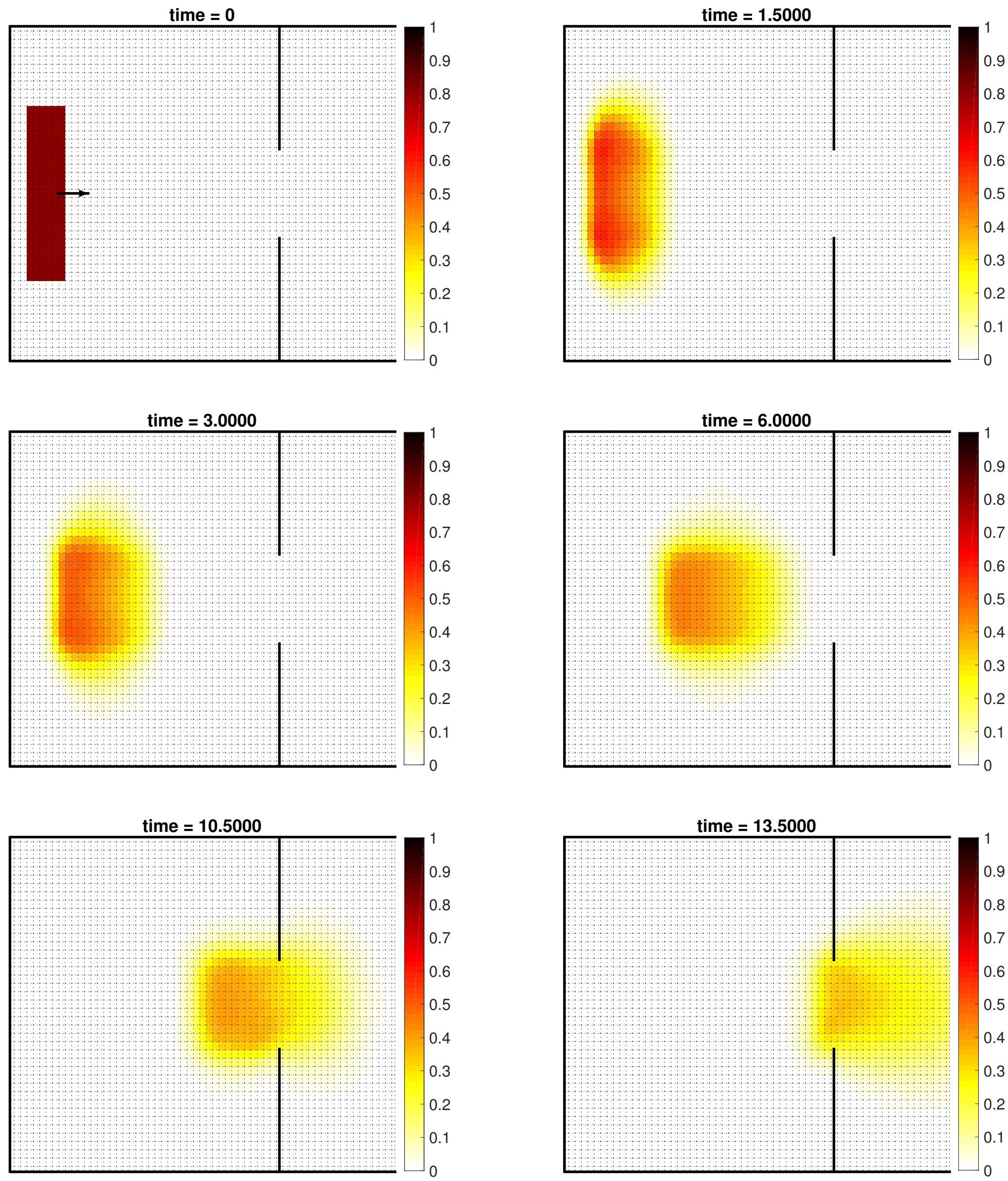

Figure 4.12: Evacuation process from a 10 m $\times$ 10 m room with a 2.6 m wide exit for $t = 0, 1.50, 3.00, 6.00, 10.50$, and 13.50 s: 44 pedestrians initially distributed in a rectangular shape moving with initial direction θ_1 with no obstacle. The color refers to density.

density computed in case c) with $\alpha = 1$ and $\alpha = 0$ in the effective area, respectively. From Figure 4.13, 4.15, and 4.17 we see that when $\alpha = 1$ pedestrians avoid the front part of the effective area. This is a possible explanation: when $\alpha = 1$, the quality of environment is at best and pedestrians can move with the maximal velocity modulus, thus the quickly adapt to the effective area through $\boldsymbol{u}_W$, but then are driven towards the exit and walk through the back part of the effective area. From Figure 4.14, 4.16, and 4.18 we observe that when $\alpha = 0$ pedestrians avoid the back part of the effective area. In this case, the possible explanation is that $\alpha = 0$ forces the pedestrians to stop, which causes higher densities in the front part of the effective area.

Finally, Figure 4.19 shows the evacuation times for the room with no obstacles and $\alpha = 1$, and for cases a), b), and c) both for $\alpha = 1$ and $\alpha = 0$. Obviously, the shortest evacuation time is for the room with no obstacles and and overall good quality of the environment. The evacuation time is slightly larger when there is one obstacle (either in the middle of the right wall or at the top) and $\alpha = 1$, and it increases again slightly when two obstacles are present and $\alpha = 1$. The evacuation times increase more significantly when we set $\alpha = 0$. In particular, when the obstacle is placed in the middle of the right wall (i.e. in front of the door), the evacuation time more than doubles. It is slightly less then double when the obstacle is at the top of the right wall. Finally, the largest evacuation time is for the room with two obstacles.

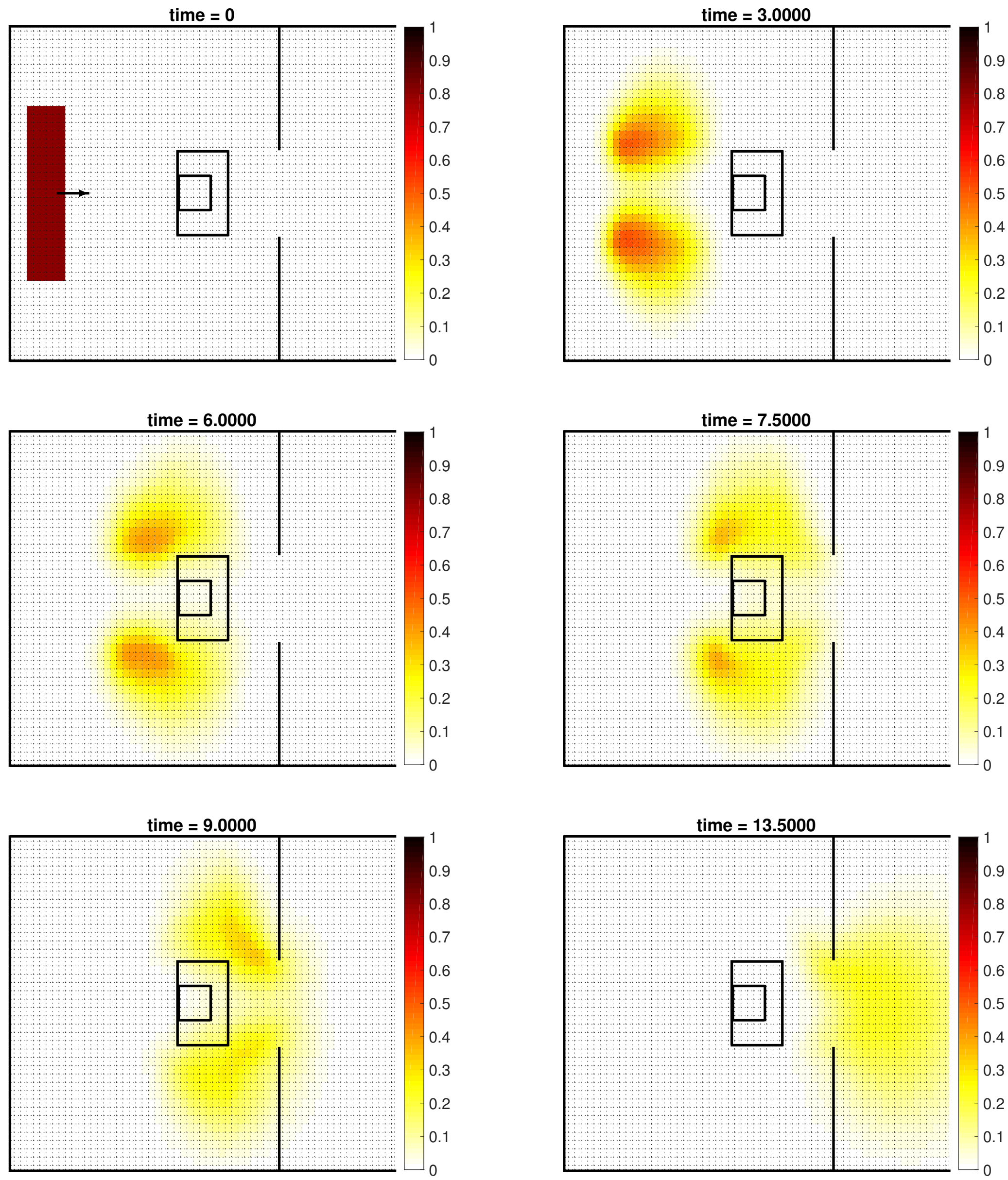

Figure 4.13: Case a)): Evacuation process of 44 pedestrians initially distributed in a rectangular shape moving with initial direction θ_1 and $\alpha = 1$ in the effective area. Computed density for $t = 0, 1.50, 3.00, 6.00, 10.50,$ and 13.50 s, respectively. The small rectangle within the effective area represents the real obstacle.

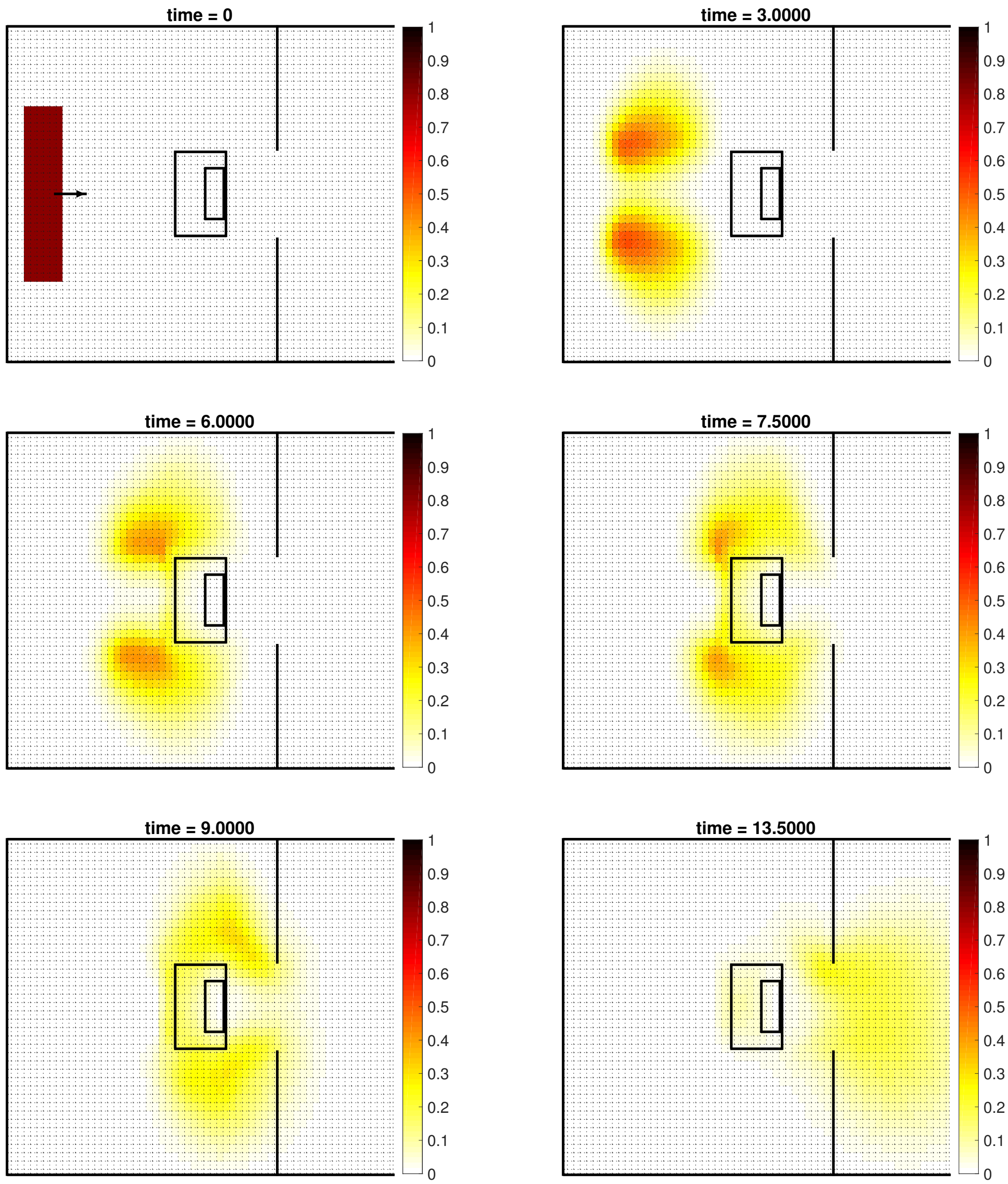

Figure 4.14: Case a): Evacuation process of 44 pedestrians initially distributed in a rectangular shape moving with initial direction θ_1 and $\alpha = 0$ in the effective area. Computed density for $t = 0, 1.50, 3.00, 6.00, 10.50,$ and 13.50 s, respectively. The small rectangle within the effective area represents the real obstacle.

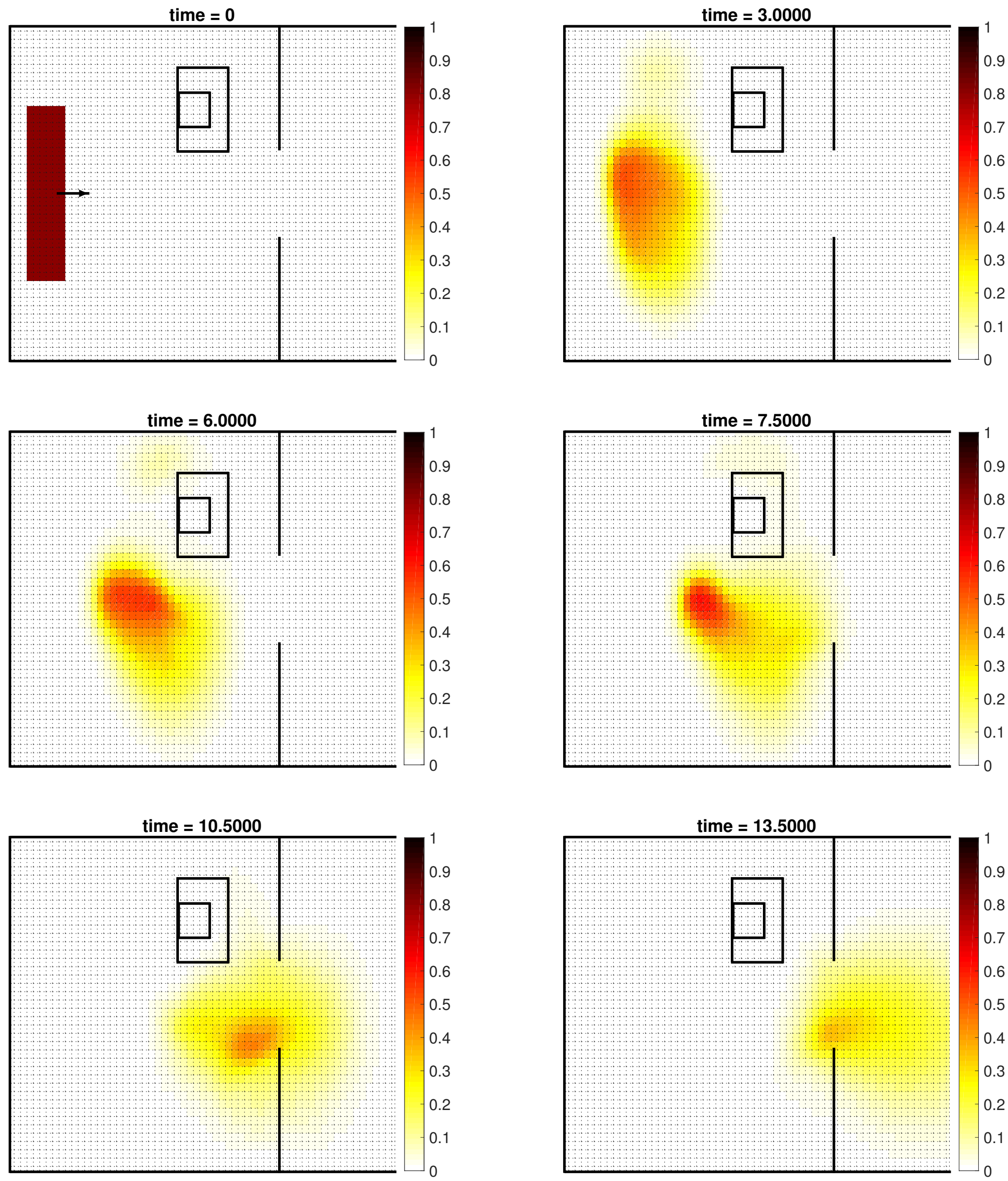

Figure 4.15: Case b)): Evacuation process of 44 pedestrians initially distributed in a rectangular shape moving with initial direction θ_1 and $\alpha = 1$ in the effective area. Computed density for $t = 0, 1.50, 3.00, 6.00, 10.50,$ and 13.50 s, repectively. The small rectangle within the effective area represents the real obstacle.

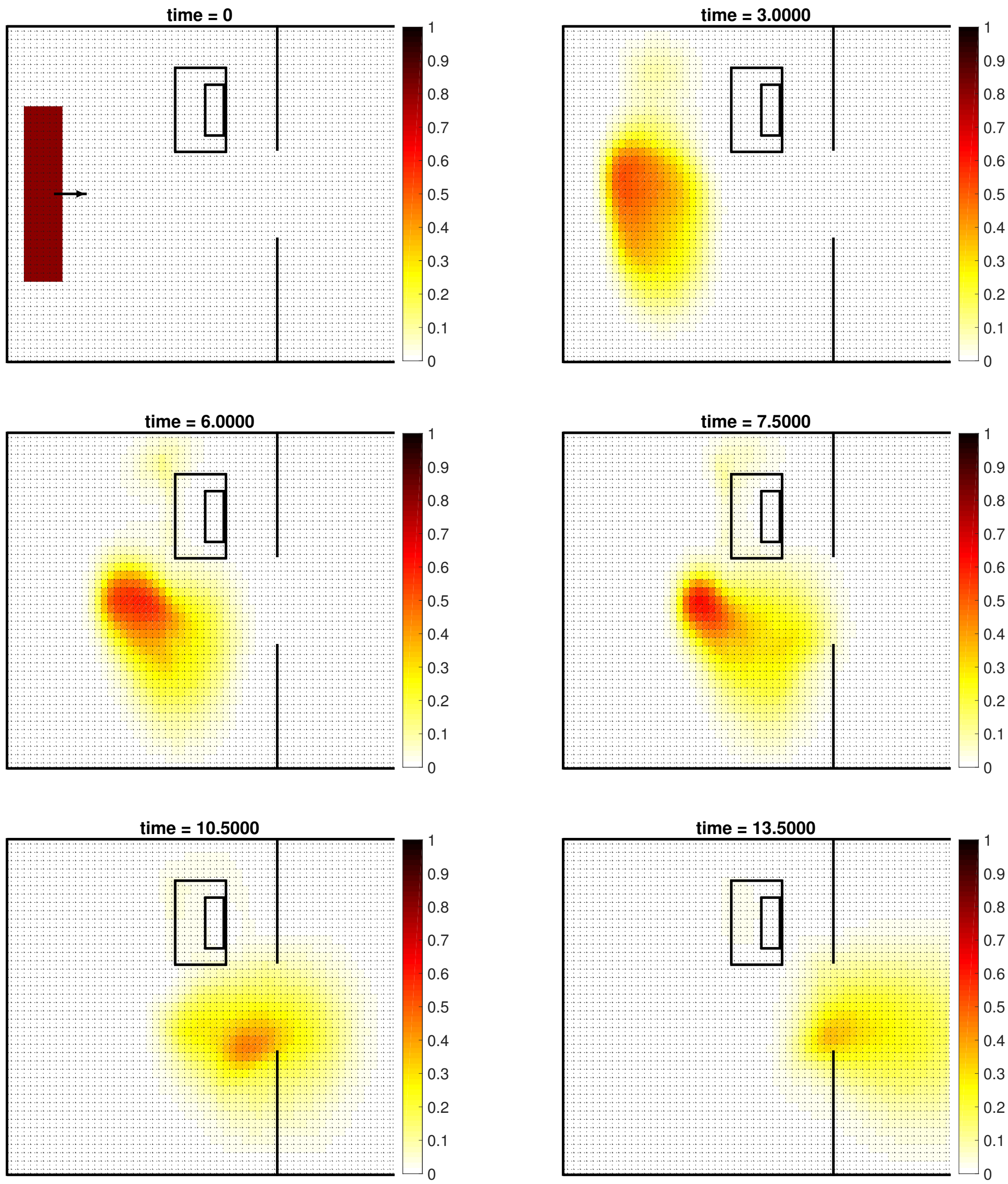

Figure 4.16: Case b)): Evacuation process of 44 pedestrians initially distributed in a rectangular shape moving with initial direction θ_1 and $\alpha = 0$ in the effective area. Computed density for $t = 0, 1.50, 3.00, 6.00, 10.50,$ and 13.50 s, repectively. The small rectangle within the effective area represents the real obstacle.

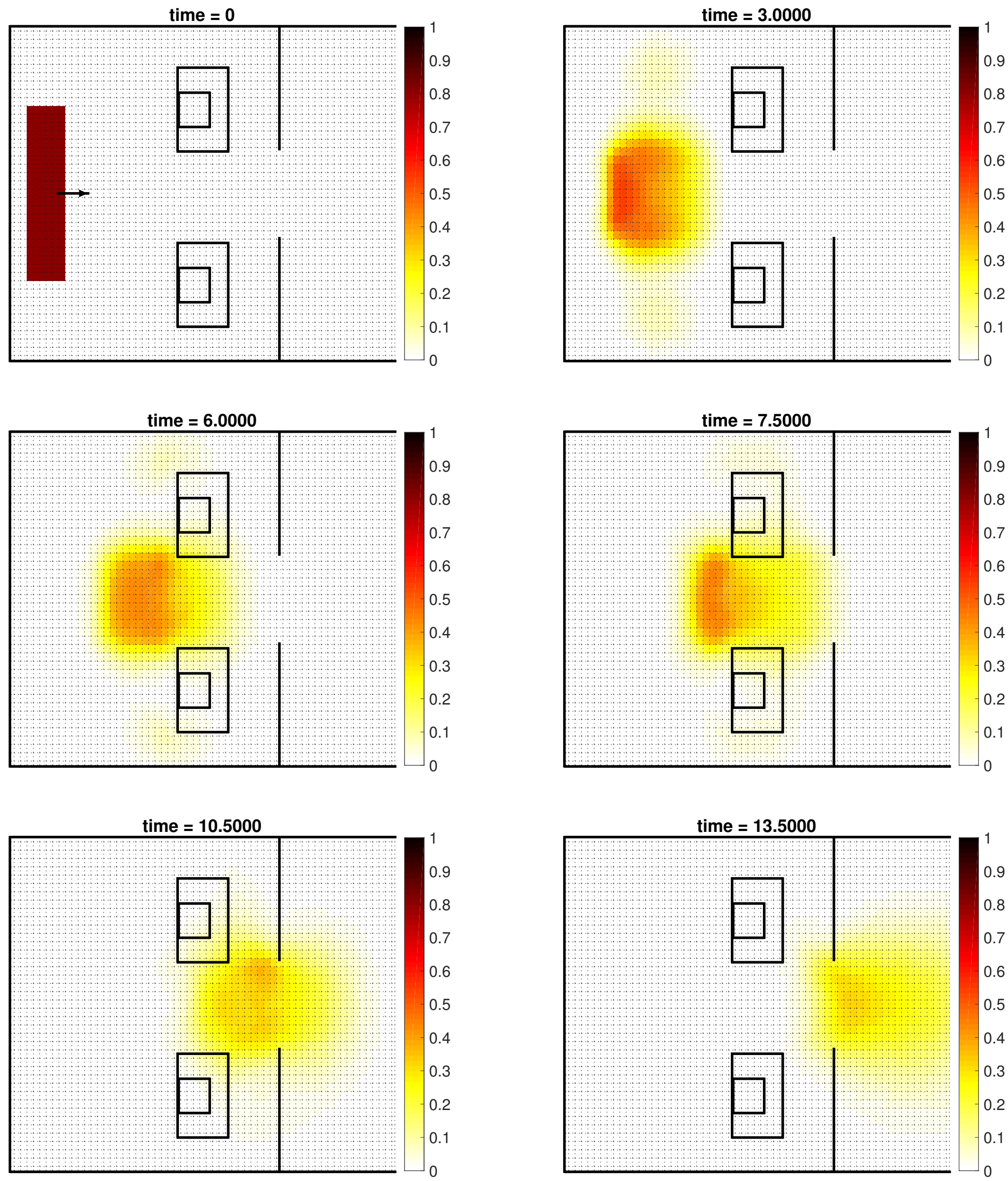

Figure 4.17: Case c): Evacuation process of 44 pedestrians initially distributed in a rectangular shape moving with initial direction θ_1 and $\alpha = 1$ in the effective area. Computed density for $t = 0, 1.50, 3.00, 6.00, 10.50,$ and 13.50 s, respectively. The small rectangle within the effective area represents the real obstacle.

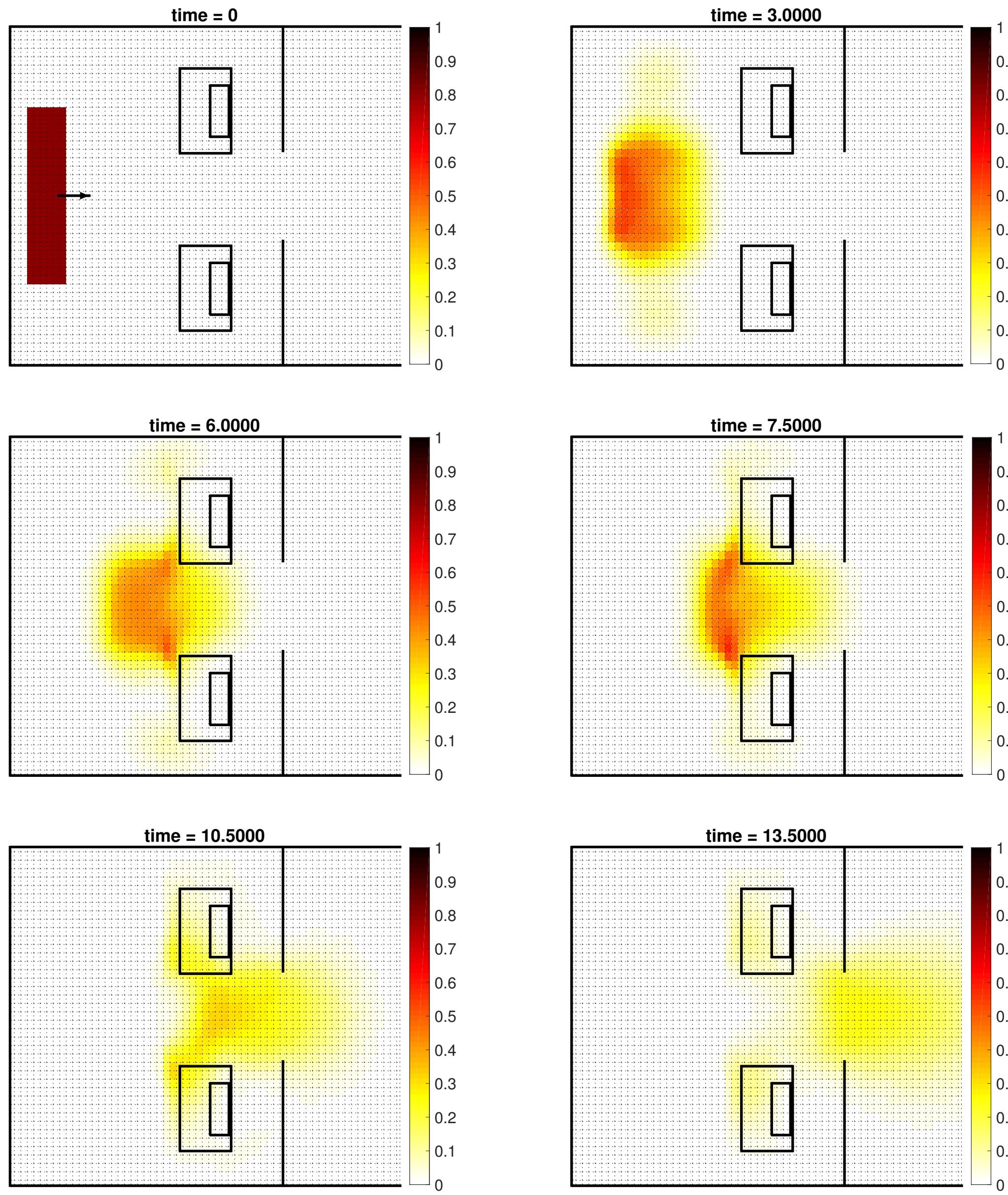

Figure 4.18: Case c): Evacuation process of 44 pedestrians initially distributed in a rectangular shape moving with initial direction θ_1 and $\alpha = 0$ in the effective area. Computed density for $t = 0, 1.50, 3.00, 6.00, 10.50,$ and 13.50 s, respectively. The small rectangle within the effective area represents the real obstacle.

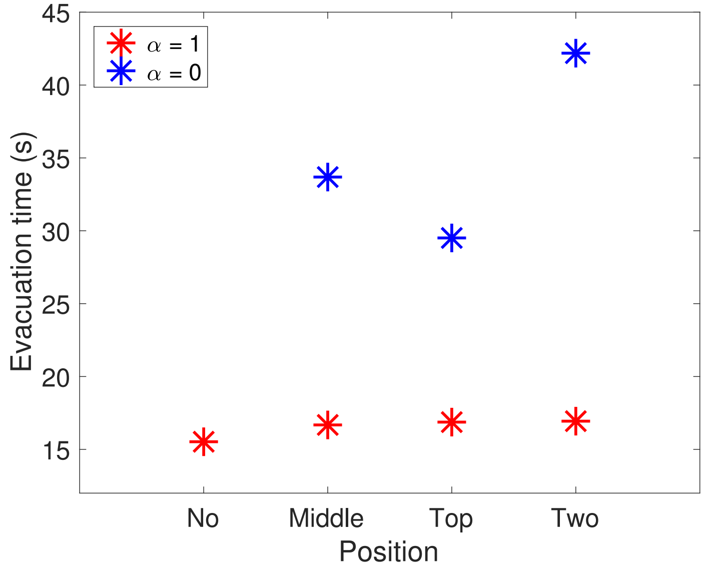

Figure 4.19: Evacuation times depending on the obstacle's positions.

4.5 Two exits

In this section, we investigate the cases of two exits [1, 50]. Following [1], in Section 4.5.1 we let the pedestrians decide actively which is the most convenient way to the exit. In the remaining subsections, we consider the case of a room with two doors of variable size and compare our results with the experimental data in [50].

4.5.1 Two identical exits

We consider again a square room of side 10 m. In the case considered in this section, two identical doors of length 2.2 m are placed symmetrically with respect to the center on the right side and they are 1 m apart. A group of 53 pedestrians are initially distributed in a circular region and they move with initial direction θ_3. We use the fine mesh previously used in the same room and Δt_{small}. All the other parameters are set like in Section 4.1.

Figure 4.20 shows the computed density at different times. Pedestrians choose the most appropriate way to the exit by taking into account not only the closeness to each door but also the less crowded path, which is similar to the results reported in [1].

4.5.2 Different exits and variable number of pedestrians

We consider the usual room of side 10 m. Two different sized exits are place on on the right side: the side length of exit ① is 0.7 m and the side length of exit ② is 1.1 m. See Figure 4.21. The distance between the two exits is 3 m. We choose this setting in order to compare with the experimental data in [50].

In [50], ten experiment runs were performed: 2 trials with 18 pedestrians, 6 trials with 40 pedestrians, and 2 trials with 138 pedestrians. The density and flow graph are reported in Figure 4.24(a) and 4.24(c), respectively. Figure 4.21, 4.22 and 4.23 show the computed densities for the evacuation of a group of 18, 40, 138, respectively. In the simulation with 18 and 40 pedestrians, the group is initially positioned in a square with higher people density towards the back of the room and they are given initial direction θ_1. In the run with 138 pedestrians, 90 of them start from the middle of a room and are also given initial direction θ_1. All the simulations use the medium mesh and Δt_{small}.

The mean density and mean flow rate computed from our simulations are given in Figure 4.24(b) and 4.24(d). The density is averaged in two 4 m^2 areas in front of the exits using the Voronoi method from [45]. Our results in Figure 4.24(b) compares

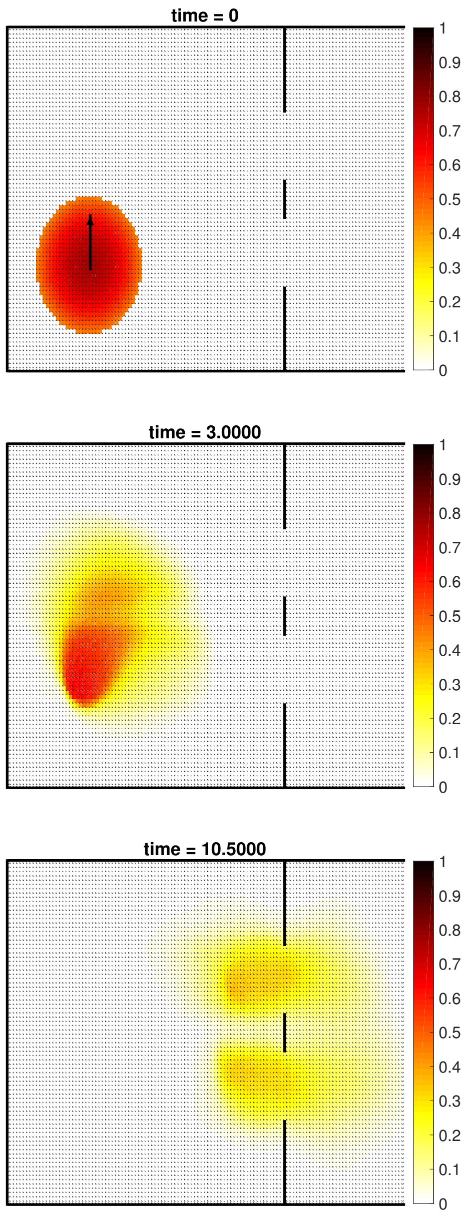

Figure 4.20: Evacuation process from the 10 m $\times$ 10 m room with two identical exits of size 2.2 m for $t = 0, 1.50, 3.00, 6.00, 10.50,$ and 13.50, respectively. The group of 53 pedestrians is initially distributed in a circular shape and moves with direction θ_3. See top left panel.

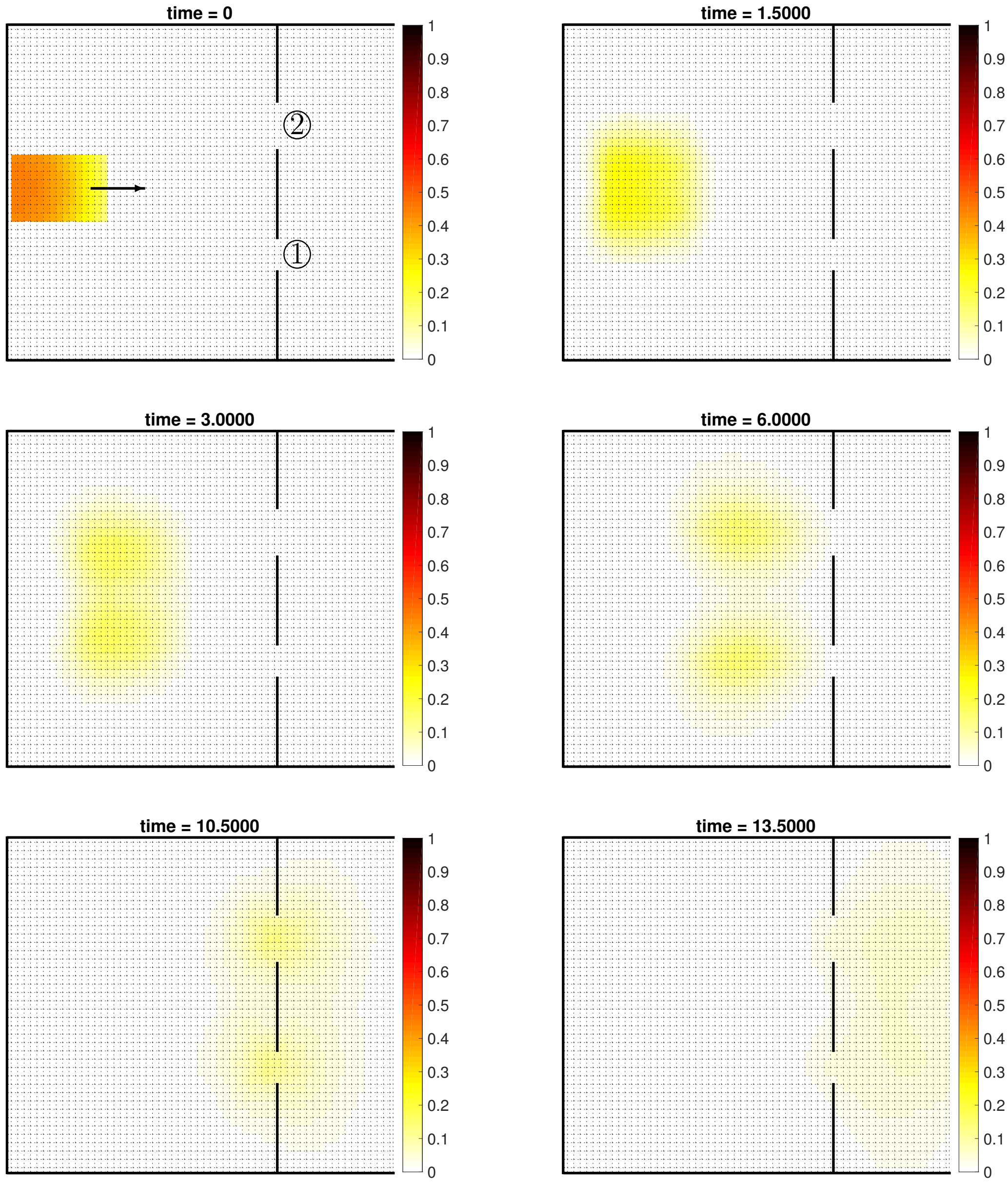

Figure 4.21: Evacuation process from a 10 m × 10 m room with exit ① 0.7 m and exit ② 1.1 m for $t = 0, 1.50, 3.00, 6.00, 10.50,$ and 13.50 s: 18 pedestrians moving with initial direction θ_1. The color refers to density.

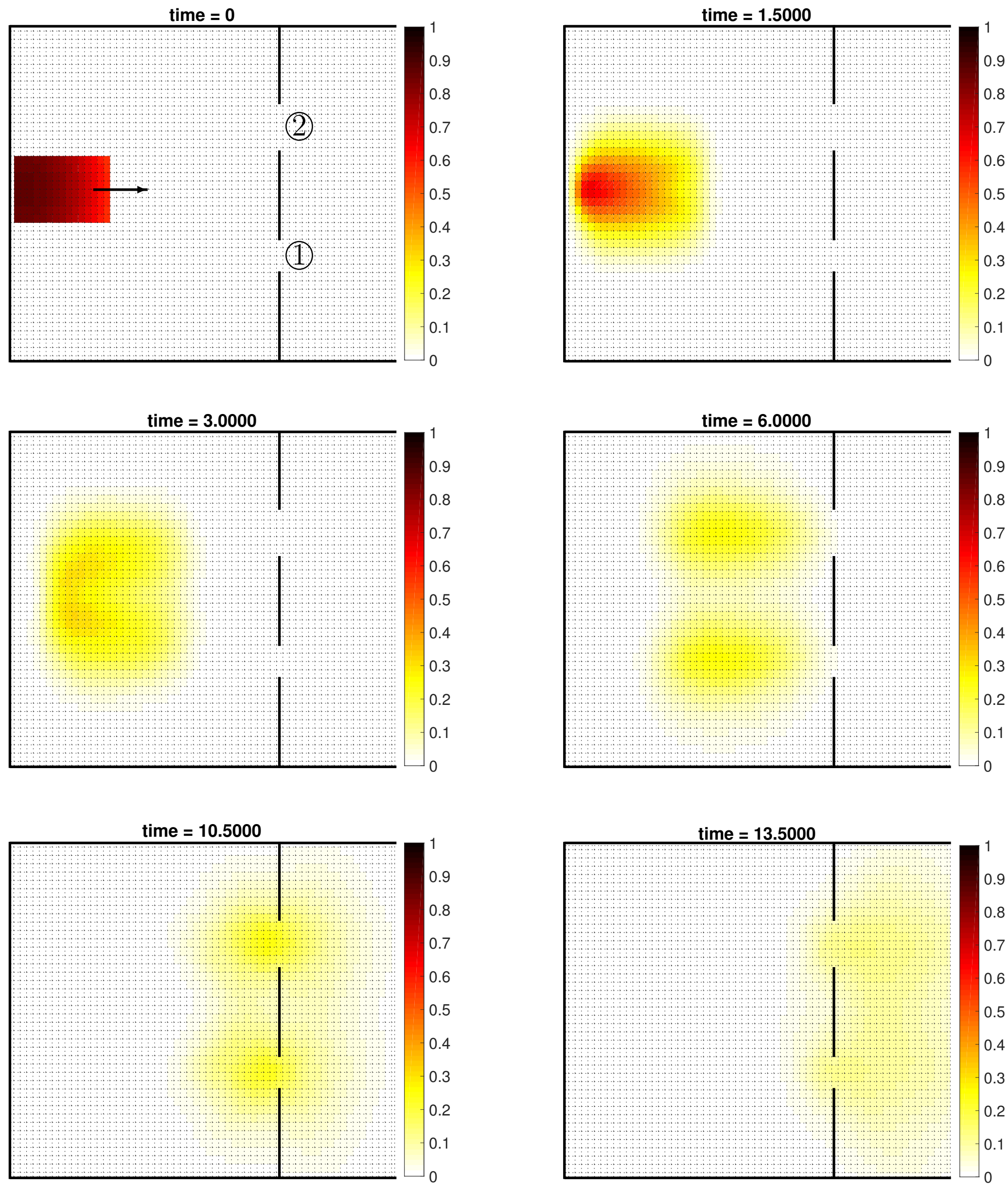

Figure 4.22: Evacuation process from a 10 m × 10 m room with exit ① 0.7 m and exit ② 1.1 m for $t = 0, 1.50, 3.00, 6.00, 10.50,$ and 13.50 s: 40 pedestrians moving with initial direction θ_1. The color refers to density.

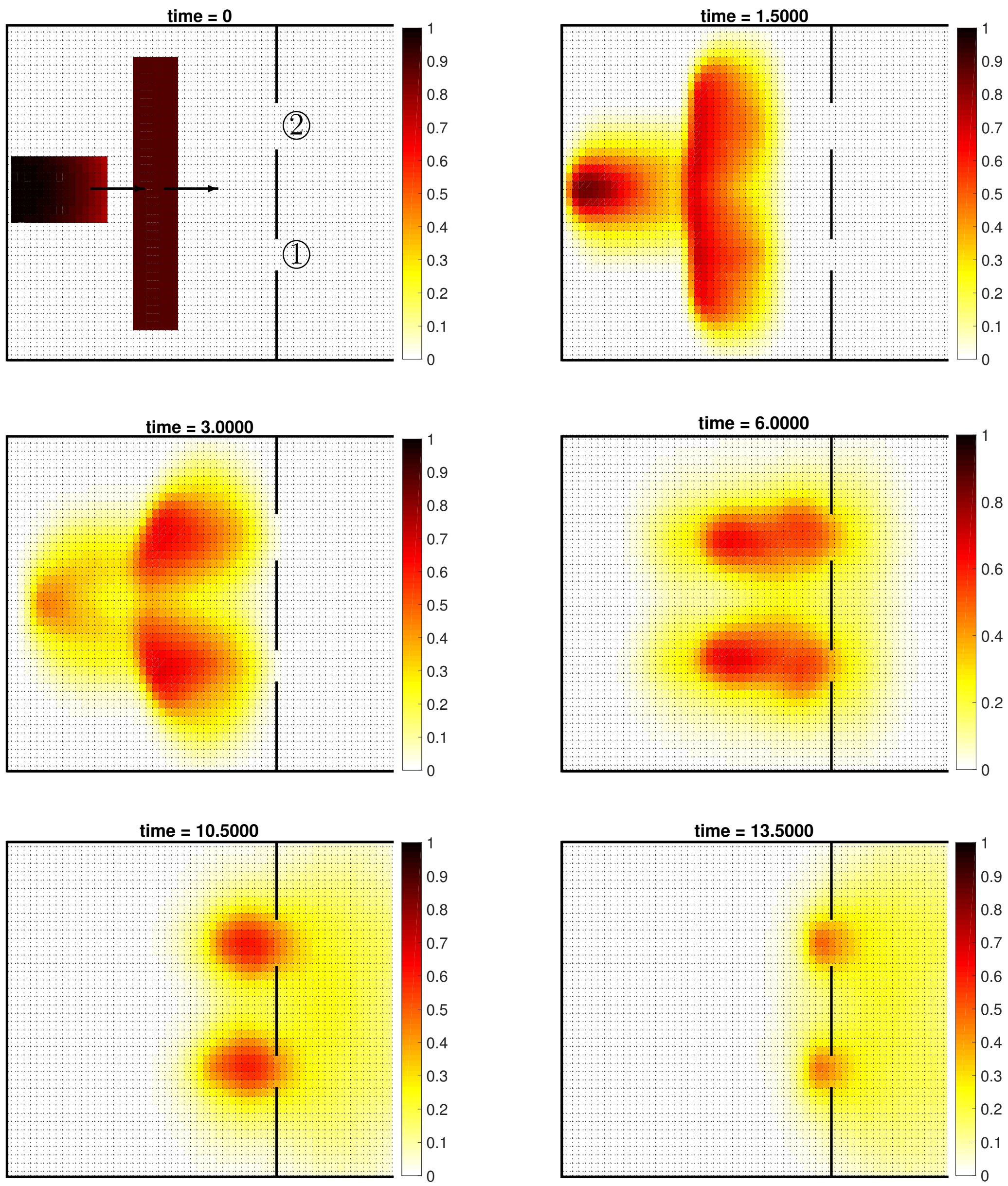

Figure 4.23: Evacuation process from a 10 m × 10 m room with exit ① 0.7 m and exit ② 1.1 m for $t = 0, 1.50, 3.00, 6.00, 10.50$, and 13.50 s: 138 pedestrians moving with initial direction θ_1. The color refers to density.

well with the experimental data in Figure 4.24(a). On the other hand, Figure 4.24(d) matches Figure 4.24(c) only when the number of pedestrians is large enough. This is to be expected: the kinetic approach is not meant to simulate the movement of a small number of pedestrians.

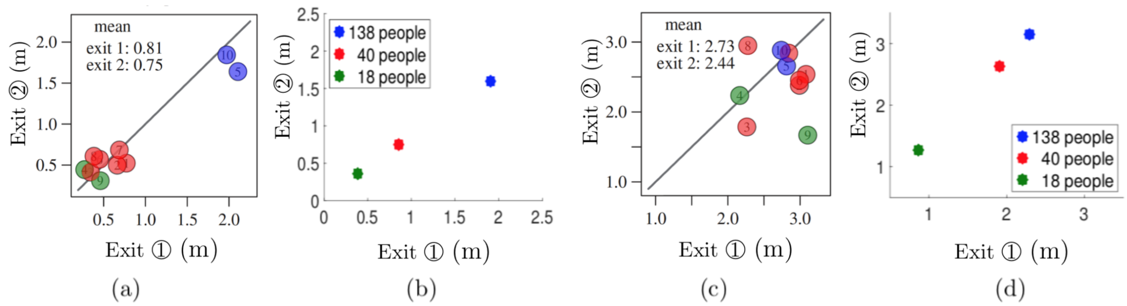

Figure 4.24: The density (ped m^{-2}): (a) empirical data in [50] and (b) our simulations, and the flow (ped m s^{-1}): (c) empirical data in [50] and (d) our simulations.

4.5.3 Different velocity moduli

This subsection considers different velocity moduli. So far, we have used the velocity modulus as (2.3). Now, simulations are preformed considering different choices for the velocity modulus. Velocity modulus (2.3) is a cubic polynomial. So, as other possible choices we consider

$$v_{purple} = v_{purple}(\rho) = (1 + \cos((\rho - 0.2)^{\frac{2}{3}}\pi/0.8^{\frac{2}{3}}))/2.$$

$$v_{orange} = v_{orange}(\rho) = (1 + \cos((\rho - 0.2)^{\frac{1}{2}}\pi/0.8^{\frac{1}{2}}))/2.$$

$$v_{blue} = v_{blue}(\rho) = (1 + \cos((\rho - 0.2)^{\frac{1}{3}}\pi/0.8^{\frac{1}{3}}))/2.$$

See Figure 4.25(a). In Figure 4.25(a), the yellow line is the original velocity modulus (2.3). Now, we consider the purple, orange, and blue curves. All the other conditions are the same as for the results in Figure 4.23, with $\alpha = 1$. The evacuation times are computed and the results are shown in Figure 4.25(b). The velocity modulus is getting lower, the evacuation requires more time.

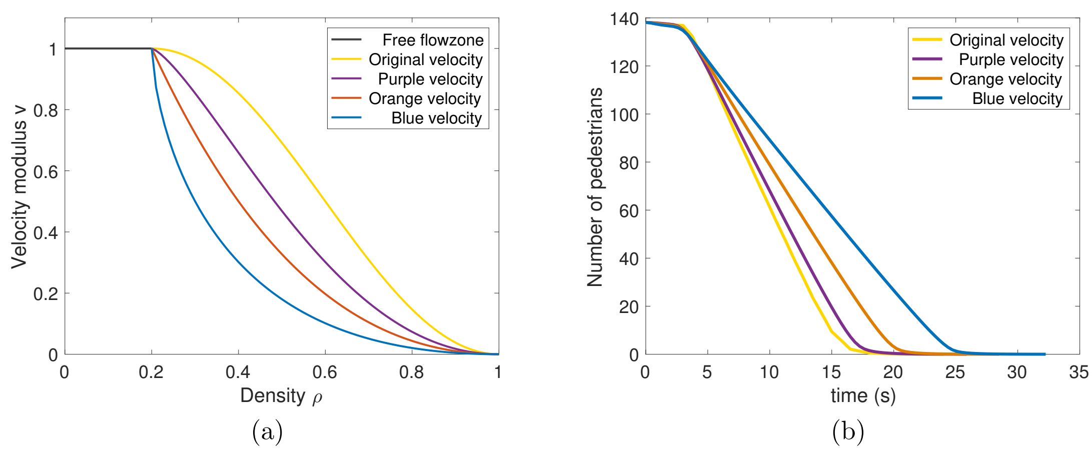

Figure 4.25: (a) The different velocity moduli and (b) Evacuation times of 138 pedestrians by different velocity moduli.

We remind that Figure 4.23 shows the evacuation process using the original velocity modulus. Figure 4.26 and 4.27 show computed density and velocity magnitude (with selected velocity vectors) for the evolution of evacuation process using the purple velocity modulus. Similarly, Figure 4.28 and 4.29 show computed density and velocity magnitude (with selected velocity vectors) for the evolution of evacuation process using the orange velocity modulus, and Figure 4.30 and 4.31 are for the case of blue velocity modulus.

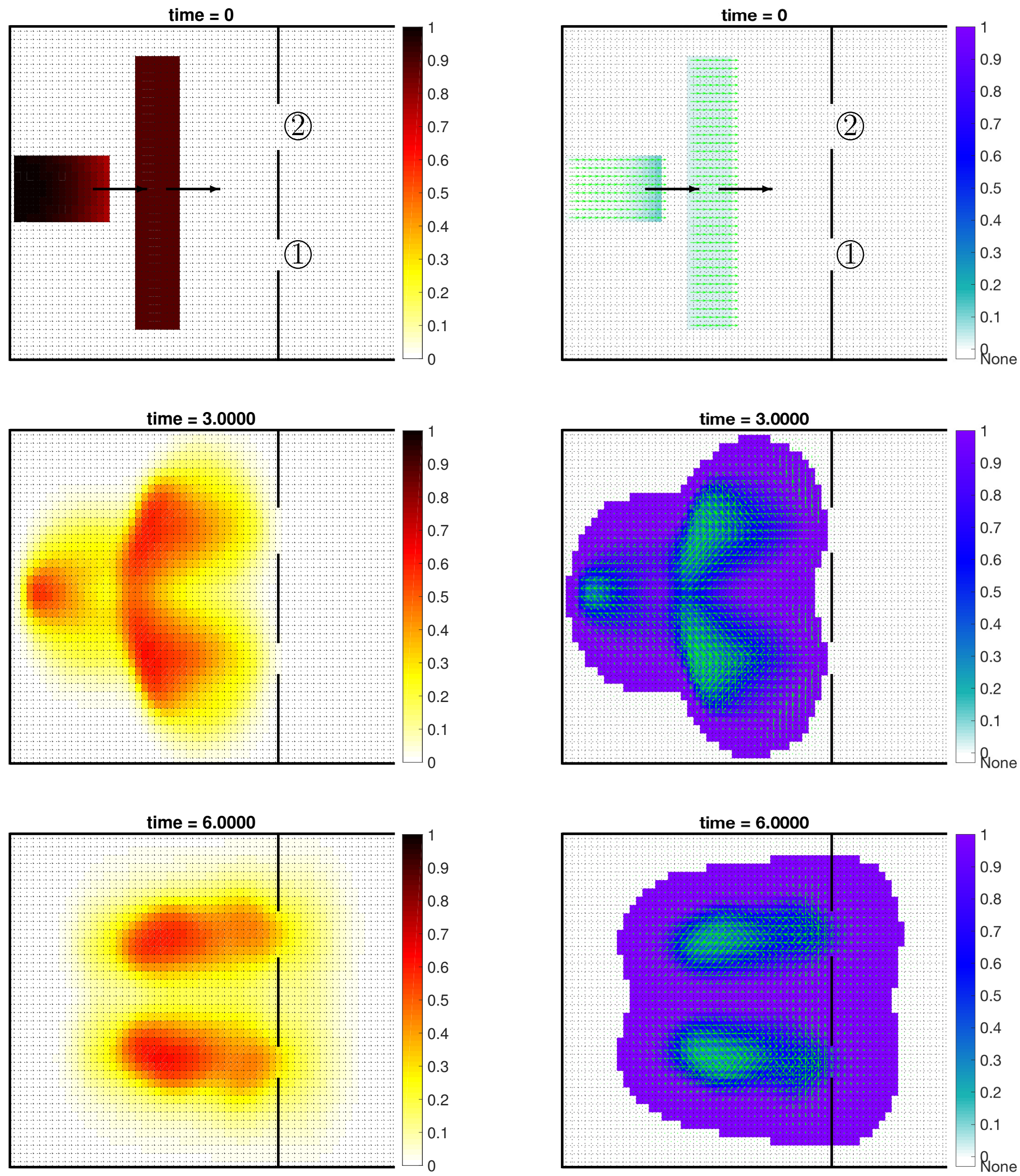

Figure 4.26: Evacuation process of 138 pedestrians in a 10 m $\times$ 10 m room for the purple velocity modulus: density (left) and velocity magnitude with selected velocity vectors (right) for $t = 0, 3.00$, and 6.00 s, respectively.

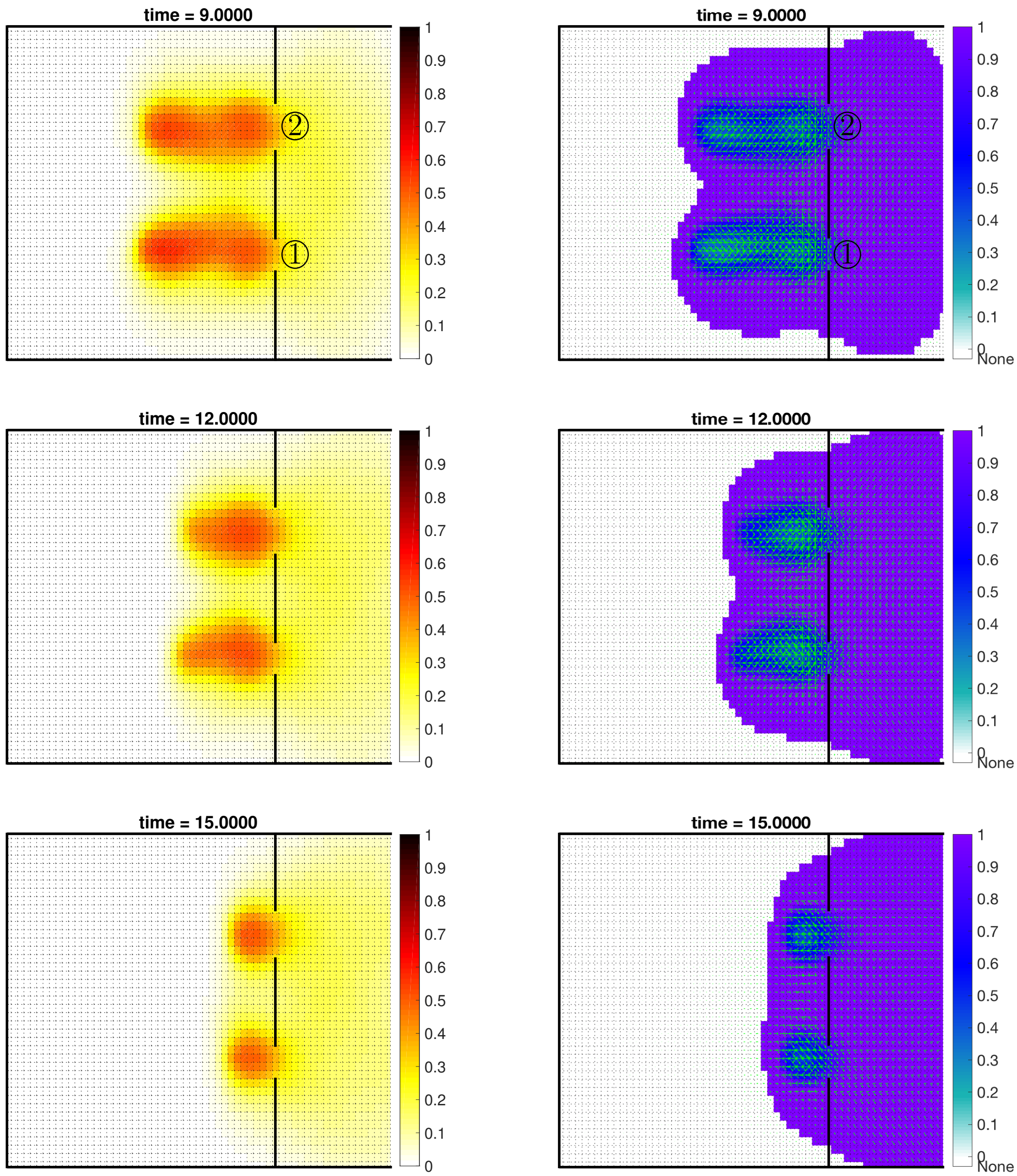

Figure 4.27: Evacuation process of 138 pedestrians in a 10 m × 10 m room for purple velocity modulus: density (left) and velocity magnitude with selected velocity vectors (right) for $t = 9.00, 12.00$, and 15.00 s, respectively.

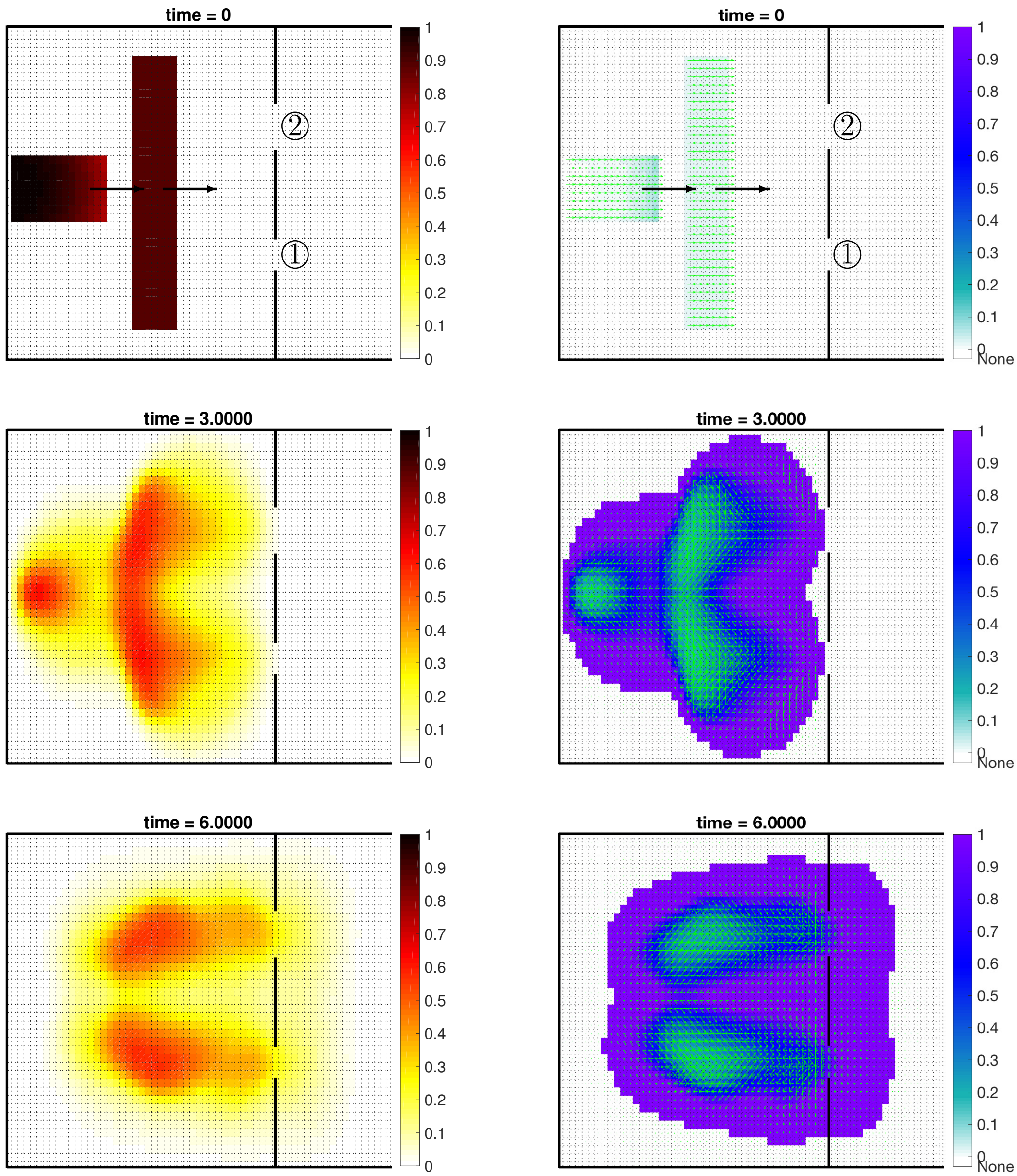

Figure 4.28: Evacuation process of 138 pedestrians in a 10 m × 10 m room for the orange velocity modulus: density (left) and velocity magnitude with selected velocity vectors (right) for $t = 0, 3.00$, and 6.00 s, respectively.

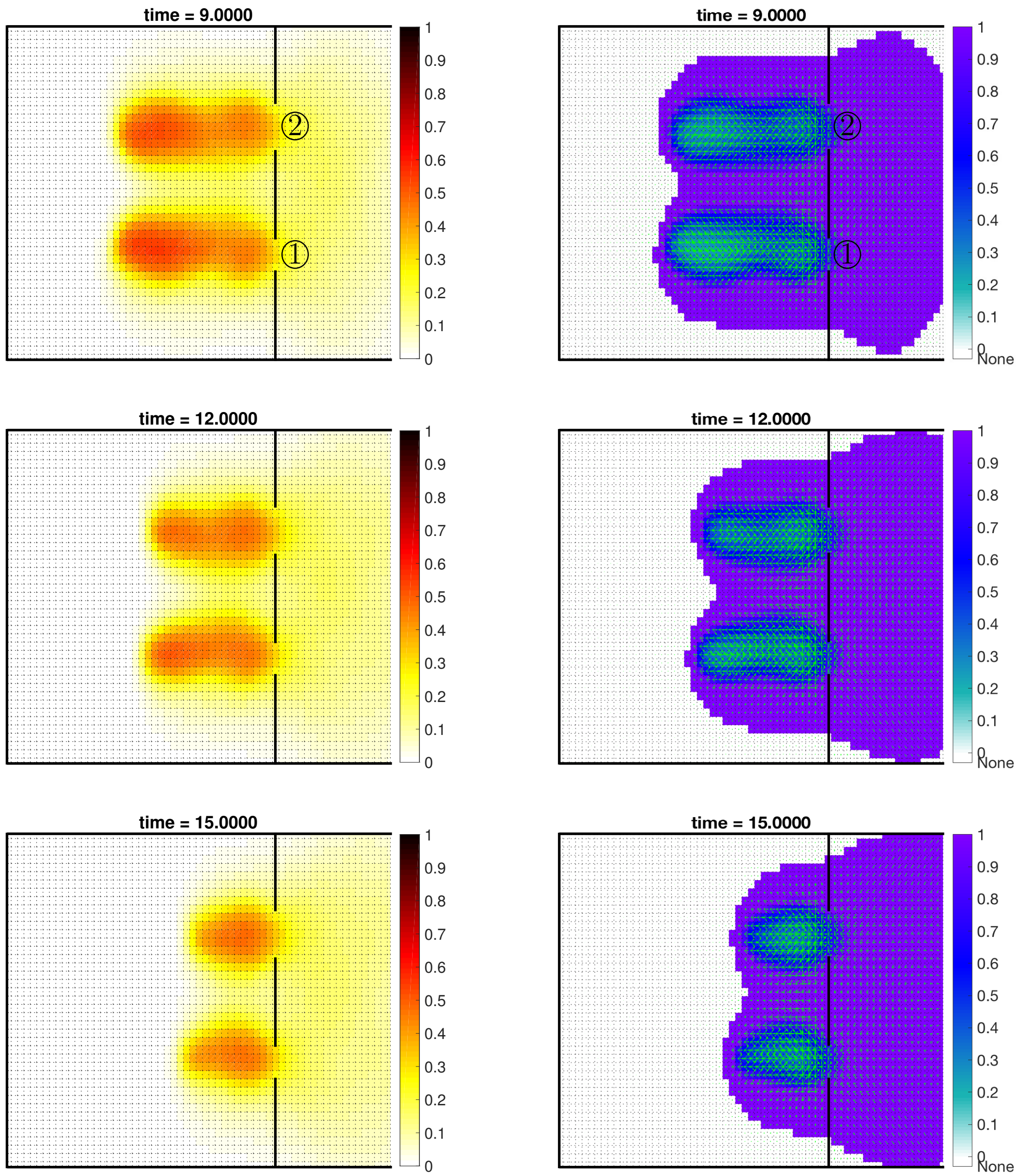

Figure 4.29: Evacuation process of 138 pedestrians in a 10 m × 10 m room for the orange velocity modulus: density (left) and velocity magnitude with selected velocity vectors (right) for $t = 9.00, 12.00$, and 15.00 s, respectively.

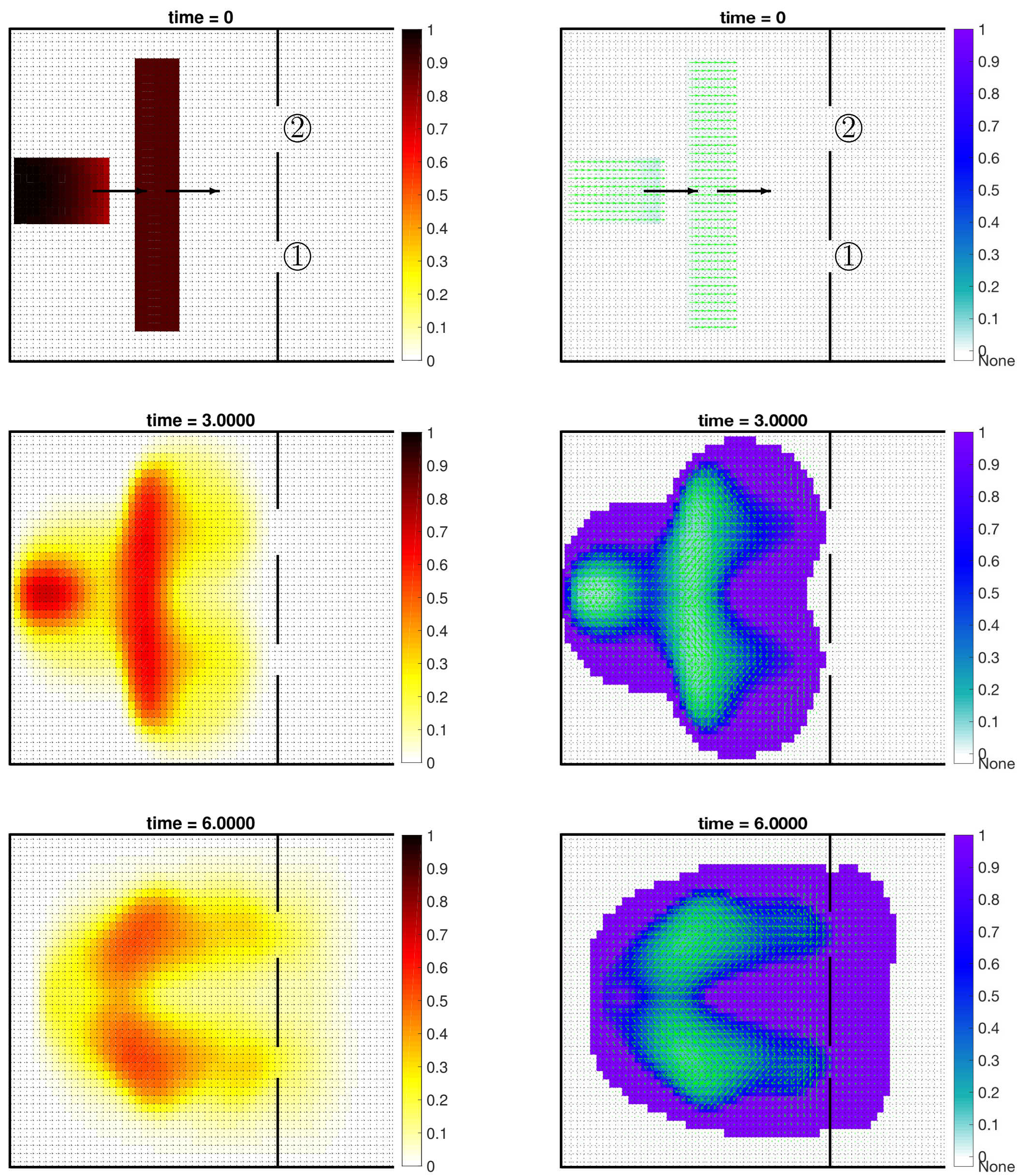

Figure 4.30: Evacuation process of 138 pedestrians in a 10 m × 10 m room for blue velocity modulus: density (left) and velocity magnitude with selected velocity vectors (right) for $t = 0, 3.00$, and 6.00 s, respectively.

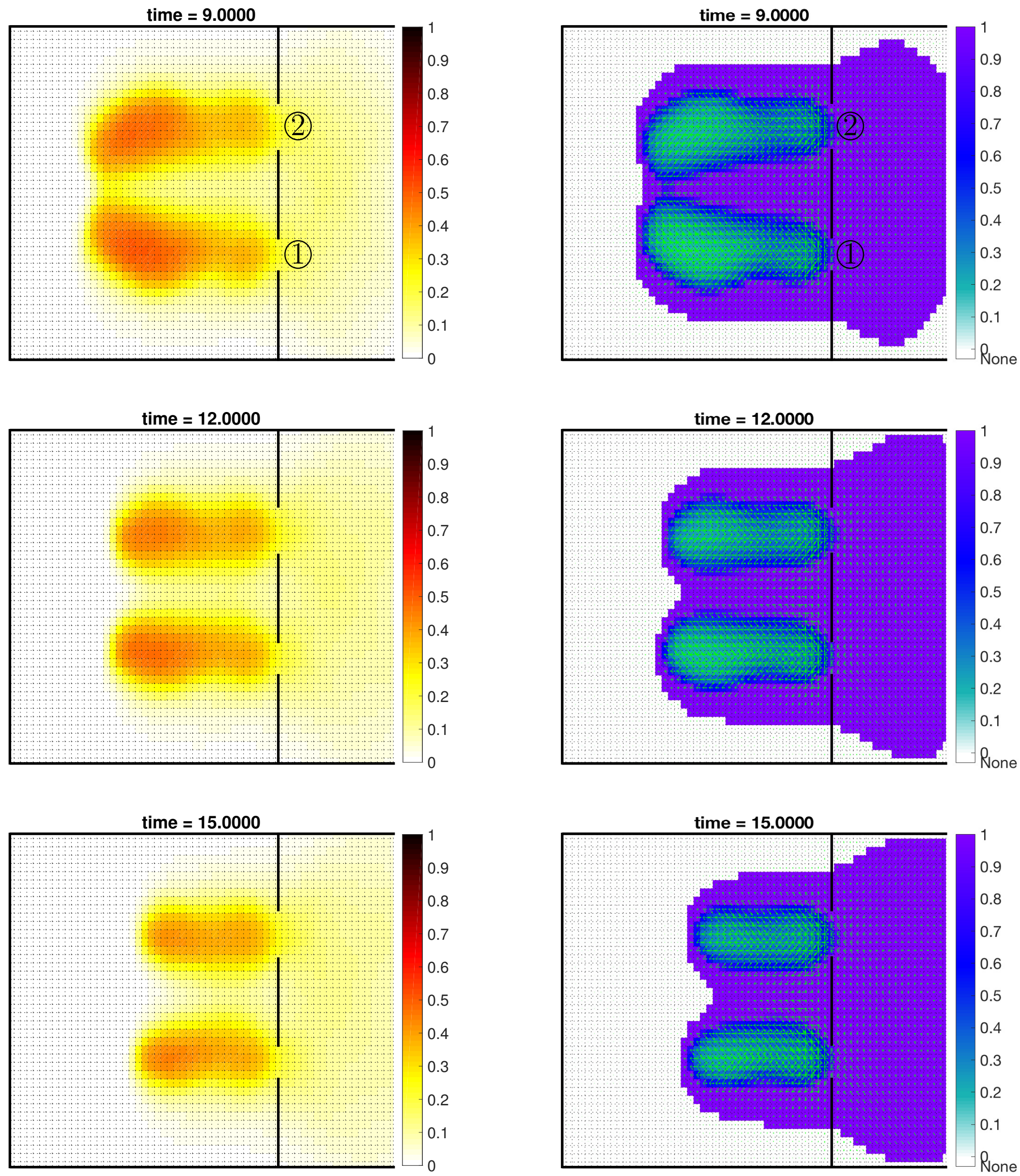

Figure 4.31: Evacuation process of 138 pedestrians in a 10 m × 10 m room for the blue velocity modulus: density (left) and velocity magnitude with selected velocity vectors (right) for $t = 9.00, 12.00$, and 15.00 s, respectively.

4.5.4 Initial positions and width ratios of two exits

In this section, we first compare two initial positioning of the pedestrians and see how that affects the overall evacuation. The first initial position is as in Figure 4.22. For the second, 40 pedestrians are placed close to the exit ①. Everything else is same as for the simulation whose results are shown in Figure 4.22. The computed density for the second initial positioning is displayed in Figure 4.32. We observe that even though the closest exit to the initial position is the exit ①, some pedestrians change the direction and head to the exit ②.

Next, let us investigate the relationship between evacuation time and the width ratio of the two exits. We fix the size and position of exit ①. Also, the position of the center of exit ② is fixed, but not size. The other conditions are exactly same as for the results in Figure 4.22. In the top left panel of Figure 4.33 we report the table of width ratios under consideration, which vary in the interval [1, 4].

Figure 4.33 and 4.34 show the distributions of 40 and 138 pedestrians, respectively, at a fixed time and for five different width ratios. One can observe that when the ratio of exit ② width/exit ① width increases, the total evacuation time decreases. Since pedestrians search for the less crowded path, the larger the ratio is, the greater is the number of pedestrians that are heading to exit ②.

4.6 Lane formation

This section is aimed at reproducing numerically a phenomenon that is observed in practice: formation of lanes when groups of pedestrians have opposite walking

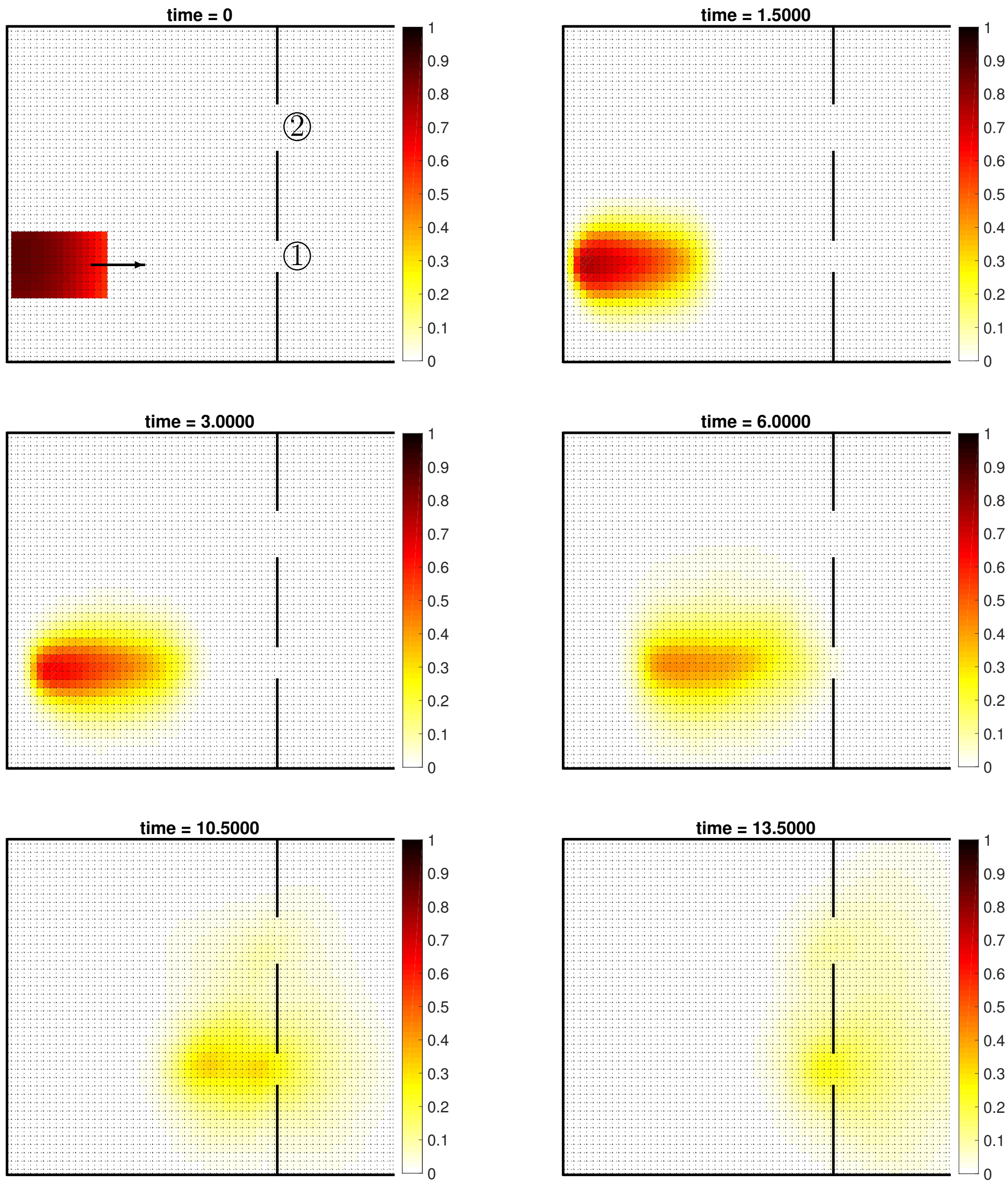

Figure 4.32: Evacuation process of 40 pedestrians initially placed near the exit ① in a 10 m × 10 m room.

Exit ② (m)	Ratio of Exit②/ Exit①
0.7	1
1.1	1.5714
1.4	2
2.1	3
2.8	4

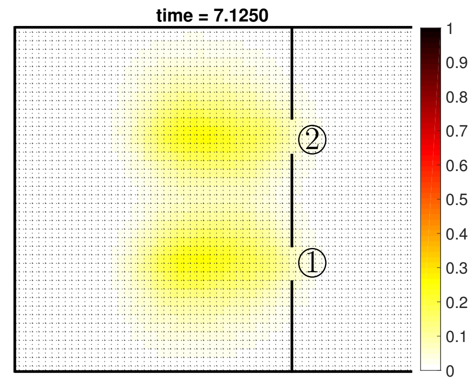

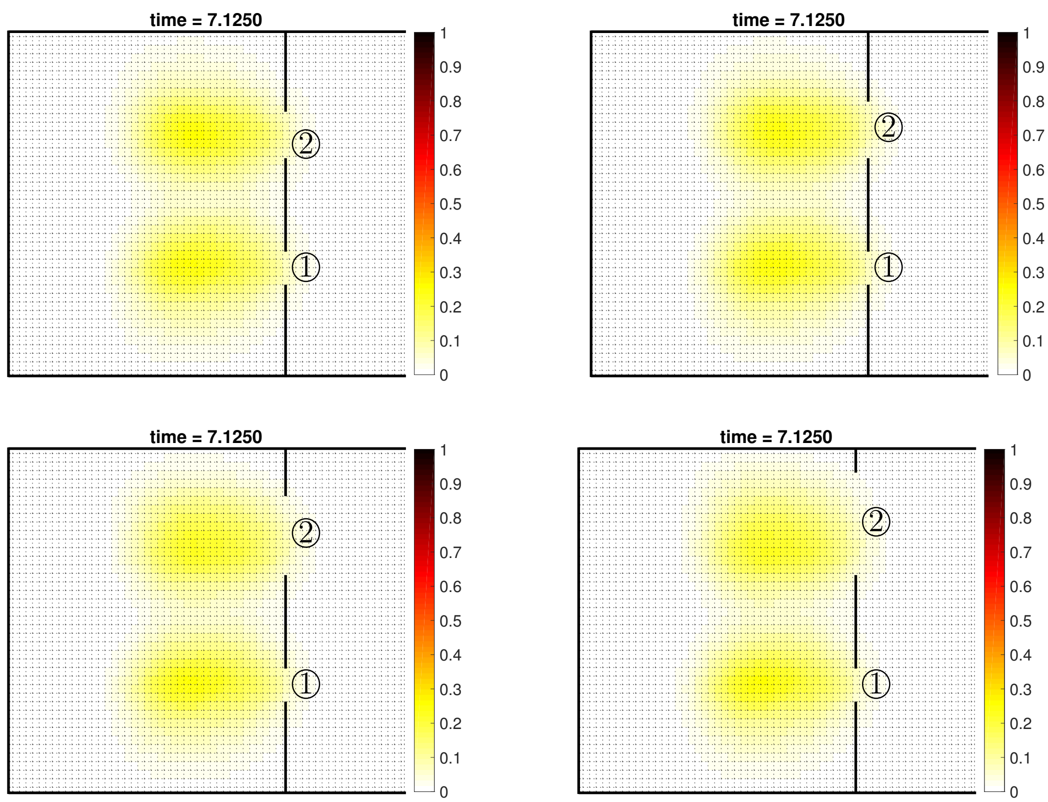

Figure 4.33: Table of the ratios of exit ② width/exit ① width and distributions of 40 pedestrians in a 10 m × 10 m room when exit ① for five different ratios at time $t = 7.1250$ s.

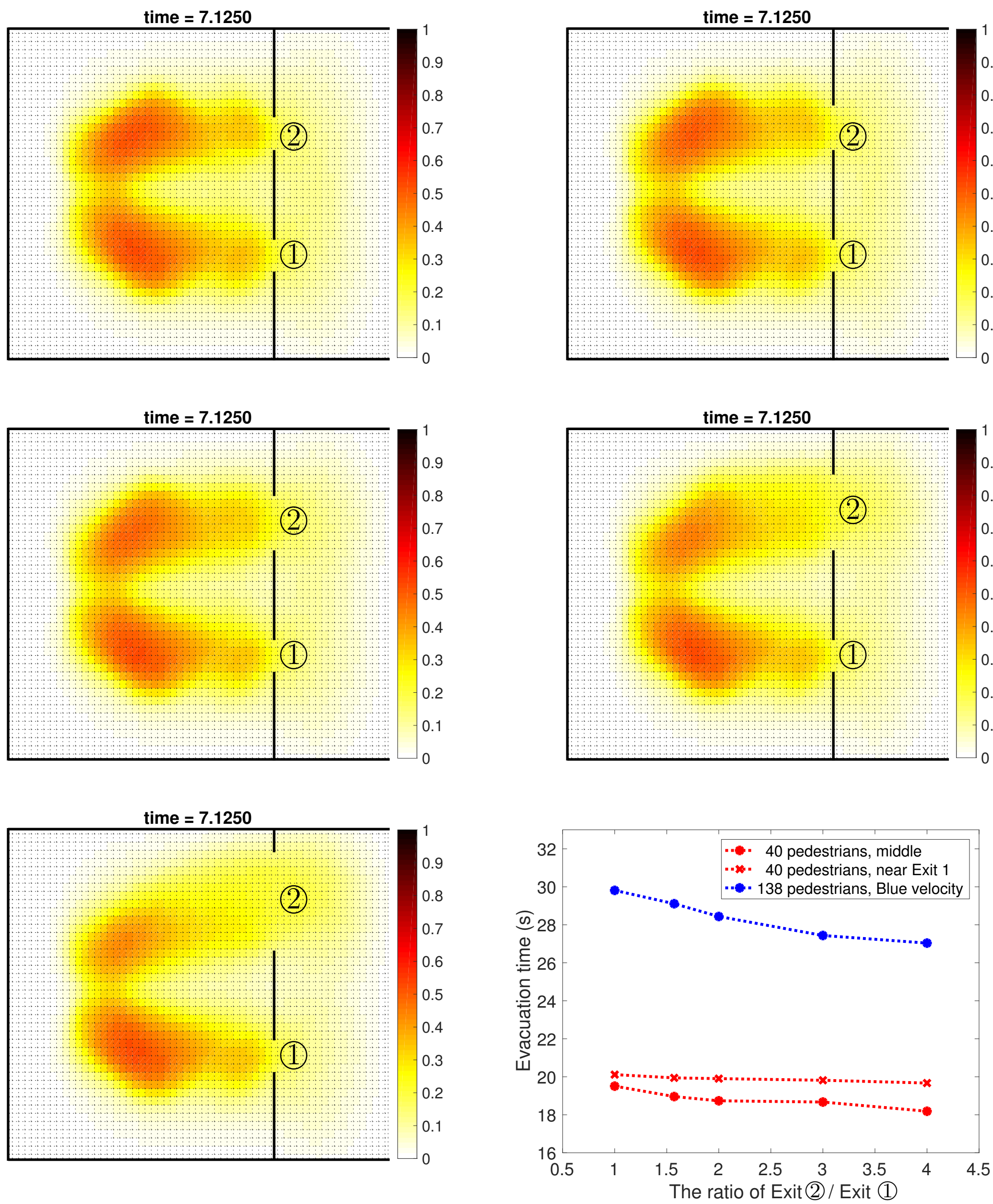

Figure 4.34: Distributions of 138 pedestrians in a 10 m × 10 m room for five different width ratios at time $t = 7.1250$ s and evacuation times for different initial positions and width ratios.

directions [28].

We consider the periodic corridor Ω of length L=20 m and width H=5 m. The diameter, the highest velocity modulus and the maximum admissible number of pedestrians per unit area are set to: $D = 5\sqrt{17}$ m, $V_M = 2$ m/s, and $\rho_M = 7$ per/m^2, respectively. The reference time is $T_M = 5\sqrt{17}/2$ s. These quantities are used to switch to dimensionless quantities as described in Section 2.1.

We consider a mesh with $\Delta x = \Delta y$=0.2 m and the time step $\Delta t = 0.3$ s. Pedestrians are initially distributed into four equal-area rectangular clusters moving with opposite initial directions θ_1 and θ_5. Figure 4.35 and 4.36 show the movement process of 98 and 188 pedestrians in the periodic corridor, respectively. Movement in opposite directions can lead to collisions. So pedestrians try to avoid contact by changing the direction, which leads to sorting and separation. From this, the lane formation emerges.

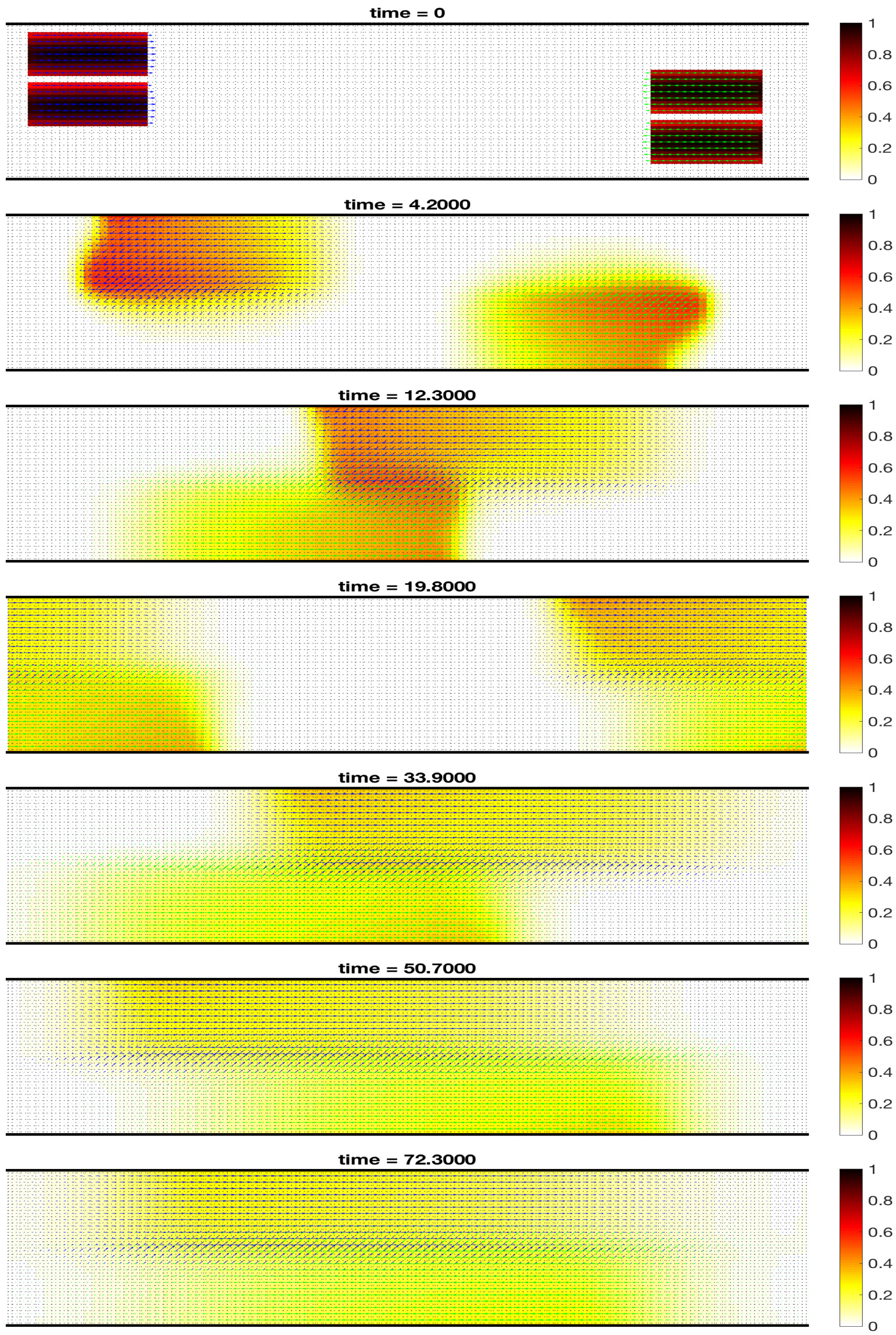

Figure 4.35: The movement process of 98 pedestrians grouped into four clusters with opposite initial direction θ_1 and θ_5 in the 20 m $\times$ 5 m periodic corridor for $t = 0, 4.20, 12.30, 19.80, 33.90, 50.70,$ and 72.30 s, respectively. The color refers to density.

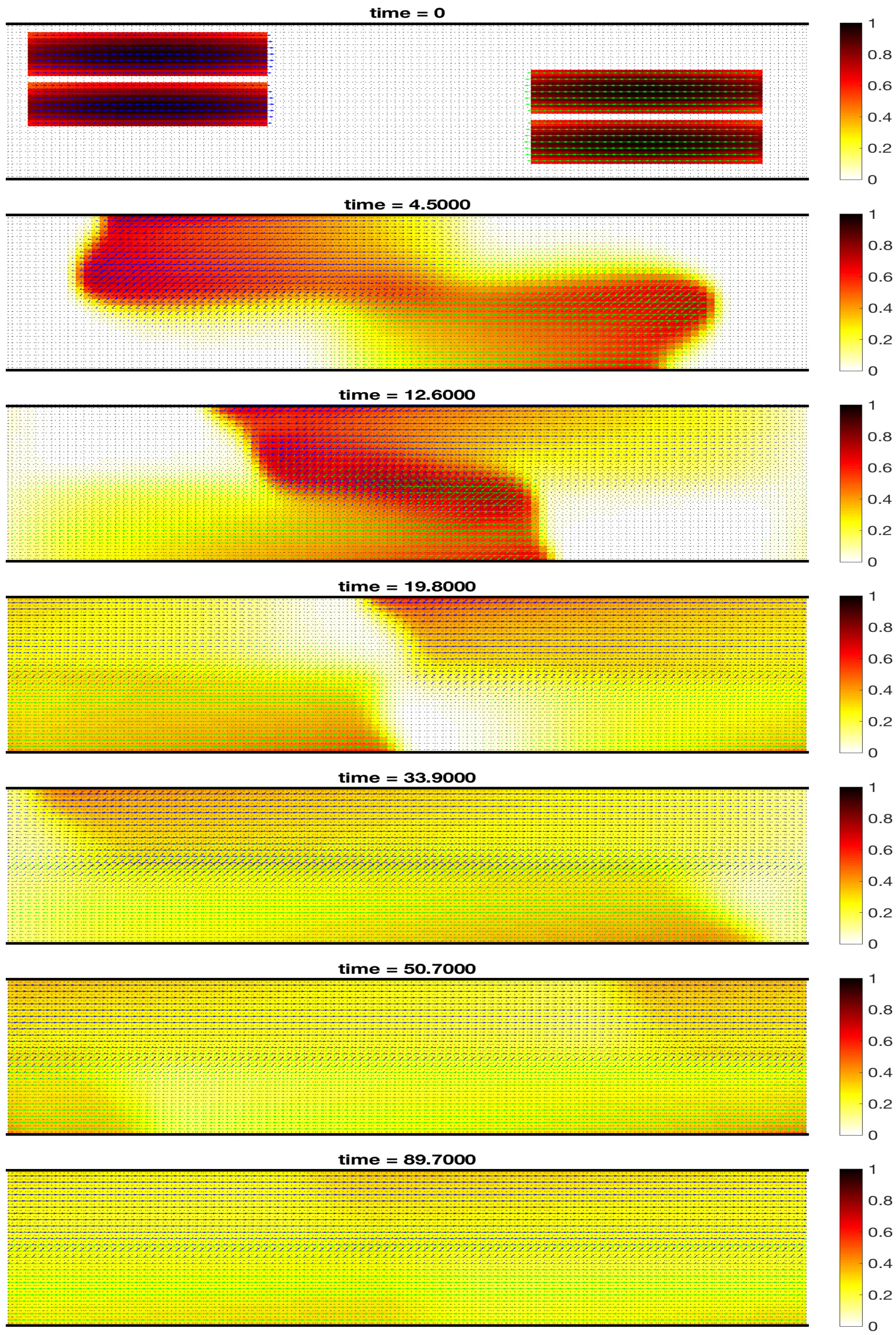

Figure 4.36: The movement process of 188 pedestrians grouped into four clusters with initial opposite direction θ_1 and θ_5 in the 20 m $\times$ 5 m periodic corridor for $t = 0, 4.50, 12.60, 19.80, 33.90, 50.70,$ and 89.70 s, respectively. The color refers to density.

Chapter 5

Contagion Model

In this chapter, we focus on a pedestrian model known as ASCRIBE [17]. This model has the interesting feature of tracking the level of fear within the individual agents, which is assumed to influence their motion. ASCRIBE has been implemented in agent-based simulation tool ESCAPES [48] that has been used to model evacuation scenarios at the International Terminal at Los Angele International Airport. Also, ASCRIBE has compared favorably to actual crowd footage of a video of Amsterdam crowd scene and recent protests in Greece relative to other pedestrian model, such as Base Models, ESCAPES, Durupinar model, in [47]. In [14], a mathematical analysis of the ASCRIBE model through particle, continuum, and kinetic descriptions was developed. In [51], two efficient numerical methods for a multi-scale kinetic equation with emotional contagion of ASCRIBE are presented. The emotional contagion model assumes that the velocity is proportional to the fear level [51], which means that agents will run faster if more scared, see also [7, 9].

5.1 Fear contagion dynamics

In this section, we briefly review the model of contagion dynamics in one dimension taken from [51]. We start with the agent-based model at the microscopic level reads

$$\frac{dx_m}{dt} = v_m = q_m; \quad \frac{dq_m}{dt} = \gamma(q_m^* - q_m); \quad q_m^* = \frac{\sum_{j=1}^{N_a} \kappa_{m,j} q_j}{\sum_{j=1}^{N_a} \kappa_{m,j}}, \quad m = 1, 2, 3, \ldots, N_a, \tag{5.1}$$

where each particle m represent a pedestrian, and $x_m(t)$, $v_m(t)$ and $q_m(t)$ are its position, velocity and fear contagion level, respectively. Here we assume that velocity is proportional to fear level, which means that agents will walk faster if more scared. The quantity q_m^* is the local "average" contagion level weighted by the distance to x and N_a is the total number of particles. In Equation (5.1), $\kappa_{m,j} = \kappa(|x_m - x_j|)$ is the interaction kernel, which serves as the weights in the average q_m^*. The interaction kernel κ is a decreasing function of the mutual distance between two particles and is parametrized by an interaction distance R, where x_m and x_j are positions in the domain L. Parameter γ describes the contagion interaction strength and it may vary with the particle for more general cases. The model works as follows: if γ is 0, there will be no contagion, if γ is not 0, there will be contagion and the higher the value, the more contagion will take place.

The microscopic system (5.1) is often too expensive to compute as N_a becomes large, in which case one needs to consider the kinetic level. Denote the empirical distribution density by

$$h^{N_a} = \frac{1}{N_a} \sum_{m=1}^{N_a} \delta(x - x_m(t))\delta(q - q_m(t)),$$

where δ is Dirac delta function. We assume that the particles remain in a fixed compact domain $(x_m(t), q_m(t)) \in \Omega \subset \mathbb{R}^2$ for all m and up to the time we consider.

Then Prohorov's theorem in [17] implies that the sequence $\{h^{N_a}\}$ is weakly * relatively compact. Therefore, there exists a subsequence $\{h^{N_k}\}_k$ such that h^{N_k} converges to h with *weak** -convergence in $\mathcal{P}(\mathbb{R}^2)$ and pointwisely in time as $k \to \infty$. Here $\mathcal{P}(\mathbb{R}^2)$ denotes the space of probability measure on $\mathbb{R}^2$. Now considering a test function $\psi \in C_0^1(\mathbb{R}^2)$, we have

$$\begin{aligned}
\frac{d}{dt}\langle h^{N_a}, \psi\rangle_{x,q} &= \frac{d}{dt}\left\langle \frac{1}{N_a}\sum_{m=1}^{N_a} \delta(x - x_m(t))\delta(q - q_m(t)), \psi \right\rangle_{x,q} \\
&= \frac{d}{dt}\frac{1}{N_a}\sum_{i=1}^{N_a} \psi(x_m(t), q_m(t)) \\
&= \frac{1}{N_a}\sum_{m=1}^{N_a} \psi_x q_m + \psi_q \gamma(q_m^* - q_m) \\
&= \langle \psi_x q_m, h^{N_a}\rangle + \frac{\gamma}{N_a}\sum_{m=1}^{N_a} \psi_q\left(\frac{\sum_{j=1}^{N_a}\kappa_{m,j}q_j}{\sum_{j=1}^{N_a}\kappa_{m,j}} - q_m\right). \qquad (5.2)
\end{aligned}$$

Here $\langle\cdot\rangle_{x,q}$ means integration against both x and q, and $\langle\cdot\rangle_x$ means integration only in x. Further,

$$\frac{1}{N_a}\sum_{m=1}^{N_a} \kappa(|x_m - x_j|) = \left\langle \kappa(|x_m - y|), \frac{1}{N_a}\sum_{j=1}^{N_a}\delta(y - x_j)\right\rangle_x = \kappa * \rho_{h_{N_a}}(x_m),$$

$$\frac{1}{N_a}\sum_{m=1}^{N_a} \kappa(|x_m - x_j|)q_j = \left\langle \kappa(|x_m - y|), \frac{1}{N_a}\sum_{j=1}^{N_a}\delta(y - x_j)q_j\right\rangle_x = \kappa * m_{h_{N_a}}(x_m),$$

where we have used the definitions

$$\rho_{h^{N_a}}(x) = \frac{1}{N_a}\sum_{m=1}^{N_a}\delta(x - x_m)$$

and

$$m_{h^{N_a}}(x) = \left\langle q, \frac{1}{N_a}\sum_{j=1}^{N_a}\delta(x - x_j)\delta(q - q_j)\right\rangle_{x,q} = \frac{1}{N_a}\sum_{j=1}^{N_a}\delta(x - x_j)q_j.$$

Then equation (5.2) reads

$$\frac{d}{dt}\langle h^{N_a},\psi\rangle_{x,q} = \langle \psi_x q, h^{N_a}\rangle_{x,q} + \gamma\left\langle h^{N_a}, \frac{\kappa * m_{h^{N_a}}}{\kappa * \rho_{h^{N_a}}}\psi_q - q\psi_q\right\rangle_{x,q},$$

which leads to

$$h_t^{N_a} + (qh^{N_a})_x = \gamma((q-q^*)h^{N_a})_q, \tag{5.3}$$

via integration by parts.

Now letting $k \to \infty$, the subsequence h^{N_k} formally leads to the limiting kinetic equation

$$h_t + (qh)_x = \gamma((q-q^*)h)_q, \tag{5.4}$$

where $h(t,x,q)$ is the probability of finding people with contagion level q at time t and position x. The quantity $q^*(t,x)$ is the local *average* contagion level of fear weighted by the distance to x:

$$q^*(t,x) = \frac{\int\int \kappa(|x-y|)h(t,y,q)q\,dq\,dy}{\int\int \kappa(|x-y|)h(t,y,q)\,dq\,dy}. \tag{5.5}$$

Finally, we define the macroscopic bulk contagion level:

$$\tilde{q}(t,x) = \int h(t,x,q)q\,dq. \tag{5.6}$$

5.1.1 Space and velocity discretization

In this sections, we present the numerical discretization in time and space for the kinetic Equation (5.4). Divide the spatial and velocity domain into a number of cells $[x_{j-\frac{1}{2}}, x_{j-\frac{1}{2}}]$ and $[q_{l-\frac{1}{2}}, q_{l+\frac{1}{2}}]$, where $j \in 1,2,\ldots,N_x$ and $l \in 1,2,\ldots,N_q$. Here N_x and N_q are the total number of points in $x-$ and $q-$ directions, respectively. Each cell is centered at x_j or q_l with a uniform length Δx and Δq. Let us denote

$h_{j,l} = h(t, x_j, q_l)$ and $q_j^* = q^*(t, x_j)$, then a first-order semi-discrete upwind scheme of the kinetic equation (5.4) reads

$$\partial_t h_{j,l} + \frac{\eta_{j+\frac{1}{2},l} - \eta_{j-\frac{1}{2},l}}{\Delta x} + \gamma \frac{\xi_{j,l+\frac{1}{2}} - \xi_{j,l-\frac{1}{2}}}{\Delta q} = 0, \tag{5.7}$$

where

$$\eta_{j,l+\frac{1}{2}} = q_l h_{j,l}, \tag{5.8}$$

$$\begin{aligned} \xi_{j,l+\frac{1}{2}} &= \frac{|q_l^* - q_{l+\frac{1}{2}}| + (q_j^* - q_{l+\frac{1}{2}})}{2} h_{j,l} + \frac{(q_l^* - q_{l+\frac{1}{2}}) - |q_j^* - q_{l+\frac{1}{2}}|}{2} h_{j,l+1} \\ &:= \xi_{j,l}^+ + \xi_{j,l+1}^-. \end{aligned} \tag{5.9}$$

Here we have used edge-values for the velocity discretization and $q_{l+\frac{1}{2}} = (q_l + q_{l+1})/2$. We compute q_j^* using a midpoint rule for the integral (5.5), i.e.,

$$q_j^* = \frac{\sum_{m,l} \kappa(|x_j - x_m|) h_{m,l} q_l \Delta x \Delta q}{\sum_{m,l} \kappa(|x_j - x_m|) h_{m,l} \Delta x \Delta q}. \tag{5.10}$$

To construct a second-order scheme in velocity, we add a flux limiter. Then equation (5.7) is modified to

$$\partial_t h_{j,l} + \frac{\eta_{j+\frac{1}{2},l} - \eta_{j-\frac{1}{2},l}}{\Delta x} + \gamma \frac{\xi_{j,l+\frac{1}{2}} - \xi_{j,l-\frac{1}{2}}}{\Delta q} + \gamma \frac{C_{j,l+\frac{1}{2}} - C_{j,l-\frac{1}{2}}}{\Delta q} = 0, \tag{5.11}$$

where $C_{j,l+\frac{1}{2}}$ is the corrector defined as

$$C_{j,l+\frac{1}{2}} = \frac{1}{2} |s_{j,l+\frac{1}{2}}| \left(1 - \frac{\Delta t}{\Delta q} |s_{j,l+\frac{1}{2}}|\right) \tilde{W}_{j,l+\frac{1}{2}}, \tag{5.12}$$

with

$$s_{j,l-\frac{1}{2}} = q_j^* - q_{l-\frac{1}{2}}, \quad W_{j,l-\frac{1}{2}} = h_{j,l} - h_{j,l-\frac{1}{2}}, \quad \tilde{W}_{j,l-\frac{1}{2}} = W_{j,l-\frac{1}{2}} \varphi\left(\frac{W_{j,\mathbf{b}-\frac{1}{2}}}{W_{j,l-\frac{1}{2}}}\right). \tag{5.13}$$

The subscript **b** is l-1 if $s_{j,l-\frac{1}{2}} > 0$ and l+1 if $s_{j,l-\frac{1}{2}} < 0$. Here φ is the slope limiter function such as the Van Leer function in [34],

$$\varphi(\theta) = \frac{|\theta| + \theta}{1 + |\theta|}. \tag{5.14}$$

5.1.2 Numerical results

We validate our implementation of the scheme presented in the previous section with a test case taken from [51]. The computational domain in the xq-plane is $[-10, 10] \times [0, 3]$. Also, N_x and N_q denote the number of points in x- and q-direction, respectively. The time step Δt is chosen as

$$\Delta t = \frac{1}{2} \min \left\{ \frac{\Delta x}{q_{max}}, \frac{\Delta q}{2 q_{max} \gamma} \right\}$$

to satisfy the Courant-Friedrichs-Lewy (CFL) condition, where $q_{max} = max_j q_j$.

The delta function in the kinetic scheme is approximated by

$$\delta(q) \sim E(q) = \frac{1}{\sqrt{\pi} R_0} e^{-\frac{q^2}{R_0^2}}, \quad R_0 = 0.04 \tag{5.15}$$

and Δq is small enough to resolve it. The interaction kernel takes the from

$$\kappa(x) = \frac{R}{(x^2 + R^2)\pi}, \tag{5.16}$$

where R is an interaction distance. In a dense crowd setting, it is reasonable to assume a relatively small interaction radius and a rather quick interaction strength.

Thus, it is natural to consider the case in which $R \to 0$ and $\gamma \to \infty$. Let us further suppose that as we approach these limiting values, the quantity $R\gamma = C$ remains fixed, so that we can use the results of Theorem 1 from [14] to determine if two particles may cross paths upon meeting. Since $R \to 0$, the particles will not interact until they are within distance R of each other for any non-zero initial spacing. When two particles are placed in the same initial position, we define that Q_L and Q_R are the largest and smallest value of q, respectively. Specifically, Theorem 1 in [14] tells us that if the greatest difference in emotion between two particles $\Delta Q = Q_L - Q_R$, satisfies $\Delta Q \le 2C$, particle paths will never cross, while if $\Delta Q > 2C$, particle paths may cross. Bigger values of γ give faster convergence rates, i.e. the disease contagion level q is inversely proportional to R.

We define the following reference quantities:

- $Q_L = 2.5$
- $Q_R = 1.5$
- $\gamma = 100$
- $R = 0.0002$

We consider a mesh with $\Delta x = 0.02$ m, $\Delta q = 0.02$, and $\Delta t = 0.001$ s. We set the initial conditions following [51].

$$\rho_I(0,x) = \sin\left(\frac{\pi x}{10}\right) + 2, \quad v_I(0,x) = \frac{1}{2}\Big(3 - \tanh x\Big),$$

$$h_I(x,q) = \rho_I(x)\left(\frac{1}{4}\,E(q - q_I(x) - 0.5) + \frac{3}{4}\,E(q - q_I(x) + 0.3)\right). \tag{5.17}$$

See Figure 5.1. Notice that $h_I(x,q)$ has two bumps in q for every x, as displayed in the Figure 5.1, left plots. As time passes, $h(t,x,q)$ starts to concentrate on $\tilde{q}(t,x)$,

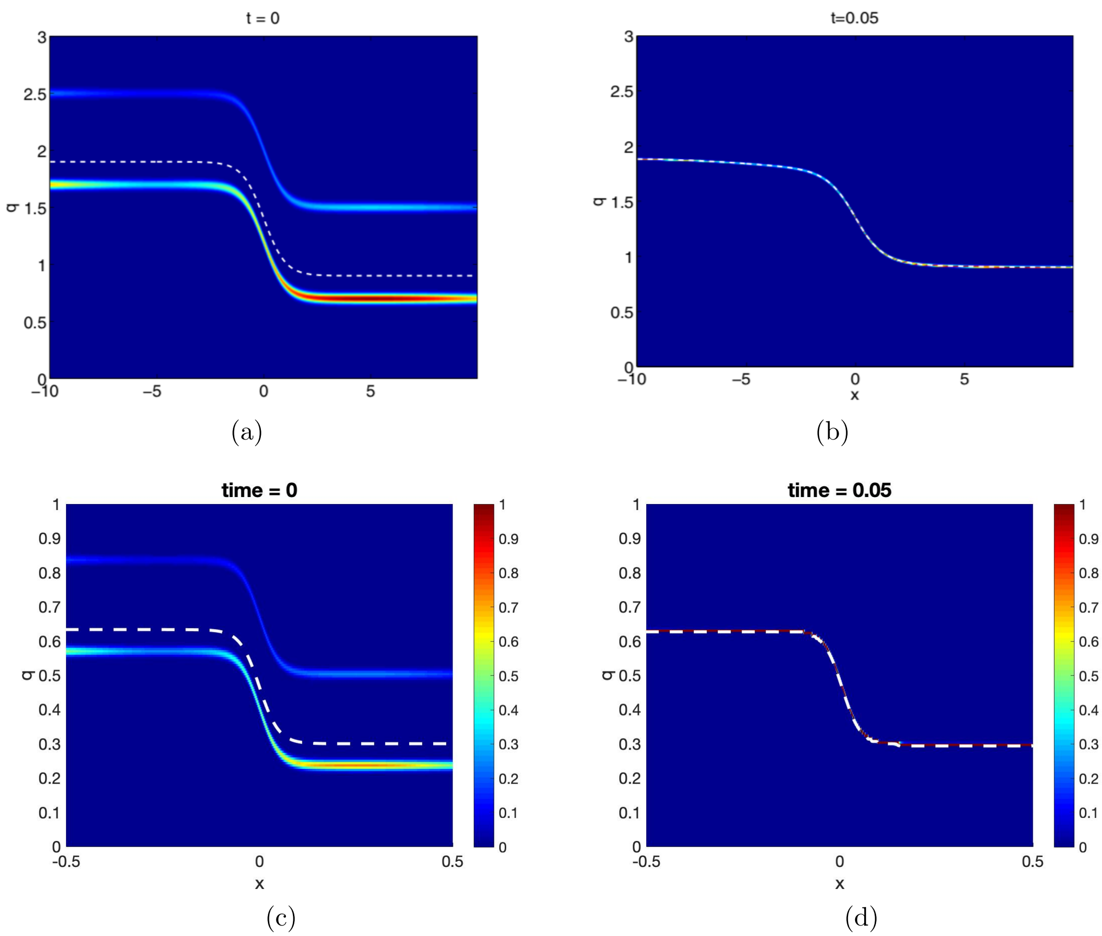

Figure 5.1: (a) Plot of $h(t, x, q)$ at $t = 0$ s and (b) at $t = 0.05$ s from [51], and (c) Plot of $h(t, x, q)$ at $t = 0$ s and (d) at $t = 0.05$ s from our simulation. The white dash line represents $\tilde{q}(t, x)$ and the color represents the probability of finding people.

as confirmed by Figure 5.1. Our results are in very good agreement with the results reported in [51].

5.1.3 Influence of the parameters γ and R

In the model (5.4), the quantity $R\gamma = C$ is fixed, where R is an interaction distance and γ is the contagion interaction strength. In this section, we are interested in looking at how the evolution of $h(t, x, q)$ changes by decreasing parameter γ and increasing parameter R at the same time, while keeping C fixed. Now, we fix $C = 0.02$ and take two cases below:

a) $\gamma = 10$, $R = 0.002$.

b) $\gamma = 1$, $R = 0.02$.

All other initial data are set in the same way as for the results in Figure 5.1.

The case a) is shown in Figure 5.2. It takes more time to concentrate on $\tilde{q}(t, x)$ by decreasing γ (and increasing R). See Figure 5.3 for the case b). It takes even longer than case a) to concentrate on $\tilde{q}(t, x)$. Moreover, after $t = 1$ s, $h(t, x, q)$ does not change substantially.

5.2 Disease contagion model

In this section, we investigate the relationship between velocity and disease contagion level. We assume that velocity modulus decreases when the disease contagion level increases, which means that pedestrians will walk slower if they get infected. Notice that this is the opposite of what happens in the case of emotional contagion. At the

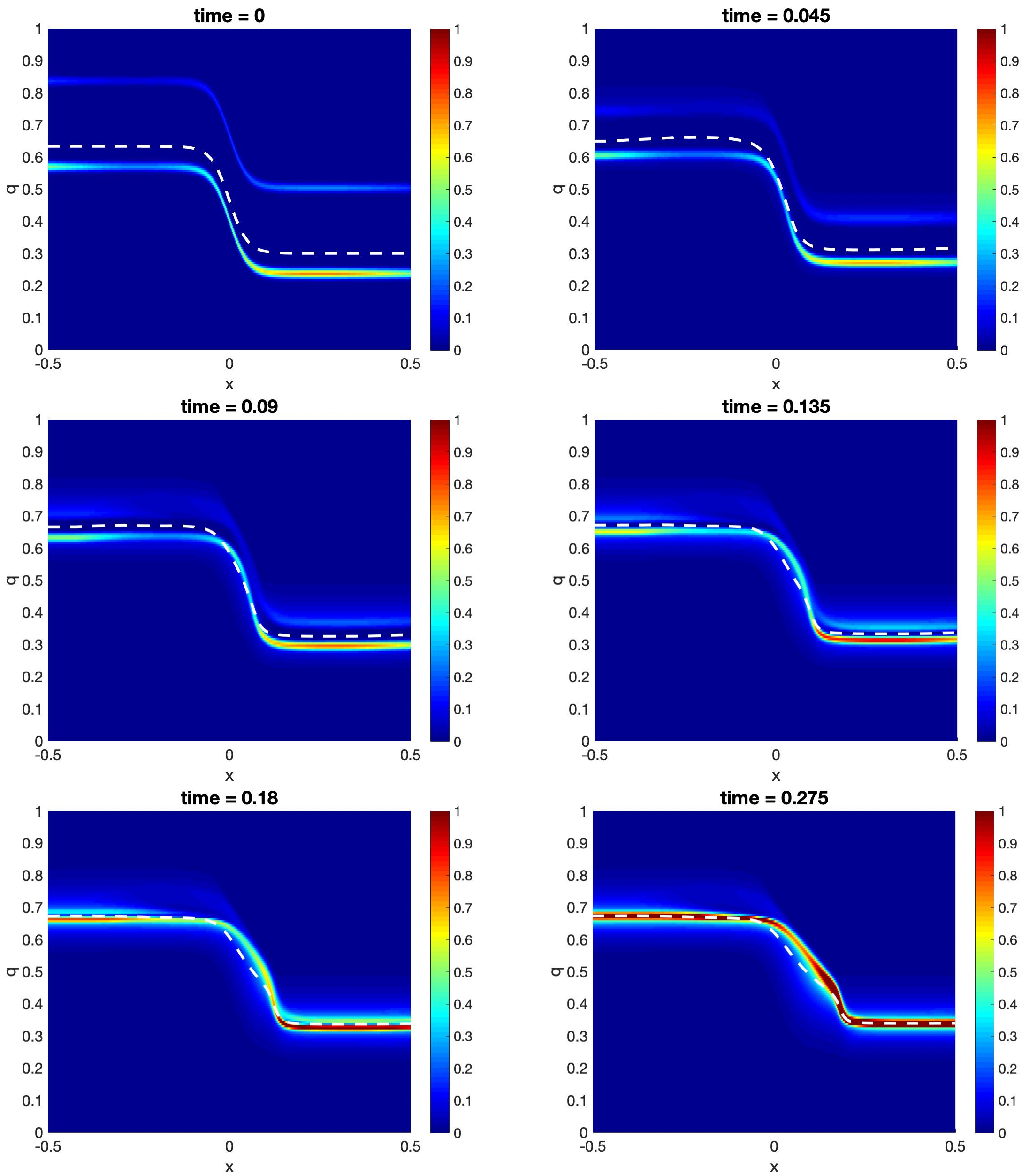

Figure 5.2: case a): Plots of $h(t,x,q)$ for $\gamma = 10$ and $R = 0.002$ at $t = 0, 0.045, 0.09, 0.135, 0.18,$ and 0.275 s, respectively. The white dash line represents $\tilde{q}(t,x)$ and the color represents the probability of finding people.

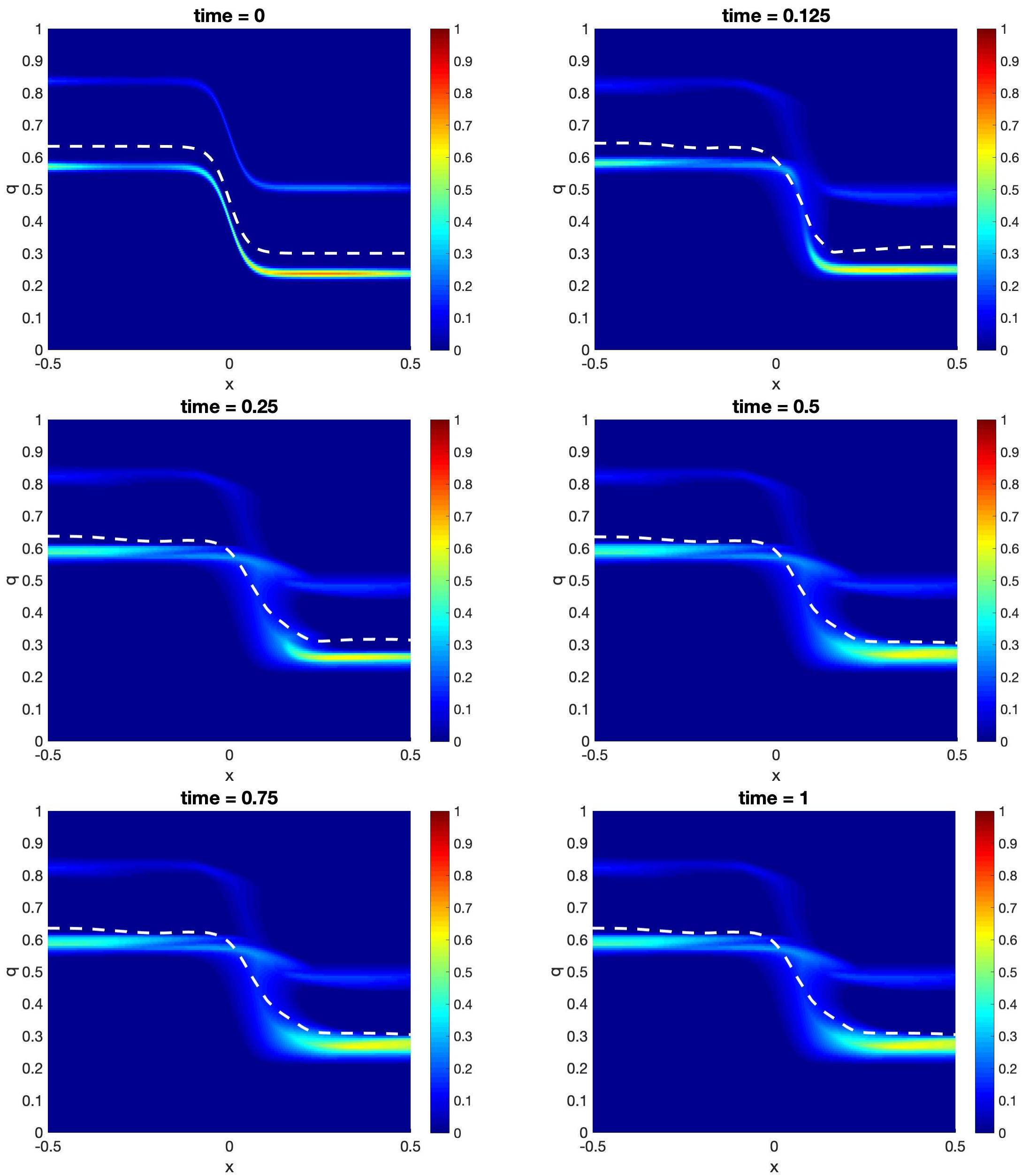

Figure 5.3: case b): Plots of $h(t, x, q)$ for $\gamma = 1$ and $R = 0.02$ at $t = 0, 0.125, 0.25, 0.05, 0.75$, and 1 s, respectively. The white dash line represents $\tilde{q}(t, x)$ and the color represents the probability of finding people.

microscopic level, we have:

$$\frac{dx_m}{dt} = v_m; \quad \frac{dq_m}{dt} = \gamma(q_m^* - q_m); \quad q_m^* = \frac{\sum_{j=1}^{N_a} \kappa_{m,j} q_j}{\sum_{j=1}^{N_a} \kappa_{m,j}}, \quad m = 1, 2, 3, \dots, N_a, \tag{5.18}$$

Notice that the only difference with respect to equation (5.1) is that $v_m \neq q_m$. Following the same procedure used to get equation (5.2) , we obtain

$$\begin{aligned}
\frac{d}{dt}\langle h^{N_a}, \psi\rangle_{x,q} &= \frac{d}{dt}\left\langle \frac{1}{N_a}\sum_{m=1}^{N_a} \delta(x - x_m(t))\delta(q - q_m(t)), \psi \right\rangle_{x,q} \\
&= \frac{d}{dt}\frac{1}{N_a}\sum_{i=1}^{N_a} \psi(x_m(t), q_m(t)) \\
&= \frac{1}{N_a}\sum_{m=1}^{N_a} \psi_x v_m + \psi_q \gamma(q_m^* - q_m) \\
&= \langle \psi_x v_m, h^{N_a}\rangle + \frac{\gamma}{N_a}\sum_{m=1}^{N_a} \psi_q \left(\frac{\sum_{j=1}^{N_a} \kappa_{m,j} q_j}{\sum_{j=1}^{N_a} \kappa_{m,j}} - q_m \right).
\end{aligned} \tag{5.19}$$

Similairly, equation (5.19) leads to

$$h_t + (vh)_x = \gamma((q - q^*)h)_q, \tag{5.20}$$

We are going to consider dimensionless quantities, like we did for the pedestrian dynamics case. We consider the following two velocity moduli

c) $v_1 = 1 - q$;

d) $v_2 = (1 - q)^2$.

See Figure 5.4, which shows how the velocity v varies with the contagion level q in the two cases.

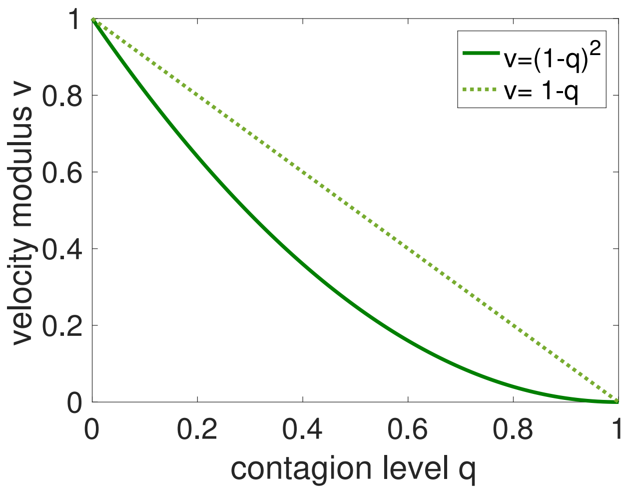

Figure 5.4: Contagion level q vs velocity modulus v.

5.2.1 Space and velocity discretization

We are considering the same approach as in Section 5.1.1. the only difference with respect to equations (5.9), (5.11), and (5.12) is that we replace q_l to v_l.

$$\partial_t h_{j,l} + \frac{\eta_{j+\frac{1}{2},l} - \eta_{j-\frac{1}{2},l}}{\Delta x} + \gamma \frac{\xi_{j,l+\frac{1}{2}} - \xi_{j,l-\frac{1}{2}}}{\Delta q} + \gamma \frac{C_{j,l+\frac{1}{2}} - C_{j,l-\frac{1}{2}}}{\Delta q} = 0, \tag{5.21}$$

where

$$\eta_{j,l+\frac{1}{2}} = v_l h_{j,l}, \quad \xi_{j,l+\frac{1}{2}} = \xi^+_{j,l} + \xi^-_{j,l+1}, \tag{5.22}$$

and

$$C_{j,l+\frac{1}{2}} = \frac{1}{2}|s_{j,l+\frac{1}{2}}| \left(1 - \frac{\Delta t}{\Delta q}|s_{j,l+\frac{1}{2}}|\right) \tilde{W}_{j,l+\frac{1}{2}}. \tag{5.23}$$

5.2.2 Numerical results

The computational domain corresponds to the setting studied in Figure 5.1.

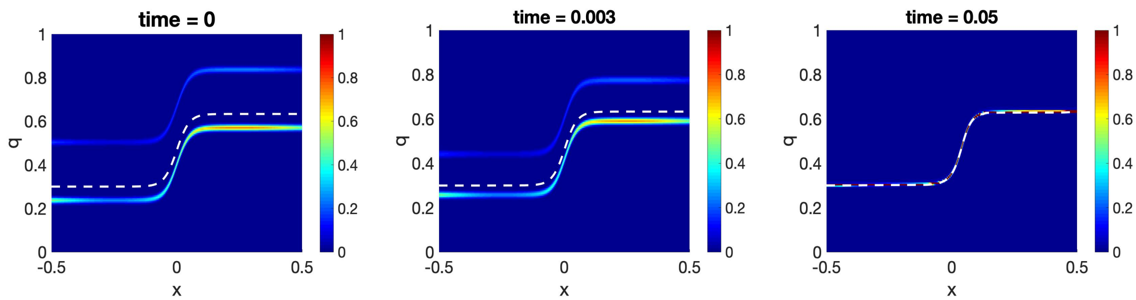

(a) case c)

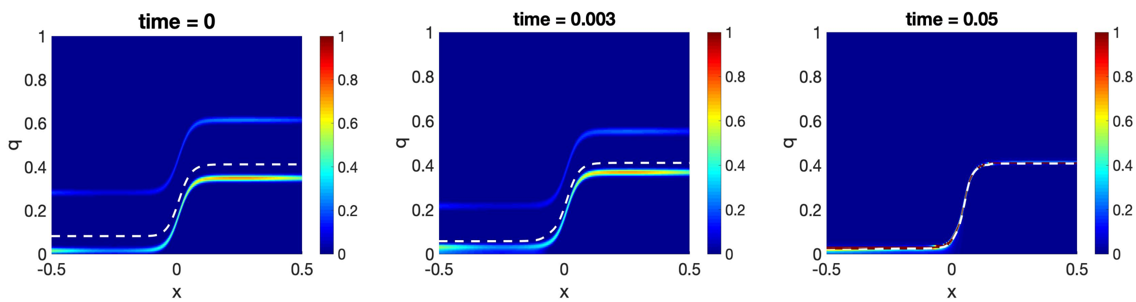

(b) case d)

Figure 5.5: Plots of $h(t, x, q)$ with (a) velocity v_1 and (b) v_2, for $t = 0, 0.003$, and 0.05 s, respectively. The white line represents $\tilde{q}(t, x)$ and the color represents the probability of finding people.

c) $v_1 = 1 - q$;

d) $v_2 = (1 - q)^2$.

And other initial data are same with Figure 5.1. The case c) has an ininital velocity v_{I_1}

$$v_{I_1}(0, x) = 3 - \frac{1}{2}\Big(3 - \tanh x\Big), \tag{5.24}$$

and the case d) has an initial velocity v_{I_2}

$$v_{I_2}(0, x) = \left(\sqrt{3} - \frac{1}{2\sqrt{3}}(3 - \tanh x)\right)^2. \tag{5.25}$$

See Figure 5.5 for the evolution of the solution in both cases. Like in Figure 5.1,

h matches well with $\tilde{q}(t,x)$ at $t = 0.05$ s in both cases.

Finally, we consider the case of $\gamma = 10$ and $R = 0.002$ for both initial velocity moduli:

e) $\gamma = 10$, $R = 0.002$, and $v_1(t,x) = 1 - q(t,x)$.

f) $\gamma = 10$, $R = 0.002$, and $v_2(t,x) = \big(1 - q(t,x)\big)^2$.

Figure 5.6 and Figure 5.7 show case e) and f), respectively. Initially, $h(t,x,q)$ has two bumps in q for every x. As time passes, $h(t,x,q)$ concentrate on $\tilde{q}(t,x)$ as we have seen also in Section 5.1.3.

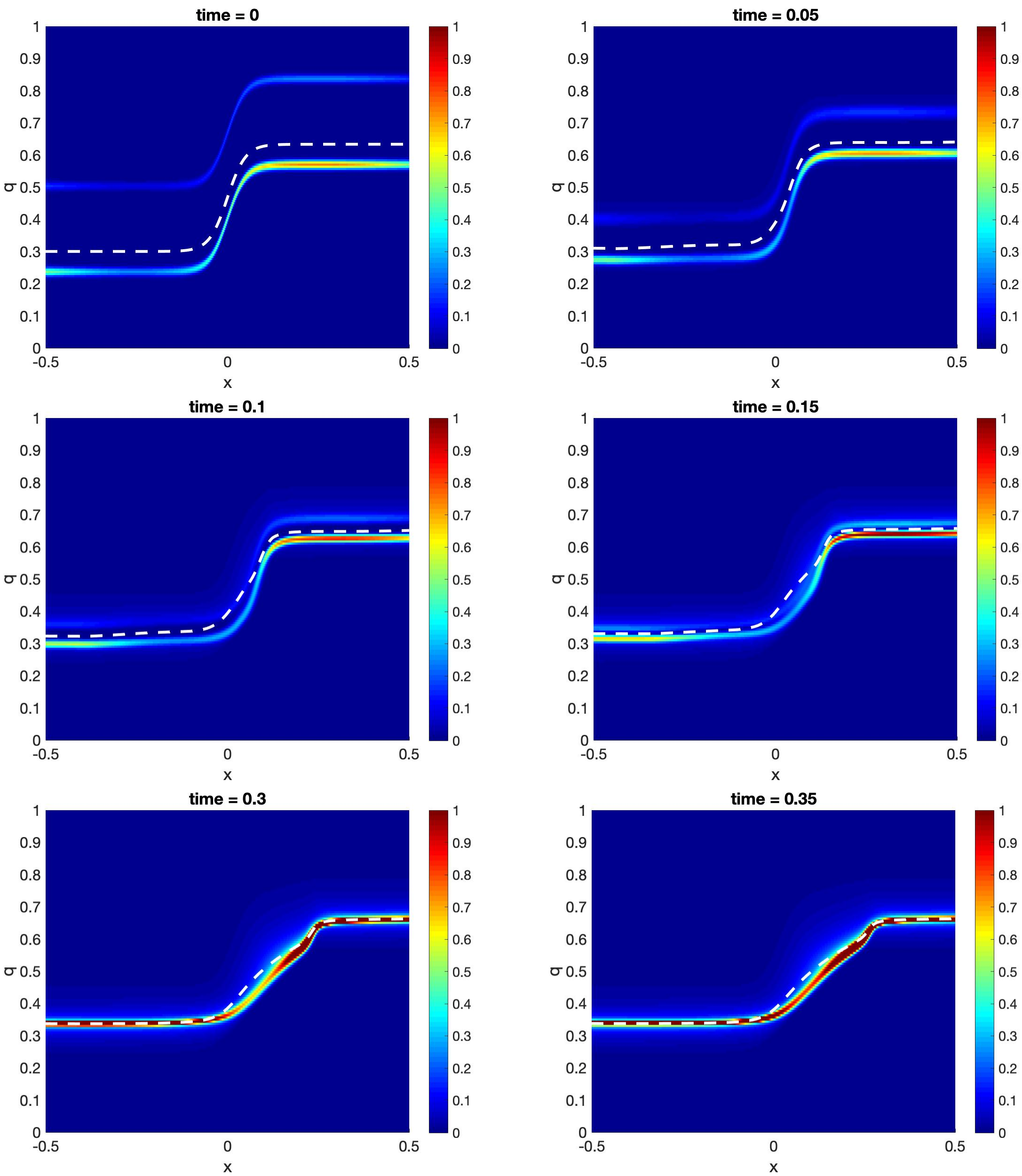

Figure 5.6: case e): Plots of $h(t, x, q)$ with $\gamma = 10$, $R = 0.002$ and $v_1(t, x) = 1 - q(t, x)$ for $t = 0, 0.05, 0.1, 0.15, 0.3$, and 0.35 s, respectively. The white line represents $\tilde{q}(t, x)$ and the color represents the probability of finding people.

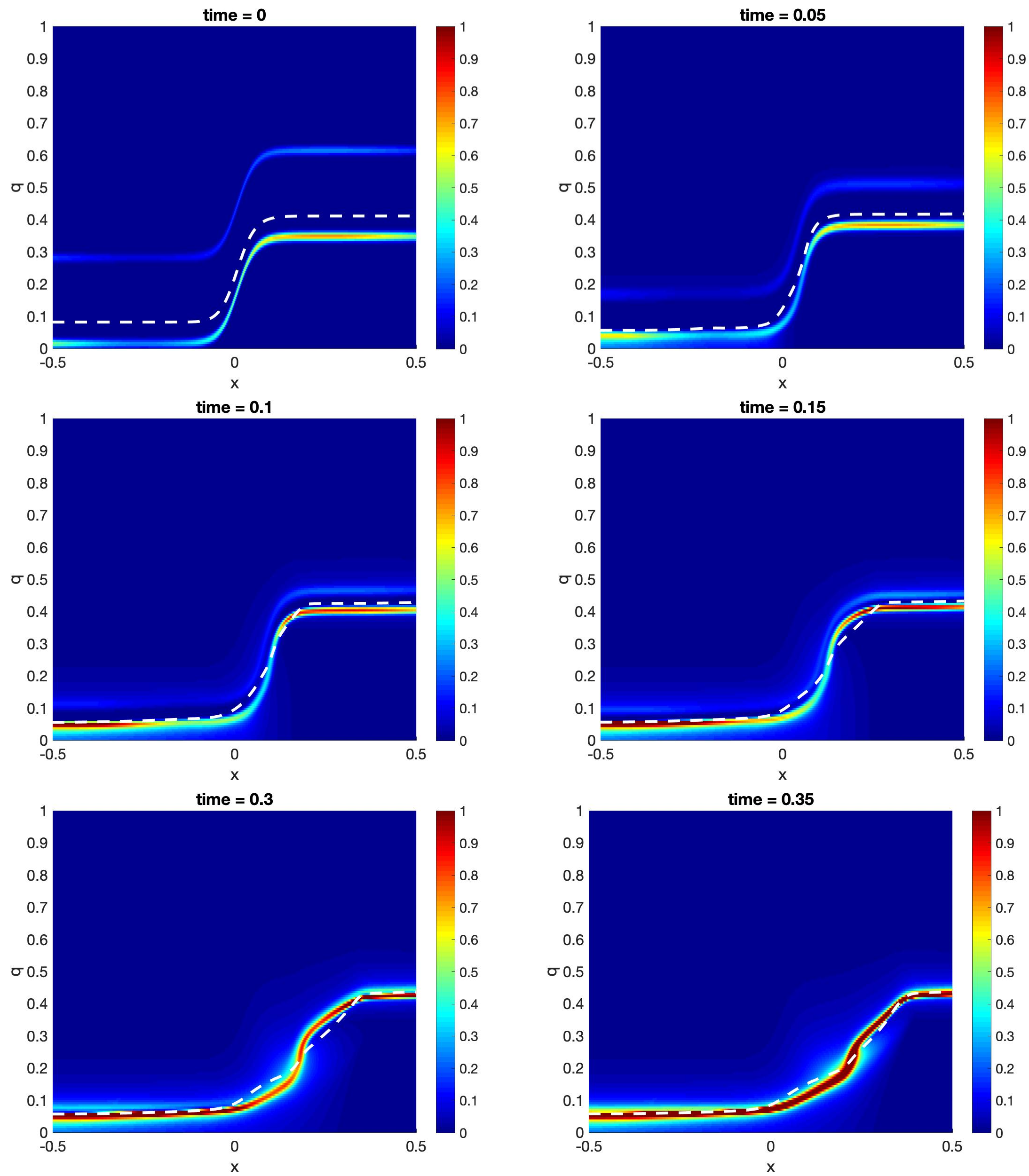

Figure 5.7: case f): Plots of $h(t, x, q)$ with $\gamma = 10$, $R = 0.002$ and $v_1(t, x) = \big(1 - q(t, x)\big)^2$ for $t = 0, 0.05, 0.1, 0.15, 0.3,$ and 0.35 s, respectively. The white line represents $\tilde{q}(t, x)$ and the color represents the probability of finding people.

Chapter 6

One Dimensional Model for Pedestrian Dynamics

In this Chapter, we present a one dimensional version of the model introduced in Chapter 2. In Chapter 7, this one dimensional model of pedestrian dynamics will be coupled with the one dimensional contagion model described in Chapter 5.

We recall a problem (2.8) and consider only the x-direction. There are two velocity directions $N_d = 2$ in the discrete set,

$$I_\theta = \left\{ \theta_i = (i-1)\pi : i = 1, 2 \right\},$$

which means people can walk back and forth without the interaction with the walls.

So, we get:

$$
\begin{aligned}
\frac{\partial f^i}{\partial t} &+ \frac{\partial \left(v^i[\rho](t,x) f^i(t,x)\right)}{\partial x} \\
&= \mathcal{J}^i[f](t,x) \\
&= \mathcal{J}^i_G[f](t,x) + \mathcal{J}^i_P[f](t,x) \\
&= \mu[\rho] \left(\sum_{h=1}^{2} \mathcal{A}_h(i) f^h(t,x) - f^i(t,x) \right) \\
&\quad + \eta[\rho] \left(\sum_{h,k=1}^{2} \mathcal{B}_{hk}(i)[\rho] f^h(t,x) f^k(t,x) - f^i(t,x)\rho(t,x) \right)
\end{aligned}
\tag{6.1}
$$

for $i = 1, 2$. Let us recall that functional $\mathcal{J}^i$ as $\mathcal{J}^i = \mathcal{J}^i_G + \mathcal{J}^i_P$, where $\mathcal{J}^i_G$ represent to goal to reach the exit and $\mathcal{J}^i_P$ is an interaction between candidate and field particles that move with direction θ_i due to interactions. See Chapter 2.

6.1 The Lie operator-splitting scheme

We apply the same scheme used in Chapter 3. Problem (6.1) will be split into a sum of two operators by applying the Lie operator-splitting scheme

1. A pure advection problem in the x direction.
2. A problem involving the interaction with the environment and other pedestrians.

Given an initial condition $f^{i,0} = f^i(0,x)$, for $i = 1, 2$, the algorithm reads: For $k = 0, 1, 2, \ldots, N_t - 2$, perform the following steps:

1. Find f^i, for $i = 1, 2$, such that

$$\begin{cases} \dfrac{\partial f^i}{\partial t} + \dfrac{\partial}{\partial x}\big((v[\rho]\cos\theta_i) f^i(t,x)\big) = 0, \ \text{ on } (t^k, t^{k+1}) \\ f^i(t^k, x) = f^{i,k} \end{cases} \tag{6.2}$$

Set $f^{i,k+\frac{1}{2}} = f^i(t^{k+1}, x)$.

2. Find f^i, for $i = 1, 2$, such that

$$\begin{cases} \dfrac{\partial f^i}{\partial t} = \mathcal{J}^i[f](t,x) \ \text{ on } (t^k, t^{k+1}) \\ f^i(t^k, x) = f^{i,k+\frac{1}{2}} \end{cases} \tag{6.3}$$

Set $f^{i,k+1} = f^i(t^{k+1}, x)$.

As in Section 3.2, once we compute $f^{i,k+1}$ for $i = 1, 2$, we use an equation (2.2) to get the density ρ^{k+1} and equations (2.3), (2.4) to get the velocity magnitude at time t^{k+1}.

6.1.1 Space and time discretization

We assume the computational domain under consideration is line segment $[0, L]$, for given L. We mesh the computational domain by choosing Δx to partition interval $[0, L]$. Let $N_x = L/\Delta x$. The discrete mesh points x_p are given by

$$x_p = p\Delta x, \quad p = 0, 1, \ldots, N_x, \tag{6.4}$$

$$x_{p+1/2} = x_p + \Delta x/2 = \Big(p + \frac{1}{2}\Big)\Delta x. \tag{6.5}$$

In order to simplify notation, let us set $\phi = f^i$, $\theta = \theta_i$, $t_0 = t^k$, $t_f = t^{k+1}$. Let M be a positive integer (≥ 3, in practice). We associate with M a time discretization step $\tau = (t_f - t_0)/M$ and set $t^m = t_0 + m\tau$. Next, we proceed with the space and time discretization of each subproblem.

Step 1

Let $\phi_0 = f^{i,k}$. Problem (6.2) can be rewritten as

$$\begin{cases} \dfrac{\partial \phi}{\partial t} + \dfrac{\partial}{\partial x}\big((v[\rho]\cos\theta)\phi(t,x)\big) = 0 \text{ on } (t_0, t_f), \\ \phi(t_0, x) = \phi_0. \end{cases} \tag{6.6}$$

The finite difference method we use produces an approximation $\Phi_p^m \in \mathbb{R}$ of the cell average

$$\Phi_p^m \approx \frac{1}{\Delta x}\int_{x_{p-1/2}}^{x_{p+1/2}} \phi(t^m, x)dx,$$

where $m = 1, \ldots, M$, $1 \leq p \leq N_x - 1$. Given an initial condition ϕ_0, function ϕ^m will be approximated by Φ^m with

$$\Phi^m\Big|_{[x_{p-1/2}, x_{p+1/2}]} = \Phi_p^m$$

The Lax-Friedrichs method for problem (6.6) can be written in conservative form as follows:

$$\Phi_p^{m+1} = \Phi_p^m - \frac{\tau}{\Delta x}\Big(\mathcal{F}(\Phi_p^m, \Phi_{p+1}^m) - \mathcal{F}(\Phi_{p-1}^m, \Phi_p^m)\Big)$$

where

$$\mathcal{F}(\Phi_p^m, \Phi_{p+1}^m) = \frac{\Delta x}{2\tau}(\Phi_p^m - \Phi_{p+1}^m) + \frac{1}{2}\Big((v[\rho_p^m]\cos\theta)\Phi_p^m + (v[\rho_{p+1}^m]\cos\theta)\Phi_{p+1}^m\Big).$$

Step 2

Let $\mathcal{J} = \mathcal{J}^i$ and $\phi_0 = f^{i,k+\frac{1}{2}}$. Problem (6.3) can be rewritten as

$$\begin{cases} \dfrac{\partial \phi}{\partial t} = \mathcal{J}[f](t,x) \text{ on } (t_0, t_f), \\ \phi(t_0, x) = \phi_0. \end{cases}$$

For the approximation of the above problem, we use the Forward Euler scheme:

$$\Phi_p^{m+1} = \Phi_p^m + \tau\Big(\mathcal{J}^m[F^m]\Big).$$

6.2 Numerical results

In this section, we consider a simple simulation: the computational domain is [0, L] with L given the real length of the domain. The door is placed at 100 m, but the domain is longer than that with a one exit at $x_{exit} = 100$ m. A group of 34 pedestrians is initially located as shown in Figure 6.1 top, left panel. See Figure 6.1. Pedestrians are moving toward the exit with the initial direction θ_1. This simulation is performed with $\varepsilon = 0.4$ and $\alpha = 1$.

We define the following reference quantities:

- $D = 100$ m;
- $v_M = 2$ m/s;
- $T = D/v_M = 50$ s;
- $\rho_M = 7$ people$/m^2$.

We use three different meshes: a coarse mesh with $\Delta x = 1$ m, a medium mesh with $\Delta x = 0.5$ m, and a fine mesh with $\Delta x = 0.25$ m. Similarly, for the time discretization we consider three different time steps: a large time step $\Delta t_{large} = 0.03$ s, a medium time step $\Delta t_{medium} = 0.015$ s, and a small time step $\Delta t_{small} = 0.0075$ s. The value of M for the Lie splitting scheme is set to 3. To avoid stability issues, we consider the following three combinations of the above meshes and time steps:

1. coarse mesh and Δt_{large};
2. medium mesh and Δt_{medium};
3. fine mesh and Δt_{small}.

Figure 6.1 shows how 34 pedestrians move for the three combinations mentioned above. From Figure 4.7, one can observe that two combinations, coarse mesh with Δt_{large} and medium mesh with Δt_{medium} are too dissipative. Hence, fine mesh and Δt_{small} is the best combination.

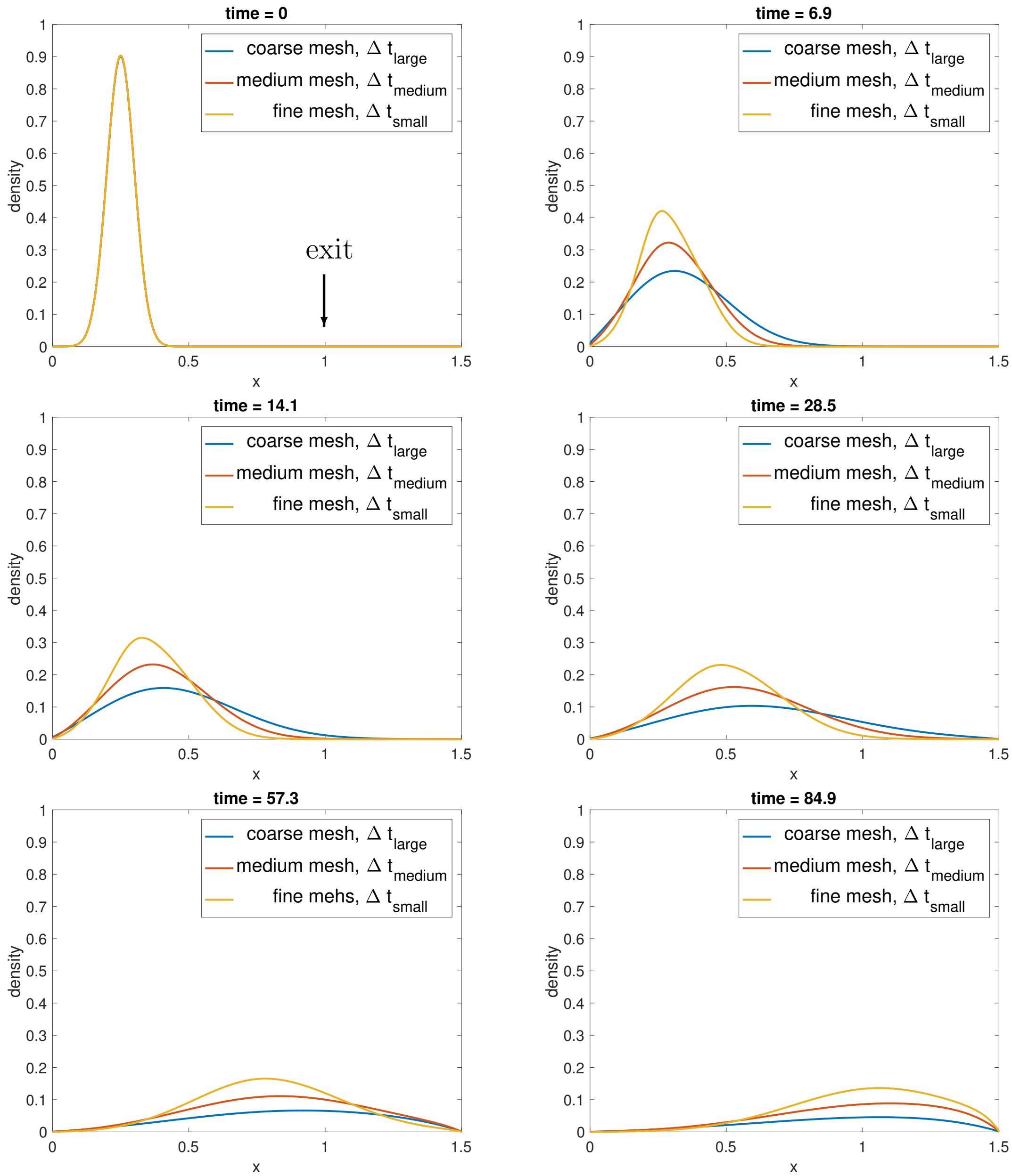

Figure 6.1: Evacuation progress of 34 pedestrians with initial direction θ_1 for three different combinations of mesh and time steps for $t = 0, 6.9, 14.1, 28.5, 57.3,$ and 84.9 s

Chapter 7

One Dimensional Pedestrian Dynamics Model Coupled to the Disease Contagion Model

In this section, we couple the one dimension pedestrian dynamics model with the model of the spreading of an infectious disease. A small number of sick people are introduced in given environment, *e.g.* a corridor or a room. We are interested in the probability of people getting infected. Let us refer to equation (6.1). Since we have different groups of people with different directions, we will have different levels of contagion q_i that are governed by the disease contagion model equation (5.20) from Section 5.2:

$$h_t^i + (v^i h^i)_x = \gamma((q^i - q^{i,*})h^i)_q, \tag{7.1}$$

where $h^i(t, x, q)$ is the probability of finding people with contagion level q at time t, position x, and direction i and v^i is the velocity with the direction θ_i. The quantity

$q^{i,*}(t,x)$ is the local *average* contagion level of infectious disease weighted by the distance to x:

$$q^{i,*}(t,x) = \frac{\int\int \kappa(|x-y|)h^i(t,y,q)qdqdy}{\int\int \kappa(|x-y|)h^i(t,y,q)dqdy}. \tag{7.2}$$

As seen in Section 5.1, the macroscopic bulk fear level is

$$\tilde{q}^i(t,x) = \int h^i(t,x,q)qdq.$$

Now, we consider the couple model:

$$\begin{cases} \dfrac{\partial f^i}{\partial t} + \dfrac{\partial\left(v^i[\rho](t,x)f^i(t,x)\right)}{\partial x} = \mathcal{J}^i[f](t,x), & (7.3) \\ \dfrac{\partial h^i}{\partial t} + \dfrac{\partial (v^i h^i)}{\partial x} = \gamma \dfrac{\partial((q^i - q^{i,*})h^i)}{\partial q}. & (7.4) \end{cases}$$

Let us find f^i and h^i for $i = 1, 2$, such that equations (6.1) and (7.1) hold.

7.1 Numerical method

From the one dimension kinetic approach pedestrian model, we can compute the distribution function $f^i(t^k, x)$ for time $t = t^k$. By summing the distribution function $f^i(t^k, x)$ with all directions i, the density $\rho(t^k, x)$ is obtained. The velocity $v^i(t^k, x)$ is computed using Equations (2.3) and (2.4), and then we use this velocity for the disease contagion model. Thus, problem (7.1) depends on the solution of Equation (6.1), but not vice versa, which means that the coupling is one way.

7.1.1 Numerical scheme

Let us apply the Lie operator-splitting scheme described in the Section 3.2 to problem (7.3). Given an initial condition $f^{i,0} = f^i(0, x)$, for $i = 1, 2$, the algorithm reads:

Given an initial condition $h^{i,0} = h^i(0,x)$, for $i = 1,2$, for $k = 0,1,2,\ldots,N_t - 2$, perform the following steps

1-a. Find f^i, for $i = 1,2$, such that

$$\begin{cases} \dfrac{\partial f^i}{\partial t} + \dfrac{\partial}{\partial x}\big((v[\rho]\cos\theta_i) f^i(t,x)\big) = 0 \;\text{ on } (t^k, t^{k+1}) \\ f^i(t^k,x) = f^{i,k} \end{cases} \tag{7.5}$$

Set $f^{i,k+\frac{1}{2}} = f^i(t^{k+1},x)$.

1-b. Find f^i, for $i = 1,2$, such that

$$\begin{cases} \dfrac{\partial f^i}{\partial t} = \mathcal{J}^i[f](t,x) \;\text{ on } (t^k, t^{k+1}) \\ f^i(t^k,x) = f^{i,k+\frac{1}{2}} \end{cases} \tag{7.6}$$

Set $f^{i,k+1} = f^i(t^{k+1},x)$. Find the velocity modulus $v(t^{k+1},x)$ by using Equations (2.3) and (2.4).

2. Find h^i, for $i = 1,2$, such that

$$\begin{cases} \dfrac{\partial h^i}{\partial t} + \dfrac{\partial (v[\rho]\cos\theta_i h^i)}{\partial x} = \gamma \dfrac{\partial((q^i - q^{i,*})h^i)}{\partial q} \;\text{ on } (t^k, t^{k+1}) \\ h^i(t^k,x) = h^{i,k} \end{cases} \tag{7.7}$$

Set $h^{i,k+\frac{1}{2}} = h^i(t^{k+1},x)$.

7.1.2 Space, contagion level and time discretization

We assume for simplicity that the computational domain under consideration is a line $[0,L]$, for given L. We discretize the computational domain $[0,L]$ by choosing

Δx to partition. Let $N_x = L/\Delta x$. Then, we define the discrete mesh points x_p by

$$x_p = p\Delta x, \quad p = 0, 1, \ldots, N_x, \tag{7.8}$$

It will also be useful to define

$$x_{p+1/2} = x_p + \Delta x/2 = \Big(p + \frac{1}{2}\Big)\Delta x. \tag{7.9}$$

For the stability, the subtime step τ is chosen the satisfy the Courant-Friedrichs-Lewy (CFL) conditions.

$$\max\left\{\frac{\tau}{\Delta x}, \frac{\tau}{\Delta y}\right\} \leq 1, \tag{7.10}$$

where $q_{max} = max_j q_j$.

In order to simplify the notation, let us set $\phi = f^i$, $\theta = \theta_i$, $t_0 = t^k$, $t_f = t^{k+1}$. Let M be a positive integer (≥ 3, in practice). We associate with M a time discretization step $\tau = (t_f - t_0)/M$ and set $t^m = t_0 + m\tau$.

Step 1-a

Let $\phi_0 = f^{i,k}$. Problem (7.5) can be rewritten as

$$\begin{cases} \dfrac{\partial \phi}{\partial t} + \dfrac{\partial}{\partial x}\big((v[\rho]\cos\theta)\phi(t,x)\big) = 0 \ \text{ on } (t_0, t_f), \\ \phi(t_0, x) = \phi_0. \end{cases} \tag{7.11}$$

The finite difference method we use produces an approximation $\Phi_p^m \in \mathbb{R}$ of the cell average

$$\Phi_p^m \approx \frac{1}{\Delta x}\int_{x_{p-1/2}}^{x_{p+1/2}} \phi(t^m, x)dx,$$

where $m = 1, \ldots, M$, $1 \leq p \leq N_x - 1$. Given an initial condition ϕ_0, function ϕ^m will be approximated by Φ^m with

$$\Phi^m \Big|_{[x_{p-1/2}, x_{p+1/2}]} = \Phi_p^m$$

The Lax-Friedrichs method for problem (7.11) can be written in conservative form as follows:

$$\Phi_p^{m+1} = \Phi_p^m - \frac{\tau}{\Delta x}\Big(\mathcal{F}(\Phi_p^m, \Phi_{p+1}^m) - \mathcal{F}(\Phi_{p-1}^m, \Phi_p^m)\Big),$$

where

$$\mathcal{F}(\Phi_p^m, \Phi_{p+1}^m) = \frac{\Delta x}{2\tau}(\Phi_p^m - \Phi_{p+1}^m) + \frac{1}{2}\Big((v[\rho_p^m]\cos\theta)\Phi_p^m + (v[\rho_{p+1}^m]\cos\theta)\Phi_{p+1}^m\Big).$$

Step 1-b

Let $\mathcal{J} = \mathcal{J}^i$ and $\phi_0 = f^{i,k+\frac{1}{2}}$. Problem (7.6) can be rewritten as

$$\begin{cases} \dfrac{\partial \phi}{\partial t} = \mathcal{J}[f](t,x) \ \text{ on } (t_0, t_f), \\ \phi(t_0, x) = \phi_0. \end{cases} \tag{7.12}$$

For the approximation of the above problem, we use the Forward Euler scheme:

$$\Phi_p^{m+1} = \Phi_p^m + \tau\Big(\mathcal{J}^m[F^m]\Big).$$

We also discretize the contagion level q by choosing $\Delta q = q_{j+1} - q_j$ and define

$$q_{j+1/2} = q_j + \Delta q_{j+\frac{1}{2}}/2, \quad j = 0, 1, \ldots, N_q,$$

where N_q denotes the total number of points in $q-$direction. The time step Δt is all chose as

$$\Delta t = \frac{1}{2} \min \left\{ \frac{\Delta x}{q_{max}}, \frac{\Delta q}{2 q_{max} \gamma} \right\}$$

to satisfy the Courant-Friedrichs-Lewy (CFL) condition, where $q_{max} = max_j q_j$.

Step 2

Denote $h^i_{p,j} = h^i(t, x_p, q_j)$ and $q^*_p = q^*(t, x_p)$. Also, let $\phi_0 = h^i_{p,j}$ and $\phi_1 = h^i_{p,j+1}$. The space discretization of problem (7.7) can be rewritten as

$$\begin{cases} \dfrac{\partial \phi}{\partial t} = -\dfrac{\eta_{p+\frac{1}{2},j} - \eta_{p-\frac{1}{2},j}}{\Delta x} - \gamma \dfrac{\xi_{p,j+\frac{1}{2}} - \xi_{p,j-\frac{1}{2}}}{\Delta q_{j+\frac{1}{2}}} - \gamma \dfrac{C_{p,j+\frac{1}{2}} - C_{p,j-\frac{1}{2}}}{\Delta q_{j+\frac{1}{2}}} \text{ on } (t_0, t_f), \\ \phi(t_0, x) = \phi_0, \end{cases} \tag{7.13}$$

where

$$\eta_{p,j+\frac{1}{2}} = v^i_p \phi_0,$$

$$\xi_{p,j+\frac{1}{2}} = \frac{|q^*_j - q_{j+\frac{1}{2}}| + (q^*_j - q_{j+\frac{1}{2}})}{2} \phi_0 + \frac{(q^*_j - q_{j+\frac{1}{2}}) - |q^*_j - q_{j+\frac{1}{2}}|}{2} \phi_1,$$

and

$$C_{p,j+\frac{1}{2}} = \frac{1}{2} |s_{p,j+\frac{1}{2}}| \left(1 - \frac{\Delta t}{\Delta q_{j+\frac{1}{2}}} |s_{p,j+\frac{1}{2}}| \right) \tilde{W}_{p,j+\frac{1}{2}},$$

with $s_{p,j-\frac{1}{2}} = q^*_p - q_{j-\frac{1}{2}}$, $W_{p,j-\frac{1}{2}} = h_{p,j} - h_{p,j-\frac{1}{2}}$, and $\tilde{W}_{p,j-\frac{1}{2}} = W_{p,j-\frac{1}{2}} \varphi\left(\frac{W_{p,\mathbf{j}-\frac{1}{2}}}{W_{p,j-\frac{1}{2}}}\right)$. The subscript **j** is p-1 if $s_{p,j-\frac{1}{2}} > 0$ and p+1 if $s_{p,j-\frac{1}{2}} < 0$. Here, φ is again the Van Leer function (5.14):

$$\varphi(\theta) = \frac{|\theta| + \theta}{1 + |\theta|}. \tag{7.14}$$

Finally, we use a first-order semi-discrete upwind scheme of problem (7.13) and a flux limiter in order to construct a second-order scheme:

$$\Phi_p^{m+1} = \Phi_p^m - \Delta t\left(\frac{\eta_{p+\frac{1}{2},j} - \eta_{p-\frac{1}{2},j}}{\Delta x} + \gamma\frac{\xi_{p,j+\frac{1}{2}} - \xi_{p,j-\frac{1}{2}}}{\Delta q_{j+\frac{1}{2}}} + \gamma\frac{C_{p,j+\frac{1}{2}} - C_{p,j-\frac{1}{2}}}{\Delta q_{j+\frac{1}{2}}}\right). \quad (7.15)$$

7.2 Numerical results

A group of 34 pedestrians is initially placed as shown in Figure 7.1 top left panel, with initial direction θ_1. All the simulations are performed with $\varepsilon = 0.4$ and $\alpha = 1$. We are going to consider dimensionless quantities as described in Section 2.1. The dimensionless quantities are obtained by using the following reference quantities:

- $L = 30$ m;
- $v_M = 2$ m/s;
- $T = D/v_M = 15$ s;
- $\rho_M = 3$ people$/m$;
- $q \in [0, 3]$;
- $\gamma = 100$;
- $R = 0.01$ m.

For the one dimension kinetic model, we consider mesh size $\Delta x_k = 0.05$ m and the time step $\Delta t_k = 0.003$ s. For the disease contagion model, we consider the mesh size $\Delta x_d = 0.025$ m and the time step $\Delta t_d = 0.00002$ s to satisfy CFL conditions. Figure 7.1 and 7.2 shows how 38 pedestrians move and how the corresponding disease contagion level can change.

See Figure 7.1 and Figure 7.2. As expected, where there is a larger crowd there is

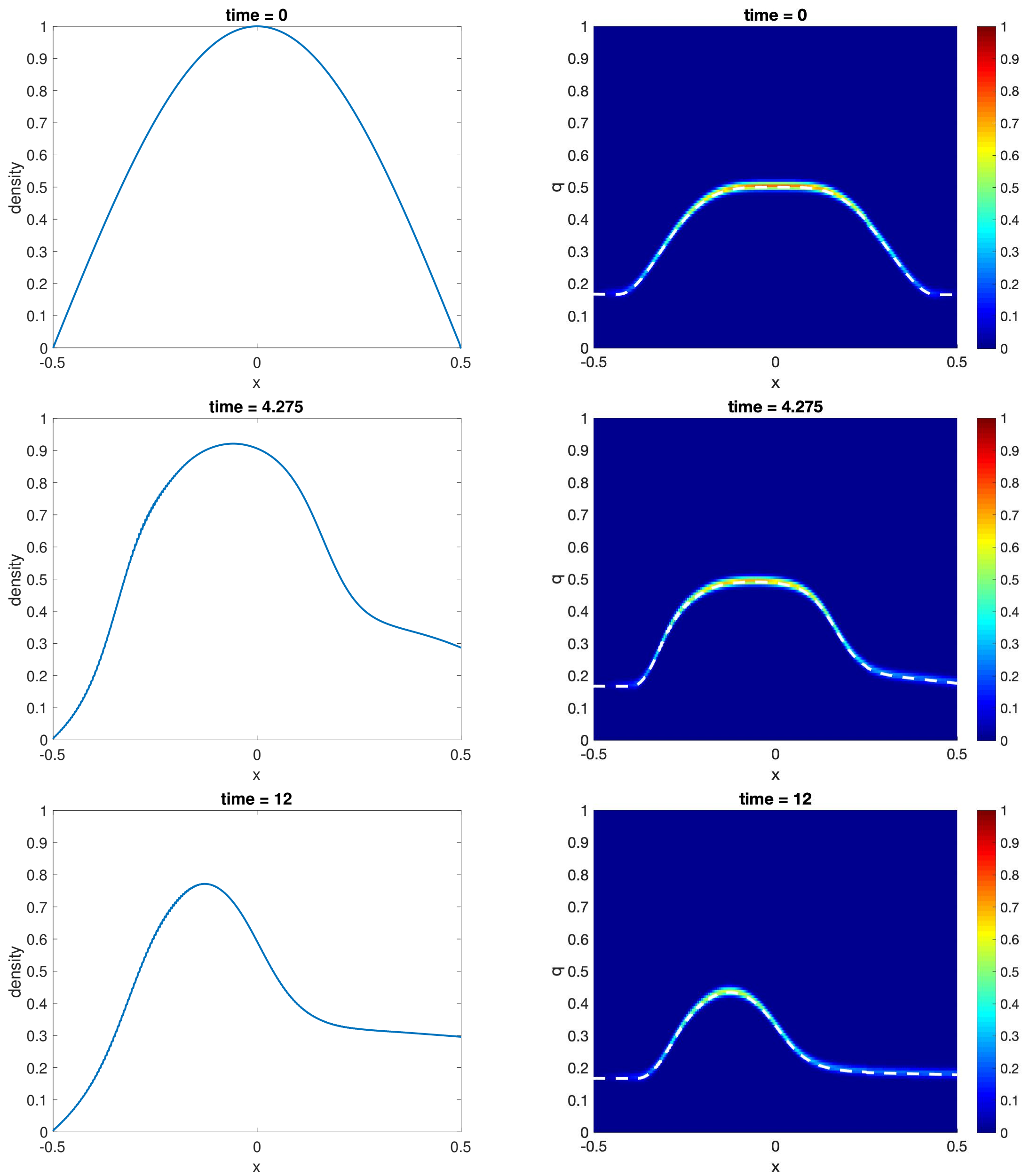

Figure 7.1: Left: Evacuation process of 38 pedestrians moving with initial direction θ_1 and Right: Plot of $h(t, x, q)$ for $t = 0, 4.275$, and 12 s. The color represents the probability of finding sick people.

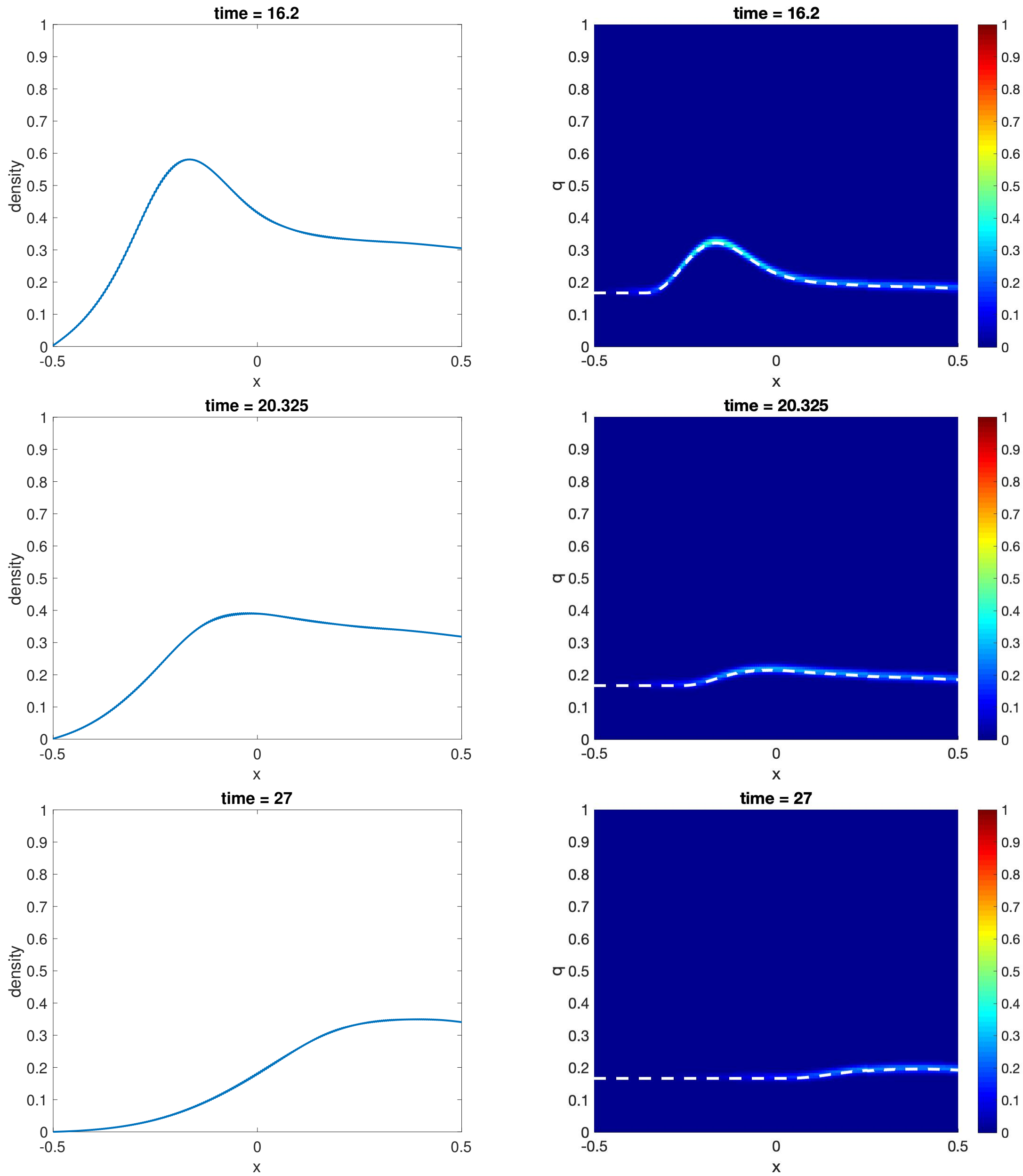

Figure 7.2: Left: Evacuation process of 38 pedestrians moving with initial direction θ_1 and Right: Plot of $h(t, x, q)$ for $t = 16.2, 20.325$, and 27 s. The color represents the probability of finding sick people.

a higher probability of getting infected. The crowded place has more higher contagion level q to get infected. See Figure 7.1 top right panel. As time passes, people move toward the exit and the contagion level q decreases.

Chapter 8

Conclusions

We considered a kinetic theory approach to model pedestrian dynamics in bounded domain and adapted it to handle obstacles. For the numerical approximation of the solution to our model, we applied the Lie splitting scheme which breaks the problem into two pure advection problems and a problem involving the interaction with the environment and other pedestrians.

Several test cases have been considered in order to show the ability of the model to reproduce qualitatively:

- evacuation from a room with one exit, without and with obstacles;
- evacuation from a room with two exits and no obstacles;
- lane formation.

In the case of the room with two exits and no obstacles, we also presented a quantitative comparison with experimental data. Numerical results and experimental data are in very good agreement for medium and medium-to-large groups of people. With the confidence in the model given by the experimental validation, we performed numerical tests to study evacuation for different scenarios in terms of exit sizes, obstacle shapes, and velocity moduli.

We considered a one dimensional model of kinetic approach known ASCRIBE that can track the level of emotional contagion. We proposed a modification to track disease contagion level. Simulations show how the infectious disease spreads for two choices of velocity moduli. Moreover, we introduced a one dimensional version of the pedestrian dynamics model and tested it with a simple benchmark combinations.

Finally, we coupled the one dimension kinetic approach for pedestrian dynamics with the disease contagion model. We applied the coupled model to study the initial spreading of an infectious disease in a corridor with one dimensional motion. Numerical results show in the crowded part of the corridor it is more likely to get infected.

Bibliography

[1] Juan Pablo Agnelli, Francesca Colasuonno, and Damian Knopoff. A kinetic theory approach to the dynamics of crowd evacuation from bounded domains. *Mathematical Models and Methods in Applied Sciences*, 25(01):109–129, 2015.

[2] Gianluca Antonini, Michel Bierlaire, and Mats Weber. Discrete choice models of pedestrian walking behavior. *Transportation Research Part B: Methodological*, 40(8):667 – 687, 2006.

[3] Miho Asano, Takamasa Iryo, and Masao Kuwahara. Microscopic pedestrian simulation model combined with a tactical model for route choice behaviour. *Transportation Research Part C: Emerging Technologies*, 18(6):842 – 855, 2010. Special issue on Transportation Simulation Advances in Air Transportation Research.

[4] Stefania Bandini, Sara Manzoni, and Giuseppe Vizzari. Agent based modeling and simulation: An informatics perspective. *Journal of Artificial Societies and Social Simulation*, 12(4):4, 2009.

[5] Nicola Bellomo and Abdelghani Bellouquid. On the modeling of crowd dynamics: Looking at the beautiful shapes of swarms. *Networks and Heterogeneous Media*, 6(3):383–399, 2011.

[6] Nicola Bellomo, Abdelghani Bellouquid, Livio Gibelli, and Nisrine Outada. A quest towards a mathematical theory of living systems. *Modeling and Simulation in Science, Engineering and Technology*, Birkhauser, 2017.

[7] Nicola Bellomo, Abdelghani Bellouquid, and Damian Knopoff. From the microscale to collective crowd dynamics. *Society for Industrial and Applied Mathematics Multiscale Modeling and Simulation*, 11:943–963, 2013.

[8] Nicola Bellomo and Christian Dogbe. On the modeling of traffic and crowds: A survey of models, speculations, and perspectives. *Society for Industrial and Applied Mathematics Review*, 53(3):409–463, 2011.

[9] Nicola Bellomo and Livio Gibelli. Toward a mathematical theory of behavioral-social dynamics for pedestrian crowds. *Mathematical Models and Methods in Applied Sciences*, 25(13):2417–2437, 2015.

[10] Nicola Bellomo and Livio Gibelli. Behavioral crowds: Modeling and Monte Carlo simulations toward validation. *Computers & Fluids*, 141:13–21, 2016.

[11] Nicola Bellomo, Livio Gibelli, and Nisrine Outada. On the interplay between behavioral dynamics and social interactions in human crowds. *Kinetic and Related Models*, 12(2):397–409, 2019.

[12] Nicola Bellomo, Damian Knopoff, and Juan Soler. On the difficult interplay between life, "complexity", and mathematical sciences. *Mathematical Models and Methods in Applied Sciences*, 23(10):1861–1913, 2013.

[13] Nicola Bellomo, Benedetto Piccoli, and Andrea Tosin. Modeling crowd dynamics from a complex system viewpoint. *Mathematical Models and Methods in Applied Sciences*, 22(supp02):1230004, 2012.

[14] Andrea L. Bertozzi, Jesús Rosado, Martin B. Short, and Li Wang. Contagion shocks in one dimension. *Journal of Statistical Physics*, 158(3):647–664, 2015.

[15] Victor Blue and Jeffrey L. Adler. Cellular automata microsimulation for modeling bi-directional pedestrian walkways. *Transportation Research Record B: Methodological*, 35:293–312, 2001.

[16] Victor Blue and Jeffrey L. Adler. Cellular automata microsimulation of bidirectional pedestrian flows. *Transportation Research Record Journal of the Transportation Research Board*, 1678:135–141, 1999.

[17] Tibor Bosse, Rob Duell, Zulfiqar A. Memon, Jan Treur, and C. Natalie van der Wal. A multi-agent model for mutual absorption of emotions. In J. Otamendi, A. Bargiela, J.L. Montes, and L.M.D. Pedrera, editors, *Proceedings of the 23rd European Conference on Modelling and Simulation*, 212–218, 2009. ECMS09.

[18] Carsten Burstedde, K Klauck, A Schadschneider, and J Zittartz. Simulation of pedestrian dynamics using a two-dimensional cellular automaton. *Physica A: Statistical Mechanics and its Applications*, 295(3):507 – 525, 2001.

[19] Carlo Cercignani, Reinhard Illner, and Mario Pulvirenti. *The Mathematical Theory of Dilute Gases*. New York : Springer-Verlag, 1994.

[20] Nitish Chooramun, Peter J. Lawrence, and Edwin R. Galea. An agent based evacuation model utilising hybrid space discretisation. *Safety Science*, 50(8):1685 – 1694, 2012. Evacuation and Pedestrian Dynamics.

[21] Mohcine Chraibi, Ulrich Kemloh, Andreas Schadschneider, and Armin Seyfried. Force-based models of pedestrian dynamics. *Networks and Heterogeneous Media*, 6(3):425–442, 2011.

[22] Jicai Dai, Xia Li, and Lin Liu. Simulation of pedestrian counter flow through bottlenecks by using an agent-based model. *Physica A: Statistical Mechanics and its Applications*, 392(9):2202–2211, 2013.

[23] Jan Dijkstra, Joran Jessurun, and Harry Timmermans. A multi-agent cellular automata model of pedestrian movement. *Pedestrian and Evacuation Dynamics*, Springer-Verlag, Berlin, 173–181, 2001.

[24] Bo Einarsson, editor. *Accuracy and Reliability in Scientific Computing*. Software, Environments and Tools. SIAM, Linköping University, Linköping, Sweden, 2005.

[25] Roland Glowinski. *Finite element methods for incompressible viscous flow, in: P.G.Ciarlet, J.-L.Lions (Eds), Handbook of numerical analysis*, volume 9. North-Holland, Amsterdam, 2003.

[26] Dirk Helbing. A mathematical model for the behavior of pedestrians. *Behavioral Science*, 36(4):298–310, 1991.

[27] Dirk Helbing. Collective phenomena and states in traffic and self-driven many-particle systems. *Computational Materials Science*, 30:180 – 187, 2004. Selected papers of the Twelfth International Workshop on Computational Materials Science (CMS2002).

[28] Dirk Helbing, Illés Farkas, Peter Molnar, and Tamás Vicsek. Simulation of pedestrian crowds in normal and evacuation situations. *Pedestrian and Evacuation Dynamics*, Springer, 21–58, 2002.

[29] Dirk Helbing and Péter Molnár. Social force model for pedestrian dynamics. *Physical Review E*, 51:4282–4286, 1995.

[30] Dirk Helbing and Tamás Vicsek. Optimal self-organization. *New Journal of Physics*, 1(1):13, 1999.

[31] Roger L. Hughes. A continuum theory for the flow of pedestrians. *Transportation Research Part B: Methodological*, 36(6):507–535, 2002.

[32] Anders Johansson, Dirk Helbing, and Pradyumn K. Shukla. Specification of the social force pedestrian model by evolutionary adjustment to video tracking data. *Advances in Complex Systems*, 10(supp02):271–288, 2007.

[33] Taras I. Lakoba, D. J. Kaup, and Neal M. Finkelstein. Modifications of the helbing-molnar-farkas-vicsek social force model for pedestrian evolution. *SIMULATION*, 81(5):339–352, 2005.

[34] R.J. LeVeque. *Numerical Methods for Conservation Laws*. Lectures in mathematics ETH Zürich. Birkhäuser Verlag, 1990.

[35] Xiaomeng Li, Xuedong Yan, Xingang Li, and Jiangfeng Wang. Using cellular automata to investigate pedestrian conflicts with vehicles in crosswalk at signalized intersection. *Discrete Dynamics in Nature and Society*, 16 pages, 2012.

[36] Shaobo Liu, Siuming Lo, Jian Ma, and Weili Wang. An agent-based microscopic pedestrian flow simulation model for pedestrian traffic problems. *IEEE Transactions on Intelligent Transportation Systems*, 15(3):992–1001, June 2014.

[37] Shaobo Liu, Lizhong Yang, Tingyong Fang, and Jian Li. Evacuation from a classroom considering the occupant density around exits. *Physica A: Statistical Mechanics and its Applications*, 388(9):1921–1928, 2009.

[38] Jian Ma, Wei guo Song, Jun Zhang, Siu ming Lo, and Guang xuan Liao. k-nearest-neighbor interaction induced self-organized pedestrian counter flow. *Physica A: Statistical Mechanics and its Applications*, 389(10):2101–2117, 2010.

[39] Mehdi Moussaïd, Dirk Helbing, Simon Garnier, Anders Johansson, Maud Combe, and Guy Theraulaz. Experimental study of the behavioural mechanisms underlying self-organization in human crowds. *Proceedings of the Royal Society of London B: Biological Sciences*, 276(1668):2755–2762, 2009.

[40] Debra Parisi and Claudio Dorso. Morphological and dynamical aspects of the room evacuation process. *Physica A: Statistical Mechanics and its Applications*, 385(1):343–355, 2007.

[41] Andreas Schadschneider, Wolfram Klingsch, Hubert Kluepfel, Tobias Kretz, Christian Rogsch, and Armin Seyfried. *Evacuation Dynamics: Empirical Results, Modeling and Applications*, 517–550. Springer, New York, 2011.

[42] Andreas Schadschneider and Armin Seyfried. Empirical results for pedestrian dynamics and their implications for modeling. *Networks and Heterogeneous Media*, 6(3):545–560, 2011.

[43] Armin Seyfried, Oliver Passon, Bernhard Steffen, Maik Boltes, Tobias Rupprecht, and Wolfram Klingsch. New insights into pedestrian flow through bottlenecks. *Transportation Science*, 43(3):395–406, 2009.

[44] Apoorva Shende, Mahendra P. Singh, and Pushkin Kachroo. Optimization-based feedback control for pedestrian evacuation from an exit corridor. *IEEE Transactions on Intelligent Transportation Systems*, 12(4):1167–1176, Dec 2011.

[45] Bernhard Steffen and Armin Seyfried. Methods for measuring pedestrian density, flow, speed and direction with minimal scatter. *Physica A: Statistical Mechanics and its Applications*, 389:1902–1910, 2009.

[46] Yusuke Tajima, Kouhei Takimoto, and Takashi Nagatani. Pattern formation and jamming transition in pedestrian counter flow. *Physica A: Statistical Mechanics and its Applications*, 313(3):709–723, 2002.

[47] Jason Tsai, Emma Bowring, Stacy Marsella, and Milind Tambe. Empirical evaluation of computational emotional contagion models. *Intelligent Virtual Agents*, 6895:384–397, 09 2011.

[48] Jason Tsai, Natalie Fridman, Emma Bowring, Matthew Brown, Shira Epstein, Gal Kaminka, Stacy C. Marsella, Andrew Ogden, Inbal Rika, Ankur Sheel, Matthew Taylor, Xuezhi Wang, Avishay Zilka, and Milind Tambe. ESCAPES - Evacuation Simulation with Children, Authorities, Parents, Emotions, and Social comparison. *International Conference on Autonomous Agents and Multiagent Systems*, Taipei, Taiwan, May 2011.

[49] Alasdair Turner and Alan Penn. Encoding natural movement as an agent-based system: An investigation into human pedestrian behaviour in the built environment. *Environment and Planning B: Planning and Design*, 29(4):473–490, 2002.

[50] A.U. Kemloh Wagoum, Antoine Tordeux, and Wilson Liao. Understanding human queuing behaviour at exits: An empirical study. *Royal Society Open Science*, 4(160896), 2017.

[51] Li Wang, Martin B. Short, and Andrea L. Bertozzi. Efficient numerical methods for multiscale crowd dynamics with emotional contagion. *Mathematical Models and Methods in Applied Sciences*, 27(1):205–230, 1 2017.

[52] Jonathan A. Ward, Andrew J. Evans, and Nicolas S. Malleson. Dynamic calibration of agent-based models using data assimilation. *Royal Society Open Science*, 3(4), 2016.

[53] Song Xu and Henry Been-Lirn Duh. A simulation of bonding effects and their impacts on pedestrian dynamics. *IEEE Transactions on Intelligent Transportation Systems*, 11(1):153–161, 2010.

[54] W. J. Yu, R. Chen, Li-Yu. Dong, and S. Q. Dai. Centrifugal force model for pedestrian dynamics. *Physical Review E*, 72(7):026112, Aug 2005.

[55] Jun Zhang, Wolfram Klingsch, Andreas Schadschneider, and Armin Seyfried. Transitions in pedestrian fundamental diagrams of straight corridors and t-junctions. *Journal of Statistical Mechanics: Theory and Experiment*, 2011(06):P06004, 2011.

[56] Bolei Zhou, Xiaogan Wang, and Xiaoou Tang. Understanding collective crowd behaviors: Learning a mixture model of dynamic pedestrian-agents. *IEEE Conference on Computer Vision and Pattern Recognition*, 2871–2878, 2012.